9950-625

BOEING ENGINEERING & CONSTRUCTION
THE BOEING ENERGY AND ENVIRONMENT DIVISION

(NASA-CR-163472) A CONCEPTUAL DESIGN STUDY OF POINT FOCUSING THIN-FILM SOLAR CONCENTRATORS Final Report (Boeing Engineering and Construction) 128 p HC A07/MF A01 CSCL 10A G3/44

N82-16492

Unclas 08834

A Conceptual Design Study of Point Focusing Thin-Film Solar Concentrators

FINAL REPORT

Jet Propulsion Laboratory
Contract 955804

November 11, 1981

A Conceptual Design Study of Point Focusing Thin-Film Solar Concentrators

FINAL REPORT

November 11, 1981

Prepared by

Solar Systems Group
Boeing Engineering and Construction

A Division of The Boeing Company
Seattle, Washington 98124

Program Manager
Donald K. Zimmerman

"This work was performed for the Jet Propulsion Laboratory, California Institute of Technology sponsored by U.S. Department of Energy through an agreement with the National Aeronautics and Space Administration."

Prepared for

Jet Propulsion Laboratory
4800 Oak Grove Drive
Pasadena, California 91103

JPL Contract
955804

ABSTRACT

This report describes a study which investigated the use of thin film for the reflective surface on solar concentrators. A conceptual design for a point-focusing concentrator with 45 gore shaped reflector panels was defined. Candidates for reflector panel design concepts, including materials and configurations, were identified. The large list of candidates was screened and reduced to the five most promising ones. Cost and technical factors were used in making the final choices for the panel conceptual design, which was a stiffened steel skin substrate with a bonded, acrylic overcoated, aluminized polyester film reflective surface. Computer simulations were run for the concentrator optics using the selected panel design, and experimentally determined specularity and reflectivity values. Intercept factor curves and energy to the aperture curves were produced. These curves indicated that surface errors of 2 mrad (milliradians) or less would be required to capture the desired energy for a Brayton cycle 816°C (1500°F) case. Two test panels were fabricated to demonstrate manufacturability and optically tested for surface error. Surface errors in the range of 1.75 mrad and 2.2 mrad were measured.

ACKNOWLEDGEMENTS

The support and advice of the Jet Propulsion Laboratory contract technical monitors, Maurice Peelgren and Ed Dennison, have provided is greatly appreciated.

The Solar Energy Systems organization within Boeing Engineering and Construction Company (a division of The Boeing Company) directed and performed the work described in this report with support from many Boeing people. Major contributors were:

Marc Berry	-	Optical Evaluation
David Kirkbride	-	Concentrator and Panel Conceptual Design
		Test Panel Fabrication
John Laakso	-	Concept Definition
		Cost Analysis
Ron Miller	-	Structural Analysis
Jim Scott	-	Fabrication of Test Coupons and Panels
Cheryl Warner	-	Thermal Analysis

Table of Contents

Table of Contents (continued)

Table of Contents (continued)

1.0 EXECUTIVE SUMMARY

This study shows that a thin film reflective surface is acceptable for use on solar concentrators, including 816°C (1500°F) applications. In addition, it shows that a formed steel sheet substrate is a good choice for concentrator panels. The concept selected and described here uses thin film adhesively bonded to the structurally stiffened formed steel sheet substrate to form a concentrator gore. A description of the design, fabrication and evaluation of two test panels is presented.

1.1 REFLECTOR PANEL CONCEPTUAL DESIGN

The objectives of Task I of this contract were to (1) identify candidate design concepts for thin-film reflector panels, (2) screen the panel concepts and (3) select an optimum panel concept for development in subsequent tasks. Table 1.1-1 lists the five most promising candidates along with comparative cost and technical data for each. The stiffened steel skin concept was the heaviest concept, but was among the lowest in material cost and bus bar energy cost and presented the lowest manufacturing complexity and technical risk. This concept is shown in Figure 1.1-1 and was selected for development.

The gore configuration selected consists of 22 gage (.76 mm) formed steel substrate, stiffened with radial and circumferential stiffeners as shown in Figure 1.1-2. The steel sheet is primed with epoxy prior to bonding the acrylic overcoated, aluminized polyester film (3M-YS91A).

The substrate/stiffeners sub-assembly was modeled and analyzed for stress and deflection with the NASTRAN computer program.

Performance of the panel concept is evaluated analytically in Section 1.3 and experimentally in Section 1.4.

1.2 CONCENTRATOR CONCEPTUAL DESIGN

The primary emphasis of this program was to identify and develop a low cost thin film concentrator panel. To provide a basis for panel design and evaluation, a representative concentrator was defined. Figures 1.2-1 and -2 show the concentrator concept description and features.

Table 1.1-1 Concept Evaluation and Ranking

Concept	Weight LB/M^2	Material cost $\$/M^2$	Manufacturing complexity	+ Technical risk	+ BBEC $mils/kW_{th}\text{-}h$	Ranking
Stiffened steel skin	21.3	11.73	Low	Low	3.7	1 (Selected)
Stiffened steel clad plastic core laminate	15.6	12.06	Moderate	Moderate	3.9	2
Stiffened steel clad WFHB core laminate	17.7	11.86	Moderate to high	Moderate	3.8	3
Aluminum clad/ paper honeycomb sandwich	11.8	15.05	High	High	4.8	5
Steel clad/paper honeycomb sandwich	14.9	14.98	High	High	4.8	4

- CONFIGURATION

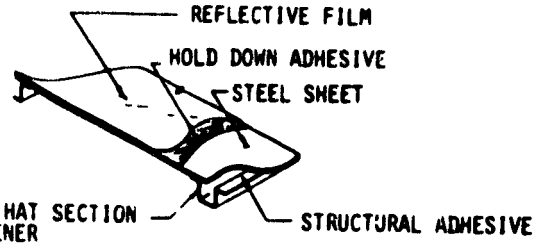

- COMPONENT/MATERIALS/COST
  - REFLECTIVE FILM/ALUMINIZED POLYESTER, ACRYLIC COATING/$5.38/M^2$
  - HOLD DOWN ADHESIVE/TYPE T.B.D./ COST ESTIMATE $6.60/kg
  - STEEL SHEET/THIN GAGE, COLD ROLLED, LOW CARBON/ $.77/kg
  - STRUCTURAL ADHESIVE/ACRYLIC OR EPOXIES/ $6.60/kg
  - STEEL STIFFENERS/THIN GAGE, COLD ROLLED, LOW CARBON/ $.77/kg

Figure 1.1-1 Stiffened Steel Skin Concept

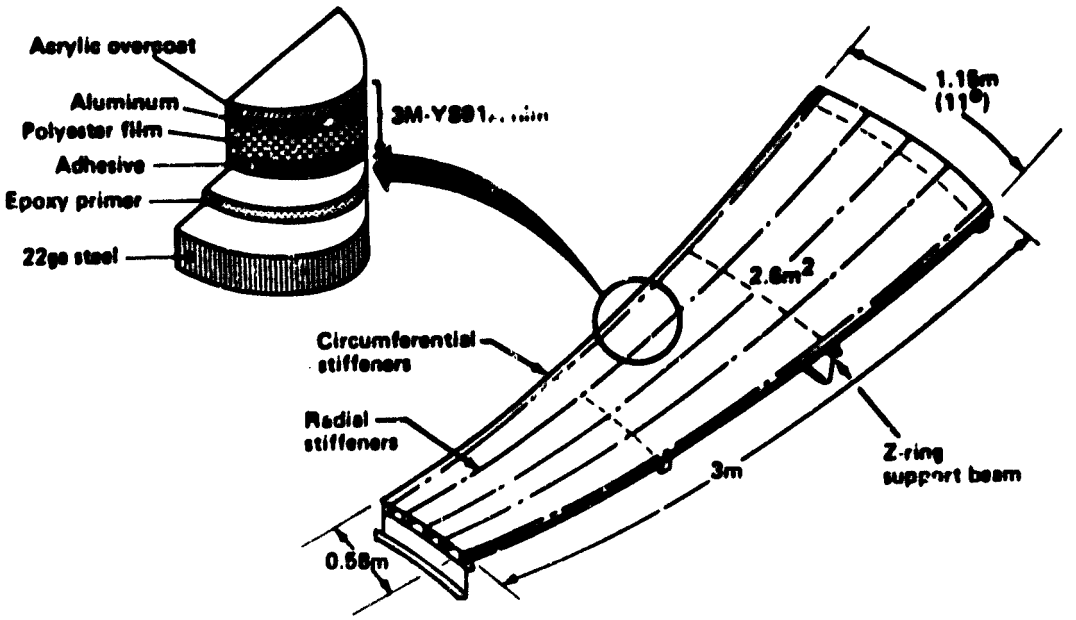

Figure 1.1-2 Outer Reflector Gore Concept

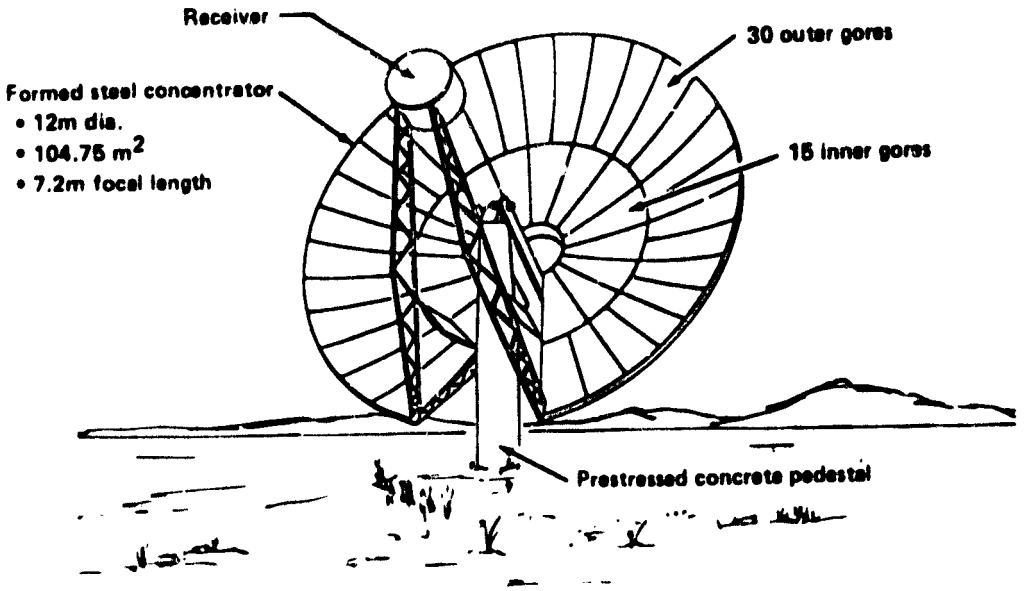

Figure 1.2-1 Thin Film Concentrator Conceptual Design

CONCENTRATOR CONCEPT FEATURES

- AZ-EL drive at C.G.
- Stand alone or field control system optional
- Inverted stow and lock-down
- Backside supported panels
- Zero blocking receiver support structure
- Pedestal mount
- Reflector panels and panel support structure 60 lbs/M^2 estimated
- 70 to 80 KW_{TH}, 816°C(1500°F) 8 inch receiver aperture

Weight

Item	Material	Weight(lb)	lb/m^2
Reflector Panels	Steel	3164	30.2
Support Structure (includes receiver support and gimbal interface)	Steel	3622	34.6
	Subtotal - gimballed weight		64.8
Gimbal Drive Unit	Steel	695	6.6
Pedestal	Concrete	7200	68.7
		14681	140.1

Figure 1.2-2 Concentrator Design Data

The concentrator reflective surface consists of 45 gore shaped panels, 15 inner and 30 outer as shown in Figure 1.2-1. The weights of the receiver and concentrator are balanced and the azimuth-elevation drive actuators are located at the center of gravity. The concentrator design allows for inverted stowage for environmental protection. Reflective panel supports are located behind the gores and the receiver support structure is aligned with the slot in the dish to eliminate blocking of the solar energy.

1.3 Concentrator Performance

Computer simulations of the concentrator optics were run using the selected reflector panel design. Experimentally determined values for reflector surface specularity and reflectivity along with dimensional data were used in the analysis. The simulations provided intercept factor and net energy into the aperture as a function of aperture size for different surface errors and pointing errors.

Figure 1.3-1 through 1.3-4 are example results of analyses for a 12 meter diameter concentrator with 1000 W/m^2 insolation. Inputs to the analyses included sun shape, hemispherical reflectance and specularity experimentally determined in coupon tests, small scale roughness (orange peel) and 3 receiver temperatures; 816°C (1500°F), 590°C (1100°F) and 370°C (700°F). Several curves are provided on each plot showing the effects of surface error on performance.

Figure 1.3-2 suggests that at 815°C a surface error of 2 mrad or less will be required to capture the desired 80 kW of thermal energy. As the surface errors increase, the net energy rapidly drops off. Larger surface errors could be tolerated on lower temperature systems. For example, at 815°C a peak energy of about 82 kW would be achieved with a 2 milliradian surface error, while at 370°C, 82 kW would be achieved with about 7 mrad surface error.

Figure 1.3-2 shows that surface errors of 1 mrad would add a few percent to the energy collected, provided the aperture diameter is reduced from .25 m (the optimum for 2 mrad surface error) to 0.175 m. However, the effects of pointing error and structural deflections also should be considered. At a 2 mrad pointing error, (Figure 1.3-4) the 2 mrad surface error/.25 m aperture drops to 76 kW, but the 1 mrad surface error/.175 m aperture drops even more

to 73 kW. Selecting the larger aperture not only permits more surface error but is also less sensitive to other errors. Allowing .5 mrad of the 1.52 mrad budgeted for environmental effects for gravity and temperature deflections, the manufactured panel error budget should be reduced to 1.5 mrad to achieve a 2 mrad total. Variable deflections due to wind loads will further degrade performance. For the average wind speed in the study (about 3 m/s) the equivalent panel surface error will be negligible. At higher wind speeds the concentrator truss deflection will have a significant effect on optical performance. This effect is not shown, but it can be concluded that losses would be lower at larger aperture sizes.

Based on these factors it is concluded that (1) achieving panel optical performance suitable for a Brayton cycle would also meet the needs for lower temperature applications, (2) a budget of 1.5 mrad RMS surface error or less for panel manufacturing tolerances is acceptable, and (3) the aperture diameter should be at least .25 m to reduce sensitivity to other errors.

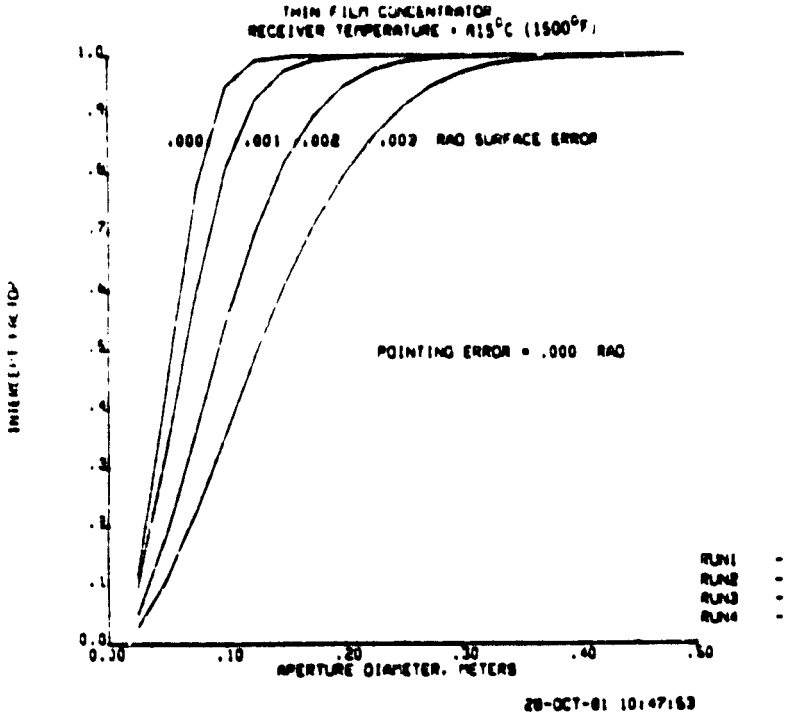

Figure 1.3-1 Intercept Factor Curve 815°C (1500°F)

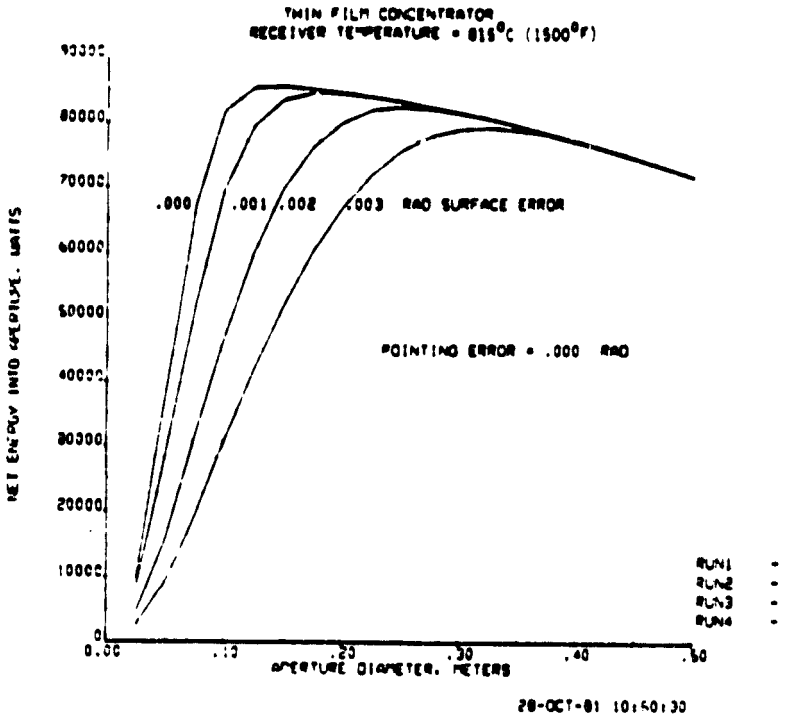

Figure 1.3-2 Net Energy Curve 815°C (1500°F)

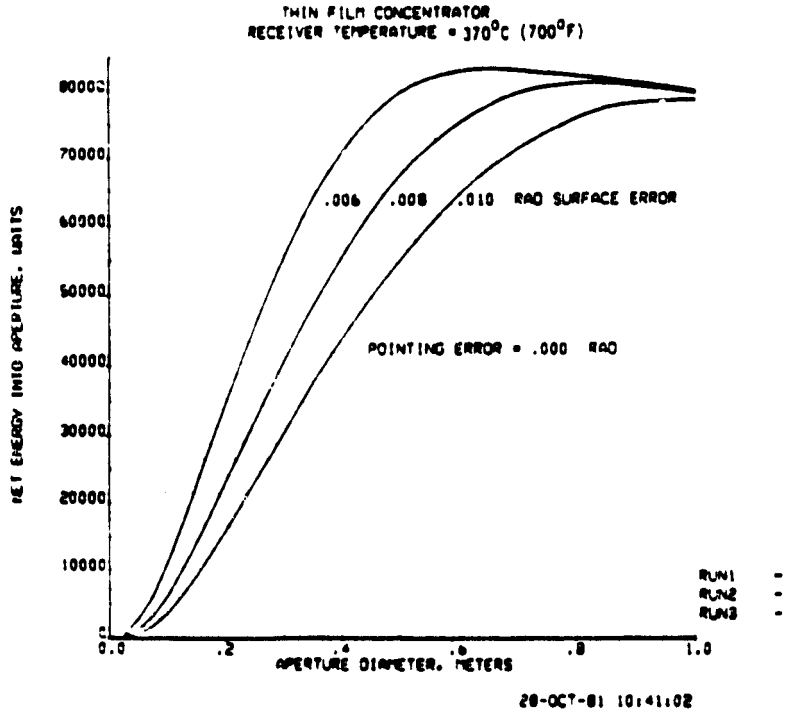

Figure 1.3-3 Net Energy Curve 370°C (700°F)

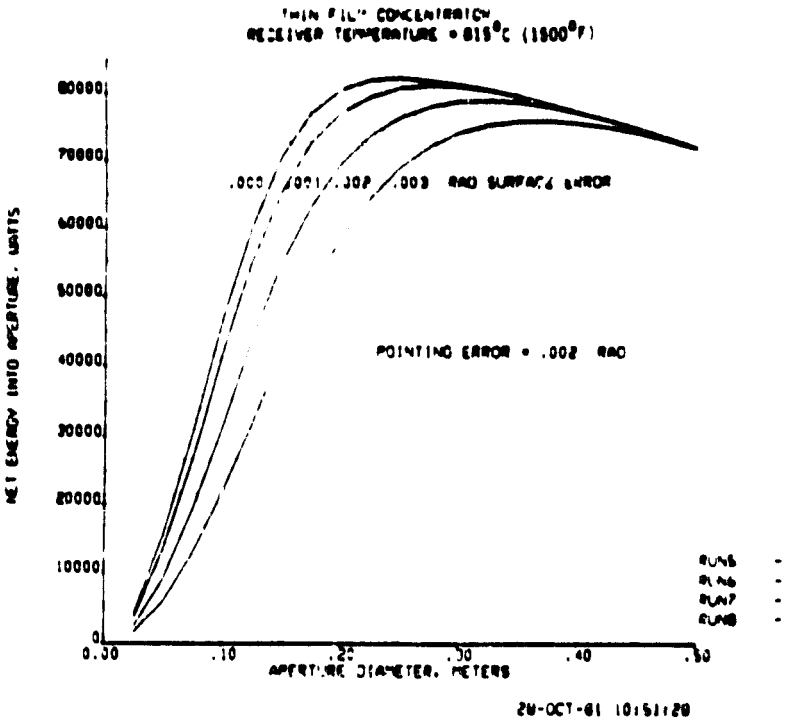

Figure 1.3-4 Net Energy Curve 815°C (1500°F)

1.4 Test Panel Development

The test panel design represents a section of a full size parabolic gore reflector panel. It uses the same stiffener configuration and its spherical radius of curvature closely matches the parabolic curvature midway on the full size panel. The design is depicted in Figure 1.4-1.

The overall dimensions of the test panel, 61 x 71 cm (24 x 28 in) and its 6.45 m (21 ft) focal length match dimensions of the JPL, glass/foamglas test bed concentrator panels. This was done to facilitate testing by JPL and allow correlation of performance versus cost per m^2 for the glass versus the aluminized thin-film concept.

The test panel design uses the materials and processes selected from the coupon development work. Test panel stiffener design and spacing was based on the full size parabolic gore reflector design.

- Basic Components
  - Reflective film
  - Steel sheet 22 gage, ASTM-A620
  - Hot section stiffeners
  - Tube end stiffeners
  - Structural adhesive
- Reflective Area
  - 0.4 M^2 (4.3 ft^2)
- Assembly Weight
  - 11.0 lbs calc.

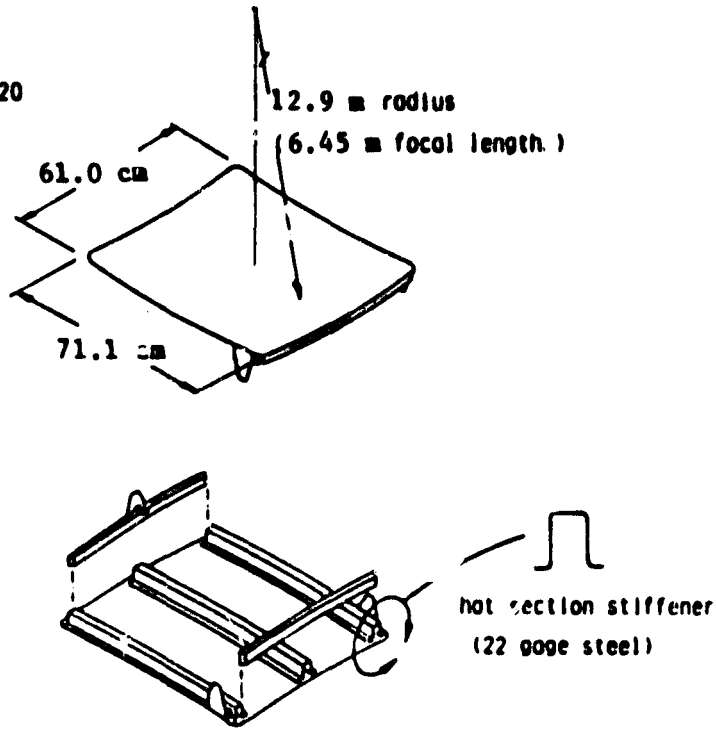

Figure 1.4-1 Test Panel

1.4.1 Panel Fabrication

The test panels were fabricated using the techniques and processes resulting from the coupon development work. The assembly sequence is shown in Figure 1.4-2. Three iterations of die fabrication were required to obtain a satisfactory radius of curvature on a part.

Square steel sheet blanks were bulge formed to the desired radius of curvature. The blanks were then cleaned and painted with zinc-rich two part epoxy primer and baked. Stiffener shapes were fabricated by brake forming. The curvatures were formed on a mechanical press and roller blocks. Stiffeners were cleaned and primed by the same method as the substrate blanks. The stiffeners were assembled with close-out tubes into a subassembly by holding the parts on the master tool while installing the fasteners. The stiffener subassembly was then bonded with gap filling epoxy adhesive to the back side of the substrate blank, which was vacuum chucked to its proper contour on the master tool. After curing, the frame side was painted with 2-part polyurethane paint. The reflector side primed surface was lightly sanded in preparation for film application. Film application was by the 3M

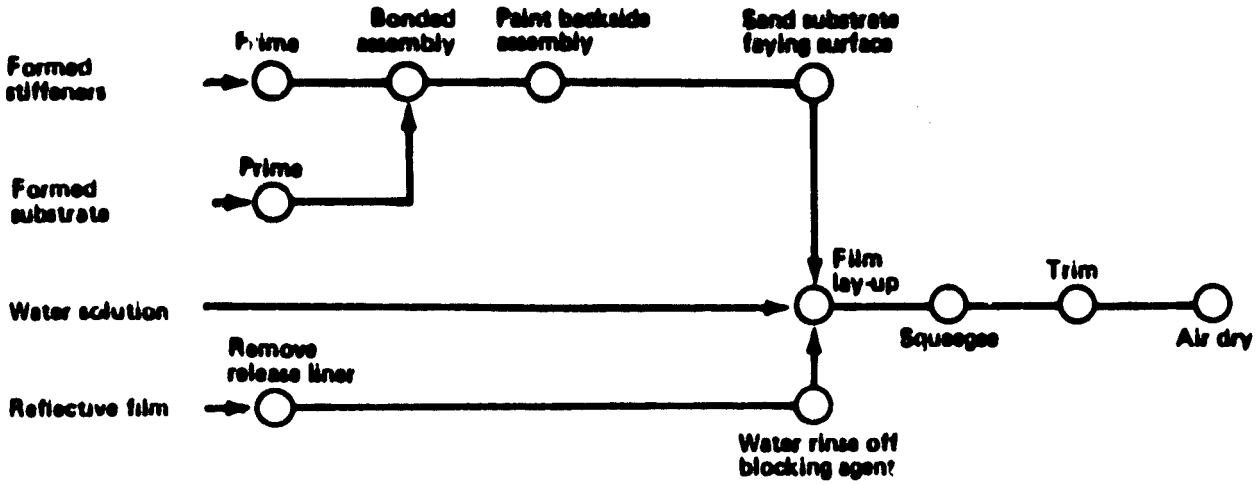

Figure 1.4-2 *Development Panel* Assembly *Steps*

"wet application" method which involved positioning the film on the wetted surface and squeegying out the trapped water and air bubbles.

Figure 1.4-3 is a photograph displaying the front and rear sides of the completed test panels.

1.4.2 Test Program

Testing under the contract consisted of 2 types:

1. coupon level development tests,
2. reflector panel tests.

Coupon Testing

Coupon tests were performed early in the program to aid the selection of materials and dimensions used in the design and to provide optical data needed in the performance analyses. Table 1.4.-1 lists the tests, their purposes, and the results.

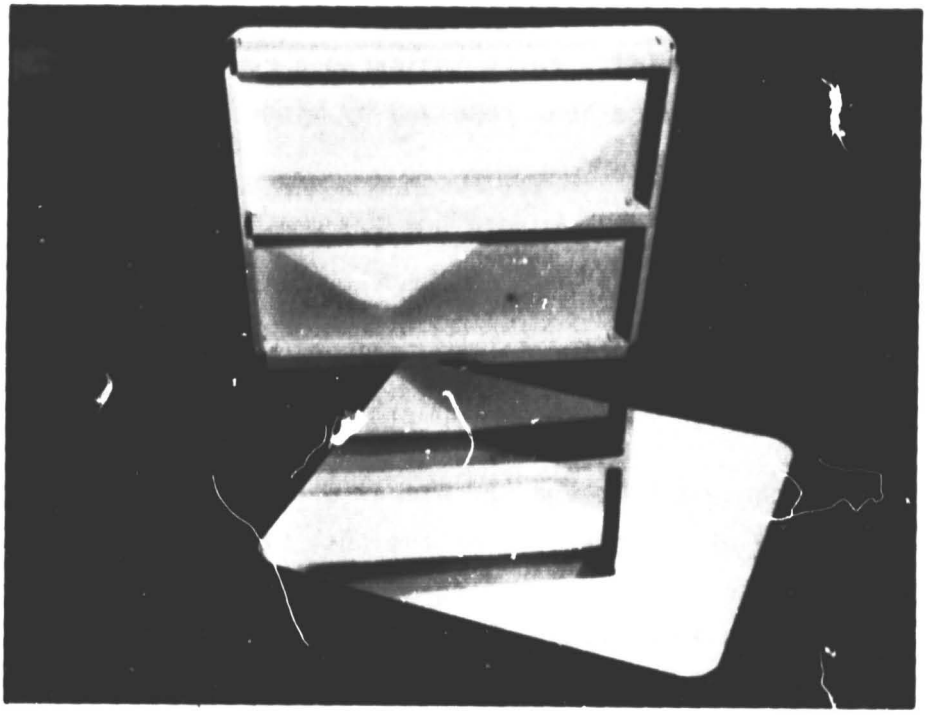

Figure 1.4-3 Test Panels S/N 7 and S/N 10

Table 1.4-1 Coupon Development Testing

TEST	PURPOSE	RESULTS	
		INITIAL CONCEPT	PRELIMINARY DESIGN
Spectral Reflectance (Air Mass 2, 29 mrad)	Coupon Screening Optical Performance Analysis	84%	85%
Specular Reflectance (1σ Half Angle Aperture), mrad		1.4 - 1.8	1.5
Reflector Figure (1σ Area Slope Error), mrad		.3 - .5	.3 - .4
Substrate Surface Roughness (RMS - micro-inches)	Substrate Design Drawings Specification	29 ✓	11 ✓
Hailstone Impact (1 Inch Diameter at 70 Ft/Sec)	Verify Substrate Thickness	0.03 Inch Marginal	
	Determine Film Damage	No Film Damage	
	Design Specification Compliance	Requires Assessment	
Temperature Extremes Soak at -30°C, +50°C	Determine Temperature Effects	Surface Pebbling at +50°C	

The selected materials and processes resulted in reflective surfaces exhibiting 85% spectral reflectance and a 1σ specular reflectance of 1.5 mrad. The .76 mm thick substrate survived hailstone impact without damage. Preliminary temperature/humidity tests indicated a potential problem with the 3M YS91A film, which has since been resolved by minor process modifications by 3M.

Panel Testing

The two test panels were subjected to two types of optical testing: (1) point source and (2) sun source.

The point source technique involved the use of a point source and a target collocated in a plane at a distance from the test panel equal to the radius of curvature. The test setup was aligned to project the image formed by the test panel onto the target. An aperture series, lenses and detector located at the target plane were used to quantify the angular scattering of light rays resulting from panel surface errors. Figure 1.4-4 shows the optical equipment and configuration.

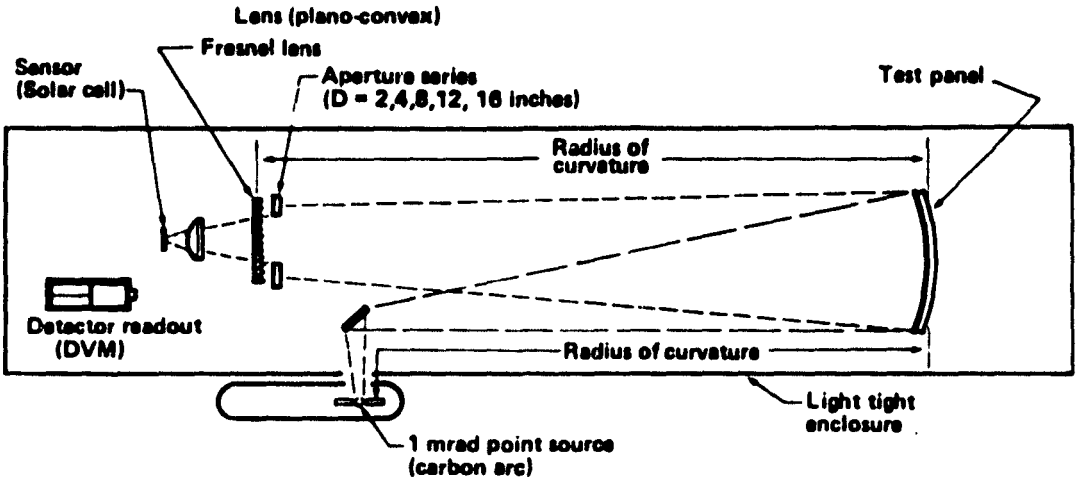

Figure 1.4-4 Point Source Panel Evaluation Apparatus

The test panel was moved towards and away from the target plane while observing the image size until the smallest diameter was observed. This established the radius of curvature. Next, apertures of 2 mrad through 16 mrad in diameter were sucessively placed in front of the image at the target plane while the response of a photovoltaic detector was observed and recorded. This process was repeated several times to allow statistical data treatment. The response data were normalized to the full open aperture (16 mrad) and tabulated.

Test results for each panel, SN7 and SN10 are plotted on the intercept factor graph shown in Figure 1.4-5 for the purpose of comparison with the analytical panel simulation. In this simulation, a one mrad source at infinity, hemispherical reflectance, specularity, and orange peel from coupon tests and zero pointing error were assumed. The solid lines are 1 surface errors of 1, 2, and 3 mrad. The dashed lines are test data. It is apparent from the graph that the surface error for both panels is between 1 and 2 mrad. Additional analyses estimate the errors to be 1.4 and 1.5 mrad for SN7 and SN10, respectively.

The sun source test was performed as an alternate approach to measuring the image size and distribution and to measure peak fluxes. Figure 1.4-6 is a photograph of the outdoor setup, which included a target board, water-cooled radiometer, digital voltmeter readout, and a manually guided test panel support. Not shown in the photograph were a 35 mm camera and an Eppley 5° normal incidence pyrheliometer (NIP).

Measurements were made by aiming the panel at the radiometer and carefully moving the image about until the peak flux was located. The image was then moved horizontally across the radiometer in one inch increments, reading the response at each increment, thereby obtaining an intensity distribution scan. Direct insolation readings were taken with the NIP and 35 mm photos were taken during the same time period.

Data from the radiometer scans and optical densitometer measurements of positive transparencies made from the 35 mm negatives indicated that negligible energy existed outside a 6 inch diameter circle. This is in close agreement with the point source data after accounting for geometry differences between the two experiments.

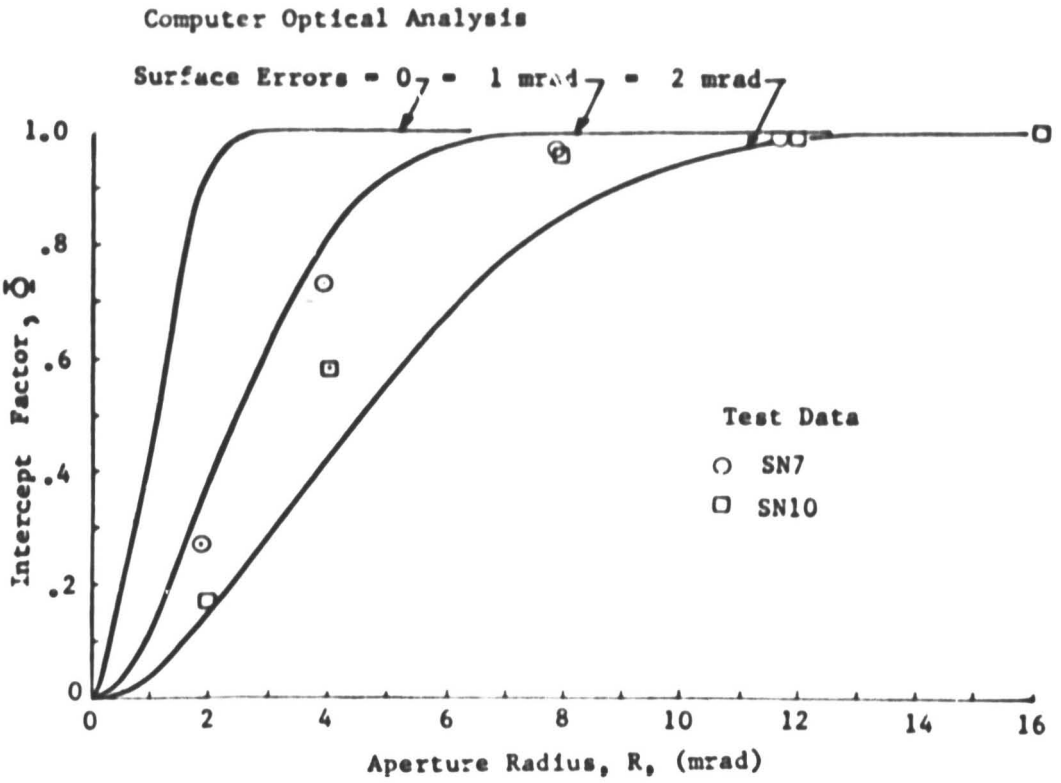

Figure 1.4-5 Test Results - Analysis Comparison

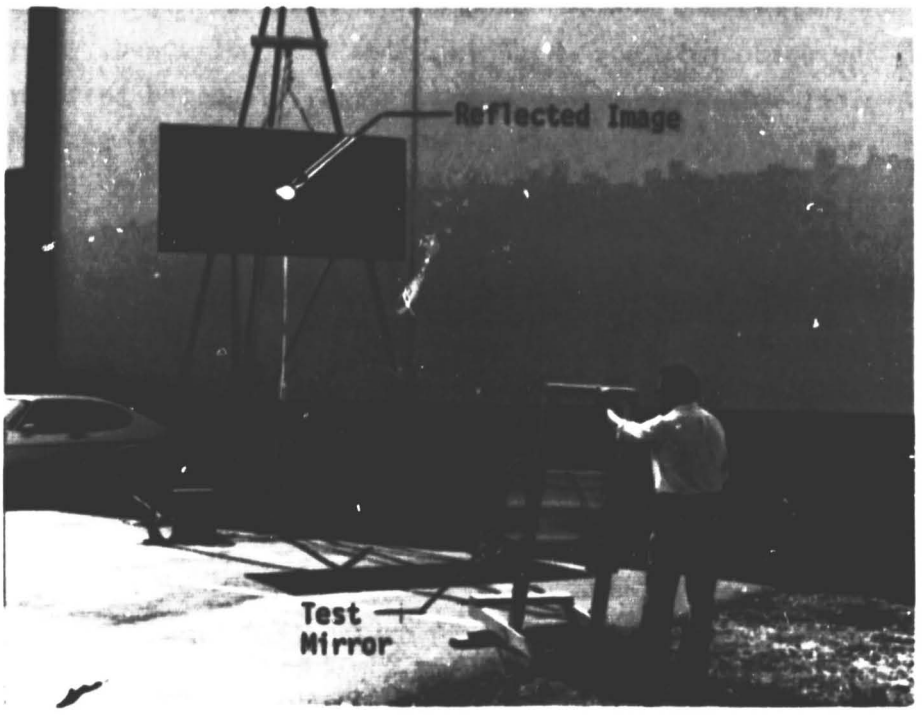

Figure 1.4-6 Sunlight Test Apparatus

Peak fluxes for the measurements were 101 suns for SN7 and 99.5 suns for SN10. This compares with 103 suns derived analytically from intercept factor curves.

1.5 Program Accomplishments

In the course of performance of this conceptual design study, several significant goals were accomplished. Included were selection of an attractive concentrator and panel concept, reflective material and process selection, optical and structural analysis, and successful demonstration of panel optical performance through test. Specific accomplishments were:

- Selected panel concept with
  - low manufacturing complexity
  - low technical risk
  - low cost at both low and high production rates

- Defined and evaluated concentrator concept, which
  - showed panel-concentrator compatibility
  - defined stiffener orientation and stiffener requirements
  - provided optical performance goals for the panel

- Validated panel concept by
  - characterizing thin film optical performance
  - demonstrating substrate/film optical compatibility
  - showing resistance to hail impact
  - fabricating test panels
  - demonstrating acceptable optical performance with the test panels

- Developed Phase 2 recommendations

1.6 Program Conclusions

This study has met its general objective of developing a rigid panel concept that utilizes a thin film reflective surface for application to a low-cost

point-focusing solar concentrator. It shows that a thin film reflective surface is acceptable for use on solar concentrators, including 1500°F applications. Additionally, it shows that a formed steel sheet substrate is a good choice for concentrator panels. The panel was shown to have good optical properties, acceptable forming tolerances, environmentally resistant substrate and stiffeners, and adaptability to low to mass production rates. The final estimates for the reflector panel material costs indicate a price of approximately $\$16/m^2$. Areas recommended for further work are: 1) weatherability of the film; 2) verification of solution to adhesive problem, and 3) forming tolerance reduction.

1.7 Recommendations

Recommendations for follow on phases based upon experience from this study have been prepared and are summarized here (see Figure 1.7-1). A Phase II is recommended that would address unresolved technical concerns, prepare a preliminary design for a dish concentrator; design, fabricate, and test panels for a 6.7 m test bed concentrator, and build and demonstrate the concentrator. The test bed concentrator would utilize the pedestal/foundation, gimbal actuator, torque tube and support beams from the existing BEC Second Generation heliostat design. Figure 1.7-2 shows the interface of the reflector panels and the existing heliostat structure. Phase II would require approximately 16 months (see Figure 1.7-3 for schedule). A Phase III would follow that would include a detail design for a dish concentrator, production planning and cost estimation, and fabrication and demonstration of a 12 m prototype concentrator.

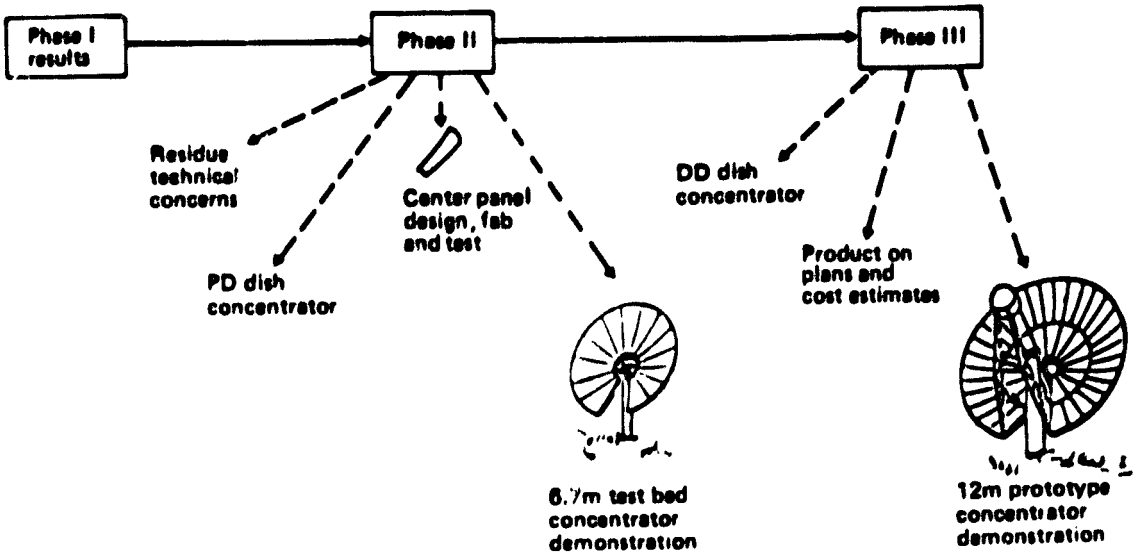

Figure 1.7-1 Program Plan Recommendation

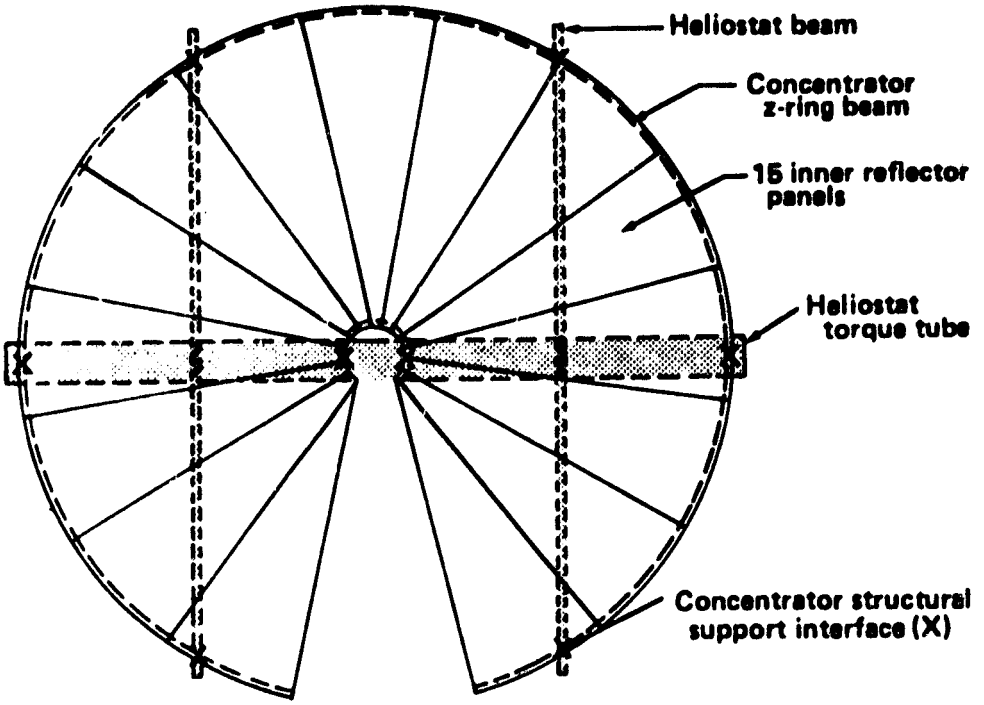

Figure 1.7-2 6.7m Concentrator/Heliostat Interface

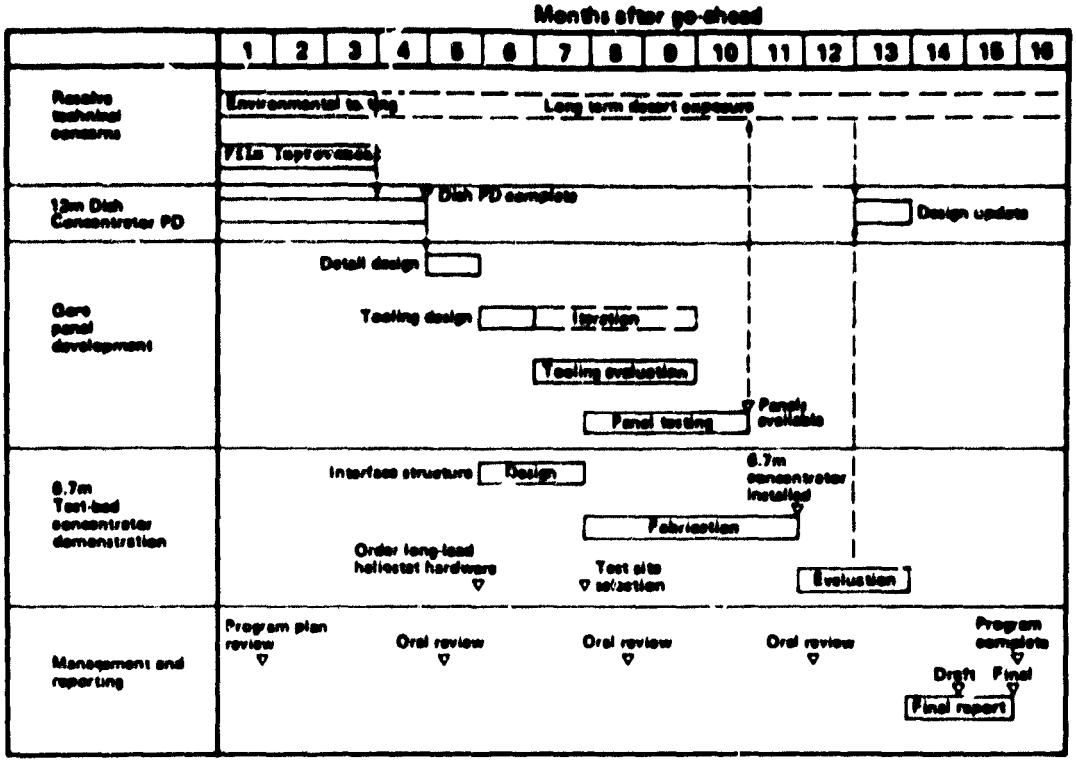

Figure 1.7-3 Phase II Recommended Schedule

2.0 INTRODUCTION

This final report summarizes all tasks of the work performed by Boeing Engineering and Construction Company Solar Systems for the Jet Propulsion Laboratory under Contract 955804, A Conceptual Design Study of Point Focusing Thin Film Solar Concentrators. This project is being managed by JPL for the Department of Energy and the National Aeronautics and Space Administration.

2.1 Study Objectives

The general objective the project was to develop a rigid panel concept that has a thin film reflective surface for application to a low cost point focusing solar concentrator. A four task program was planned to accomplish the objective.

The specific objectives of Task 1, Concept Definition and Parameter Optimization, were to 1) identify candidate design concepts for thin film reflector panels; 2) screen the panel concepts; and 3) to select an optimum panel concept for development in subsequent tasks. The Task 1 activities consisted of conceptual design, structural analysis, parametric cost analysis, manufacturing studies, and concept screening.

The specific objectives of Task 2, Concentrator Preliminary Design, were to develop a preliminary panel design for the selected panel concept and to 1) perform optical, thermal and structural performance studies, 2) define fabrication method; and) identify technology and materials development needed to insure or improve performance, life, and costs of the design. Task 2 activities consisted of coupon development, panel preliminary design, and concentrator conceptual design.

The specific objectives of Tasks 3 and 4 were to prepare a test plan and to fabricate and test coupons and test panels.

2.2 Study Approach

The use of thin film as the reflective surface for concentrator panels was the central theme of this study. Thin films referred to here are thin (a few mils) polymeric sheets that have been metalized to a highly reflective finish.

An overcoating is generally required for weatherization. The films are applied to a rigidizer or substrate which imparts the necessary structural support for shape, stiffness, and strength. The baseline film was YS91A, an acrylic overcoated, aluminized polyester film, manufactured by the 3M company.

The basic approach to this study was to extend and develop the baseline concentrator design with emphasis on the reflector panels. Early in the study a concentrator conceptual design was selected to provide a basis for the panel screening effort. While the baseline panel utilized woodfiber hardboard/paper honey comb sandwich for the panel substrate, several other candidates were identified for screening.

2.3 Report Organization

This section is preceded by Section 1.0, the Executive Summary, which gives program highlights, major findings, accomplishments and conclusions. Section 3.0 presents the reflector panel concept development. The concentrator conceptual design is described in Section 4.0. Design, fabrication and evaluation of the reflector test panels is presented in Section 5.0. Conclusions appear in Section 6.0, recommendations in Section 7.0, and references are in Section 8.0.

3.0 Reflector Panel Concept Development

This section of the report describes the evolution of the panel concept from the baseline design, through candidate screening/selection, concluding with feasibility verification with coupon level testing.

3.1 Concept Definition

3.1.1 Baseline

The baseline concept proposed initially consisted of coated aluminized polyester film bonded to a molded wood fiber hardboard which was in turn bonded to a paper honeycomb core. Another wood fiber hardboard sheet was bonded to the back side completing the sandwich. Urethane adhesives were used to bond the sandwich parts together and to apply the thin film. Panel edges were sealed with metal edge trim and elastomeric sealant.

The film selected for the baseline reflective surface was YS-91, which is produced by 3M Company. This film is currently in production and has undergone extensive environmental testing. The YS-91 film is furnished by 3M with a primer applied to enhance bonding to the underlying rigidizing material. Weather-proofing of YS-91 is accomplished by use of a UV-stabilized polyester base film and an acrylic overcoating. Since the aluminum layer is in front of the polyester, the primary structural film is protected from UV radiation. 3M has product improvement programs in progress that should result in enhanced reflectance and weatherability. Therefore, for a production period five years away, a weatherable film having specular reflectance above 0.85 can be reasonably anticipated. Urethane adhesive, such as 34 Type 3532, was selected as the baseline adhesive with polysulfide as an alternate. Application of the film would be accomplished by stretching the film facedown over a contoured tool, applying the adhesive to the preprimed film surface and positioning the prefabricated sandwich panel over the film, vacuum holding until adhesive hardened.

Selection of the sandwich panel materials was based on low cost, structural efficiency, and thermal expansion considerations. An attractive material for sandwich face sheets was woodfiber hardboard which has low cost, low thermal expansion, and attractive specific strength and stiffness properties.

After reviewing design requirements for doubly-curved panels, the Weyerhauser Company recommended using a woodfiber hardboard product called PRES-TOCK (a Weyerhauser Trademark). The Masonite Corporation, also recommended a similar product.

For the sandwich core, a commercial grade of kraft paper honeycomb produced by Hexcel was selected because of low cost; it also has very low thermal expansion. A fast-curing, one part urethane adhesive (MOR-AD 336) produced by Morton Chemical would be used to bond the sandwich parts. This adhesive is widely used in high-rate production of sandwich panels for recreational vehicles and mobile homes.

3.1.2 Reflector Panel Candidates

Identification of additional reflector panel design candidates, screening of the candidates, and selection of the optimum concept were objectives of Task 1. The general design requirements were: 1) utilize existing materials and fabrication technology; 2) minimize the need for research and development, 3) employ reasonable limited production techniques compatible with mass production methods. Performance requirements were: 1) 30-year operational life in specified environment; 2) wind induced surface slope error of 1.5 mrad (rms) at 14 m/sec (31 mph) wind speed; 3) minimum maintenance consistent with low life cycle cost.

Based on these requirements, panel concepts were established and screened to create a set of candidates. Candidates for the reflective film were investigated separately from the remainder of the panel.

3.1.2.1 Reflector Film Candidates and Selection

Requirements for the reflective film are high specular reflectance, abrasion resistance, soiling resistance, long life, and commercial availability. Table 3.1-1 lists the final film options.

Table 3.1-1 Reflective Film Options

• COMMERCIALLY AVAILABLE FILMS

SUPPLIER	DESIGNATION	DESCRIPTION	REFLECTANCE	$/M^2
3M	YS91	ALUMINIZED 2 MIL POLYESTER ACRYLIC OVERCOAT	82% - 85%	5.38
3M	FEK244	ALUMINIZED 4 MIL ACRYLIC ACRYLIC OVERCOAT	82% - 85%	15.60

• FILMS UNDER DEVELOPMENT

SUPPLIER	FILM	OVERCOAT	REFLECTANCE	$/M^2
DOW CORNING	POLYESTER	SILICONE/SILICA	82% - 85%	T.B.D

• REFLECTIVE FILM COMPONENTS

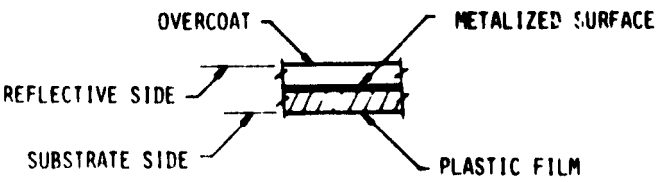

The reflective film component of the concentrator panel is the part that governs life cycle performance and also will be a significant portion of the panel's selling price. 3M's YS-91 aluminized polyester film was selected as a baseline material because it has reasonable cost, 130 cm (51 inch) available width, and acrylic overcoating.

The YS-91 film material was used to fabricate panel specimens during Task 4. YS-91's 2 mil polyester substrate is mechanically and physically equivalent to several other available films so use of YS-91 verifies film-to-panel application techniques for other films as well.

3.1.2.2 Panel Substrate Candidates

Requirements for the panel substrate are to:

a. Maintain panel design shape within specified deflection limits under operating conditions.

b. Provide impact resistant backing for film.

c. Have a minimum effect on the finished panel's specular reflectance.

d. Provide structural rigidity for concentrator support structure.

e. Achieve 30-year useful life with zero maintenance.

f. Minimum cost.

A number of prospective panel materials and rigid construction concepts were identified and are shown in Tables 3.1-2, 3.1-3, and 3.1-4. Based on cost/stiffness parameters, steel and wood fiber products have the best potential for achieving low overall panel cost. The structural configuration options shown utilize solid sheet steel products as well as metal-clad laminates which are currently being developed by the automotive industry. These laminates attempt to exploit the (1) good cost/tensile stiffness of steel used as laminate cladding and (2) good cost/bending stiffness of wood fiber products used as a filler ply.

Table 3.1-2 Structural Material Options

- PROSPECTIVE COMPOSITE SANDWICH CORE MATERIALS

MATERIAL	$/FT^2 ($/M^2)	CORE DENSITY LB/FT^3
• KRAFT PAPER HONEYCOMB TREATED 1.3 cm CELL 2.5 cm DEEP	0.43 (4.63)	2.0
• CARDBOARD EXPANDED GRID UNTREATED 7.6 cm CELL 2.5 cm DEEP	0.03 (0.32)	0.78
• FOAMED PLASTICS RIGID 2.5 cm DEEP	0.17 (1.83)	2.0
• CELLULAR GLASS BOROSILICATE 2.5 cm DEEP	0.45 (4.84)	12.5

Table 3.1-3 Structural Material Options

- PROSPECTIVE LAMINATE, SANDWICH SKINS, MONLITH, AND STIFFENED SKIN MATERIALS

MATERIAL	$/LB	DENSITY LB/In^3	MOD OF ELAST X 10^6 PSI	RELATIVE $ TEN STIFF[1]	RELATIVE $ BEND STIFF[2]
STEEL SHEET, t = 0.008 in	0.35	0.29	29	1	1
STEEL FOIL t = 0.006 in	0.45	0.29	29	1.25	1.25
ALUMINUM FOIL t = 0.005 in	1.33	0.10	10	3.30	2.00
ALUMINUM SHEET t - 0.006 in	1.07	0.10	10	3.30	1.40
GLASS REINFORCED PLASTIC	1.00	0.067	2.3	10.0	1.70
GLASS REINFORCED CEMENT	0.38	0.072	2.5	3.30	5.00
TREATED PAPER	0.58	0.03	0.5	10.0	0.70
WOOD FIBER HARDBOARD	0.17	0.04	0.9	2.16	0.21
POLYETHYLENE OR POLYPROPOLENE	1.00[3]	0.33	0.2	471.00	17.0

(1) $\frac{\text{RELATIVE \$}}{\text{TEN STIFF}} = \frac{\$_2 \rho_2}{E_2}\left(\frac{E_1}{\$_1 \rho_1}\right)$ steel sheet

(2) $\frac{\text{RELATIVE \$}}{\text{BEND STIFF}} = \frac{\$_2 \rho_2}{E_2^{1/3}}\left(\frac{E_1^{1/3}}{\$_1 \rho_1}\right)$ steel sheet

(3) INCLUDES ADHESIVE COSTS

Table 3.1-4 Structural Configuration Options

CONFIGURATION	EXAMPLE
STIFFENED MONOCOQUE SKINS	METAL FOILS OR SHEETS WITH LOCAL STIFFENERS TO RESIST BENDING.
MONOLITHS	SOLID SHEET MATERIALS WITH ADEQUATE THICKNESS TO RESIST BENDING.
COMPOSITE LAMINATES	SOLID PLY MATERIALS WITH CONTINUOUS BOND INTERFACES (METAL SKINS BONDED TO A PLASTIC SHEET CORE).
COMPOSITE SANDWICHES	SAME AS LAMINATES EXCEPT FOR CELLULAR CORE CONSTRUCTION METAL SKINS ON PAPER HONEYCOMB.
HYBRIDS	STIFFENED LAMINATE SKIN.

Figure 3.1-1 presents a matrix of all possible combinations of potential materials/configurations and the resultant positive and negative characteristics.

A large number of panel concepts were identified from the listed materials and configurations. These combinations were narrowed down to six candidate concepts by considering practicability and potential for low cost. Two generic forms, stiffened skin and sandwich, were selected for subsequent screening evaluations. Tables 3.1-5, 3.1-6, 3.1-7, and 3.1-8) show the logical sequence of selection of the potential, then preferred combinations, the rejected combinations, and finally the six candidates identified for screening. It should be noted that the baseline substrate of stiffened skin with wood fiber hardboard was rejected here due to difficulties in environmental sealing.

Stiffened Skin Panel Concepts

Representative stiffened skin panel concepts and their respective components, materials and material costs are illustrated in Figures 3.1-2, 3.1-3, and 3.1-4.

Sandwich Panel Concepts

Representative sandwich panel concepts and their respective components, materials and material costs are shown in Figures 3.1-5 and 3.1-6.

3.1.2.3 Panel Substrate Evaluation and Final Selection

The stiffened skin and sandwich panel concepts were evaluated with respect to material costs, total costs, busbar energy costs, manufacturing operations, and technical risks.

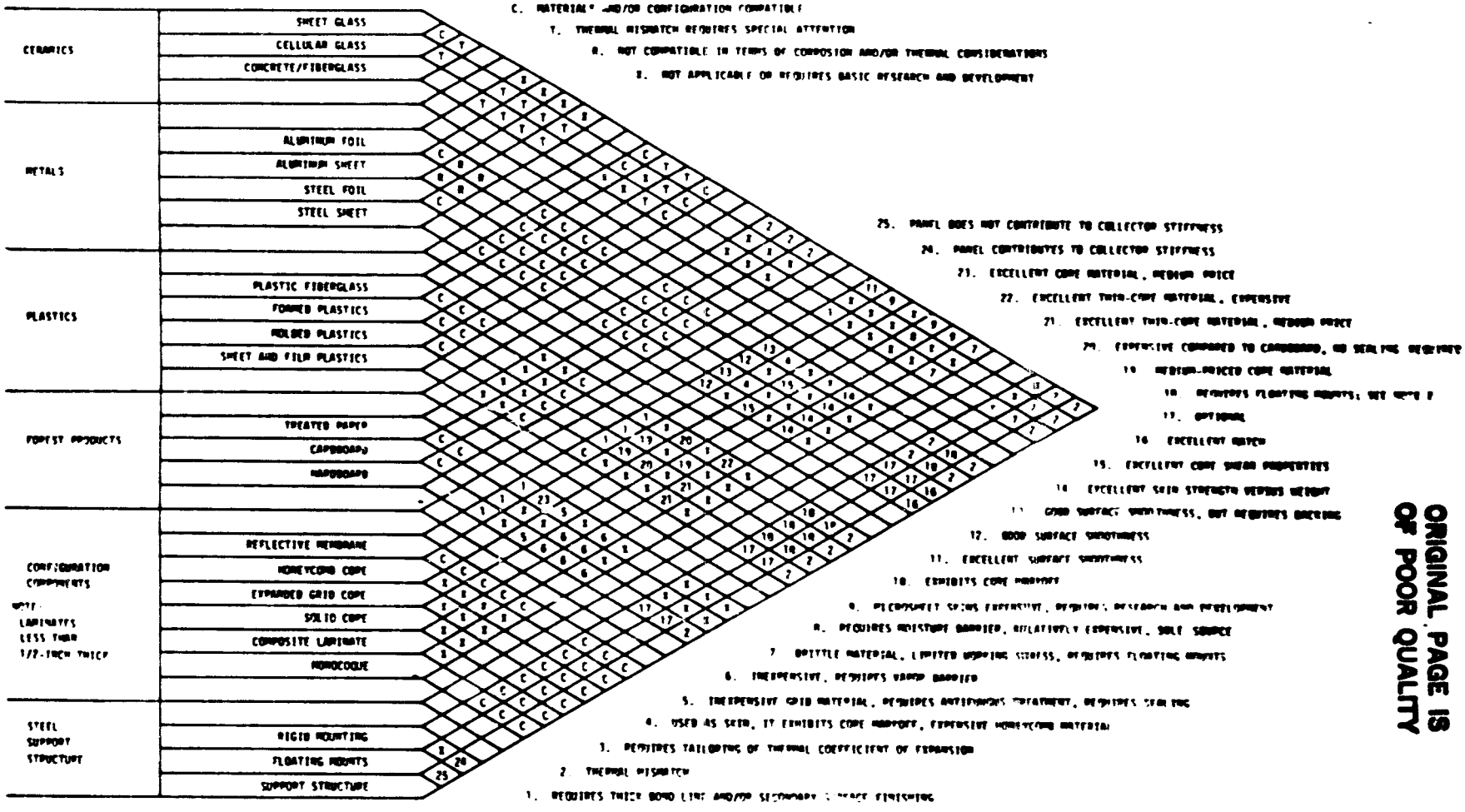

Figure 3.1-1 Potential Material - Configuration Combinations

Table 3.1-5 Configuration/Material Combinations

ESTIMATE OF PROBABLE COMBINATIONS		
CONFIGURATION	MATERIAL CHOICES	RESULTANT PROBABLE COMBINATIONS
MONOLITHS	5	5
STIFFENED SKINS	7	7
COMPOSITE LAMINATES	4 CORES 5 SKINS	20
COMPOSITE SANDWICHES	4 CORES 5 SKINS	20
HYBRIDS:		
STIFFENED SKIN/ COMPOSITE LAMINATE		20
COMPOSITE SANDWICH/ COMPOSITE LAMINATES		20
		92 TOTAL

Table 3.1-6 Configuration/Material Combinations

PREFERRED COMBINATIONS		
CONFIGURATION	MATERIAL CHOICES	RESULTANT PREFERRED COMBINATIONS
MONOLITH	STEEL SHEET	1
STIFFENED SKIN	STEEL SHEET WOODFIBER HARDBOARD (WFHB)	2
COMPOSITE LAMINATE	STEEL FOIL SKINS ALUMINUM FOILS SKINS PLASTIC CORE PLY WFHB CORE PLY PAPERBOARD CORE PLY	6
COMPOSITE SANDWICHES	STEEL SHEET SKINS ALUMINUM SHEET SKINS PAPER HONEYCOMB CORE EXPANDED CARDBOARD GRID CORE	4
HYBRIDS:		
STIFFENED SKIN/ COMPOSTIVE LAMINATE	STEEL FOIL SKINS PLASTIC CORE PLY WFHB CORE PLY PAPER CORE PLY	3
		16 TOTAL

Table 3.1-7 Rejected Combinations

MONOLITH/STEEL SHEET	INEFFICIENT MATERIAL USAGE VS. COST EXCESSIVE WEIGHT
STIFFENED SKIN/WFHB	LONG TERM ENVIRONMENTAL SEALING DIFFICULT TO IMPOSSIBLE
COMPOSITE SANDWICHES/ EXPANDED CARDBOARD CORE	REQUIRED HERMETIC SEALING RESULTS IN TEMPERATURE INDUCED PRESSURE GRADIENTS ACROSS SKINS LEADING TO POTENTIAL STRESS/FATIGUE FAILURES AND/OR OIL CANNING
COMPOSITE LAMINATES	NOT COST/WEIGHT COMPETITIVE WITH HYBRID STIFFENED SKIN/COMPOSITE LAMINATES BASED ON PRELIMINARY STRUCTURAL COMPUTER ANALYSIS
HYBRIDS STIFFENED SKIN/ COMPOSITE LAMINATES	ALUMINUM SKIN COMBINATIONS NOT COST COMPETITIVE WITH STEEL SKINS. ALUMINUM SKINS NOT COMPATIBLE WITH STEEL STIFFENERS

Table 3.1-8 Candidate Concepts

- 6 CANDIDATE CONCEPTS IDENTIFIED FOR MORE DETAILED SCREENING

CONFIGURATION	MATERIALS
STIFFENED SKIN	• LIGHT GAGE FORMED STEEL SHEET WITH FORMED STEEL HAT SECTION STIFFENERS
COMPOSITE SANDWICHES	• LIGHT GAGE STEEL CLADDING ON KRAFT PAPER HONEYCOMB • LIGHT GAGE ALUMINUM CLADDING ON KRAFT PAPER HONEYCOMB
HYBRID: STIFFENED SKIN/ COMPOSITE LAMINATES	• LIGHT GAGE STEEL CLADDING ON: PAPERBOARD CORE PLY WOOD FIBER HARDBOARD CORE PLY PLASTIC CORE PLY ALL COMBINATIONS STIFFENED WITH STEEL HAT SECTIONS.

- CONFIGURATION

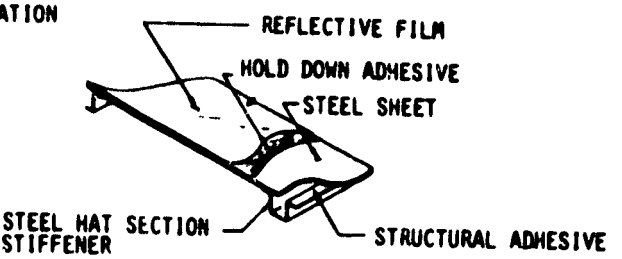

- COMPONENT/MATERIALS/COST
  - REFLECTIVE FILM/ALUMINIZED POLYESTER, ACRYLIC COATING/$5.38/m^2
  - HOLD DOWN ADHESIVE/TYPE T.B.D./ COST ESTIMATE $6.60/kg
  - STEEL SHEET/THIN GAGE, COLD ROLLED, LOW CARBON, $.77/kg
  - STRUCTURAL ADHESIVE/ACRYLIC OR EPOXIES/ $6.60/kg
  - STEEL STIFFENERS/THIN GAGE, COLD ROLLED, LOW CARBON/$.77/kg

Figure 3.1-2 Stiffened Steel Skin Concepts

- CONFIGURATION

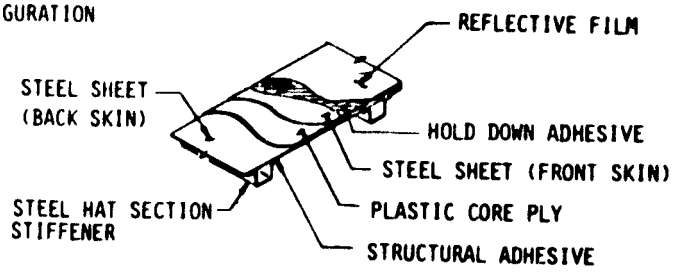

- COMPONENT/MATERIAL/COST
  - REFLECTIVE FILM/ALUMINIZED, POLYESTER, ACRYLIC COATING/$5.38/m^2
  - HOLD DOWN ADHESIVE/TYP T.B.D./COST ESTIMATE $6.60/kg
  - STEEL SHEET (FRONT SKIN)/THIN GAGE, COLD ROLLED, LOW CARBON/ $.77/kg
  - PLASTIC CORE PLY/POLYCARBONATE WITH ADHESIVE/ $2.20/kg
  - STEEL SHEET (BACK SKIN)/THIN GAGE, COLD ROLLED, LOW CARBON/ $.77/kg
  - STRUCTURAL ADHESIVE/ACRYLIC OR EPOXIES/ $6.60/kg
  - STEEL STIFFENERS/THIN GAGE, COLD ROLLED, LOW CARBON/$.77/kg

Figure 3.1-3 Stiffened Steel Clad/Plastic Core Laminate Concept

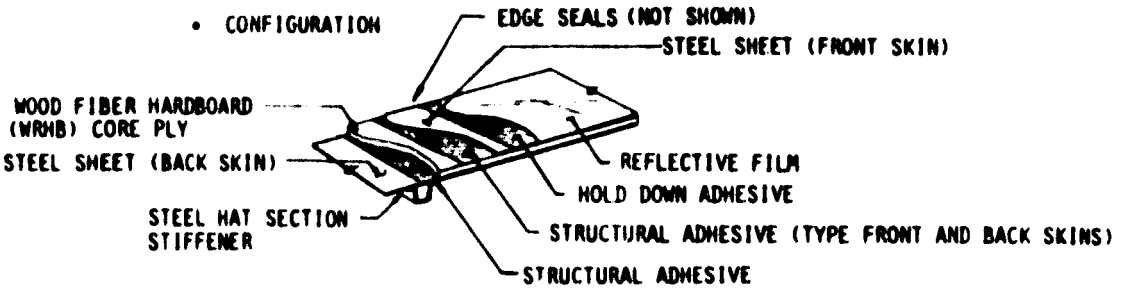

- COMPONENT/MATERIAL/COST
  - REFLECTIVE FILM/ALUMINIZED POLYESTER, ACRYLIC COATING/$5.38/$m^2$
  - HOLD DOWN ADHESIVE/TYPE T.B.D./COST ESTIMATE/**$6.60/kg**
  - STEEL SHEET (FRONT SKIN)/THIN GAGE, COLD ROLLED, LOW CARBON/**$.77/kg**
  - STRUCTURAL ADHESIVE/ACRYLIC OR EPOXIES/**$6.60/kg**
  - STEEL SHEET (BACK SKIN)/THIN GAGE, COLD ROLLED, LOW CARBON/ **$.77/kg**
  - STEEL STIFFENERS/THIN GAGE, COLD ROLLED, LOW CARBON/ **$.77/kg**
  - EDGE SEALS/ALUMINUM FOIL, BUTYL BACKING/ **$.23/m**
  - CORE PLY/WFHB/ **$.37/kg**

Figure 3.1-4 Stiffened Steel Clad/WFHB Core Laminate Concept

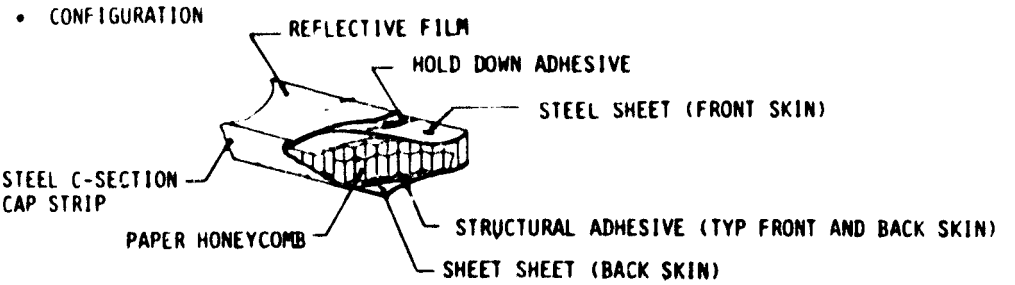

- COMPONENTS/MATERIALS/COST
  - REFLECTIVE FILM/ALUMINIZED POLYESTER, ACRYLIC COATING/$5.38/$m^2$
  - HOLD DOWN ADHESIVE/TYP T.B.D./COST ESTIMATE **$6.60/kg**
  - STEEL SHEET (FRONT SKIN)/THIN GAGE, COLD ROLLED, LOW CARBON/ **$.77/kg**
  - STRUCTURAL ADHESIVE/ACRYLIC OR EPOXIES/**$6.60/kg**
  - PAPER HONEYCOMB/KRAFT PAPER, **1.3cm** CELLS, **2.5cm** DEEP/$4.63/$m^2$
  - STEEL SHEET (BACK SKIN)/THIN GAGE, COLD ROLLED, LOW CARBON/**$.77/kg**
  - STEEL CAP STRIP/THIN GAGE, COLD ROLLED, LOW CARBON/**$.77/kg**

Figure 3.1-5 Composite Sandwich Steel Clad Paper Honeycomb Concept

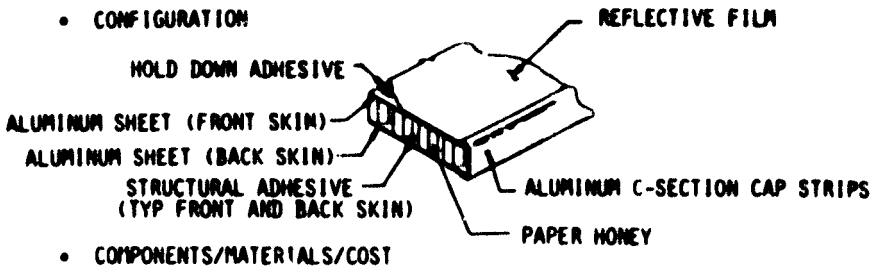

• COMPONENTS/MATERIALS/COST

- REFLECTIVE FILM/ALUMINIZED POLYESTER, ACRYLIC COATING/$5.38/m^2
- HOLD DOWN ADHESIVE/TYP T.B.D./COST ESTIMATE $6.60/kg
- ALUMINUM SHEET (FRONT SKIN)/THIN GAGE 5000 SERIES/ $2.35/kg
- STRUCTURAL ADHESIVE/ACRYLIC OR EPOXIES/ $6.60/kg
- PAPER HONEYCOMB/KRAFT PAPER, 1.3cm CELL, 2.5cm DEEP/$4.63/M^2
- ALUMINUM SHEET (BACK SKIN)/THIN AGE, 5000 SERIES/ $2.35/kg
- ALUMINUM CAP STRIP/THIN GAGE, 5000 SERIES/$2.35/kg

Figure 3.1-6 Composite Sandwich Aluminum Clad Paper Honeycomb Concept

Panel Sizing

The candidate panel concepts were sized, using a computer-aided approach, to obtain weight and material cost data sufficient for concept screening purposes. Both deflection (slope errors) and stresses were treated in the sizing analyses; deflection constraints generally governed panel designs. Because of light panel weights, wind induced deflections are significantly larger than gravity deflections. Consequently, the panel sizing was performed by analyzing only wind induced deflections using a conservative analytical approach.

For purposes of concept screening, the panel sizing was constrained by a wind-induced peak slope error budget of 1.52 mrad at a wind speed of 14 m/s (maximum operational condition). A study was made of wind data from Edwards

AFB furnished by JPL that verified that the assumed panel error budget, combined with wind induced truss deflection errors, will result in nearly full energy capture in typical wind conditions at the site (see Figures 3.1-7, 3.1-8, 3.1-9, and 3.1-10). This study utilized concentrator performance predictions developed previously on the JPL/BEC Low Cost Concentrator Program. (Reference 3-1)

The large number of panel sizing cases were evaluated using a computer model that has the following features:

- o Treats stiffened skin and sandwich construction
- o Performs deflection (slope error) analysis at operational wind conditions (see Table 3.1-9)
- o Performs stress (strength) analysis at the ultimate wind condition (see Table 3.1-9)
- o Computes weights
- o Computes structural material costs
- o Generates data for a specific range of key design dimensions
- o Outputs design data for each dimension case in a summary table format that is useful for concept screening

Table 3.1-10 summarizes how the model features are applied to each concept.

Deflection slope errors are computed using a conservative simply-supported panel approach. In actual construction, panel-to-truss connections will provide fixity which effectively reduces panel deflections. Also, the model is based on flat plate idealizations so actual deflections will be reduced by doubly-curved shell behavior. Model details are shown in Figure 3.1-11.

Panel sizing was governed by ground rules adopted to develop data meaningful for panel screening (Table 3.1-11). Material gages were selected on the basis of minimum thickness consistent with availability and expected hailstone resistance. Also, a gore configuration judged to be representative was selected mainly to reduce the number of variable parameters. The panel sizing strategy was to hold these dimensional parameters fixed while the "first order" variables -- stiffener spacing, stiffener height, and sandwich core thickness -- were optimized to produce least cost for each material/generic concept option.

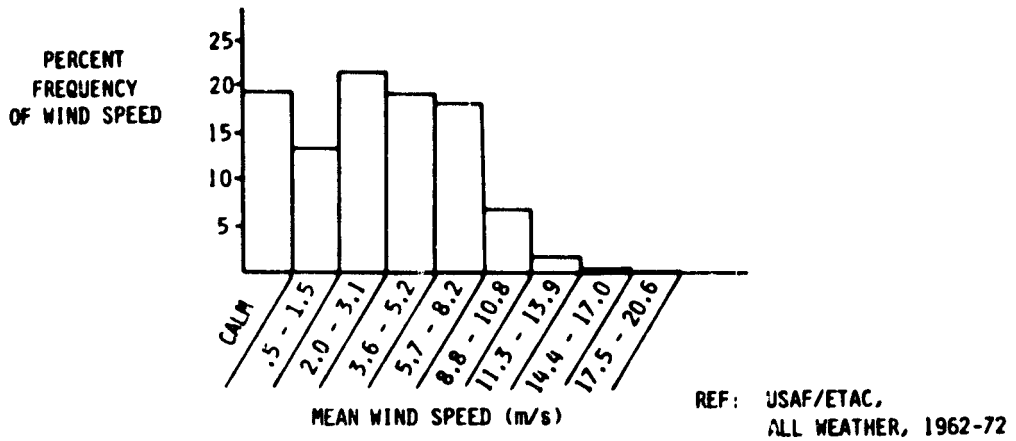

Figure 3.1-7 Surface Wind Conditions at Edwards AFB

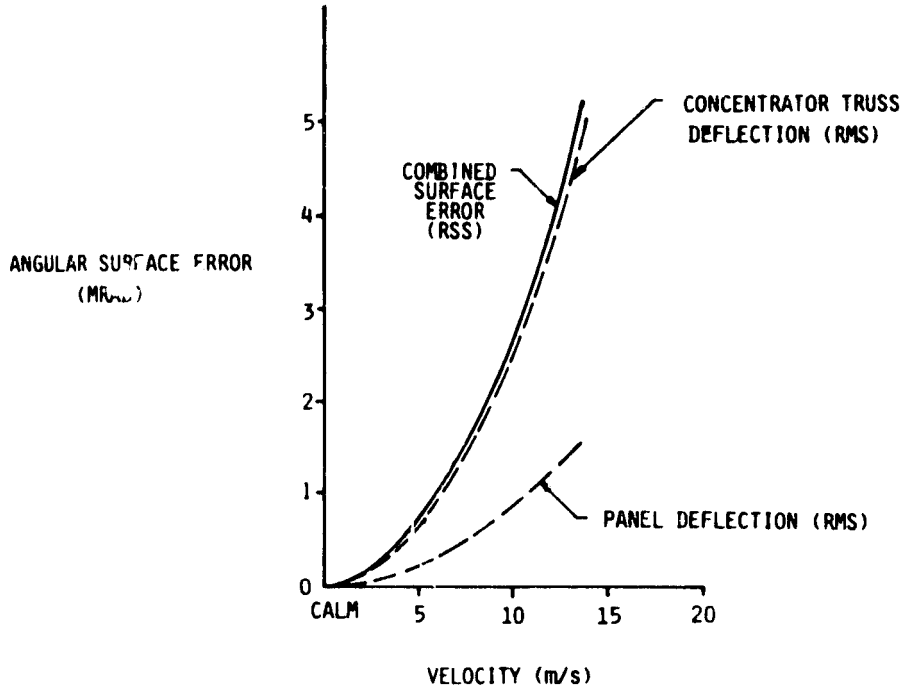

Figure 3.1-8 Wind Related Surface Error Budgets

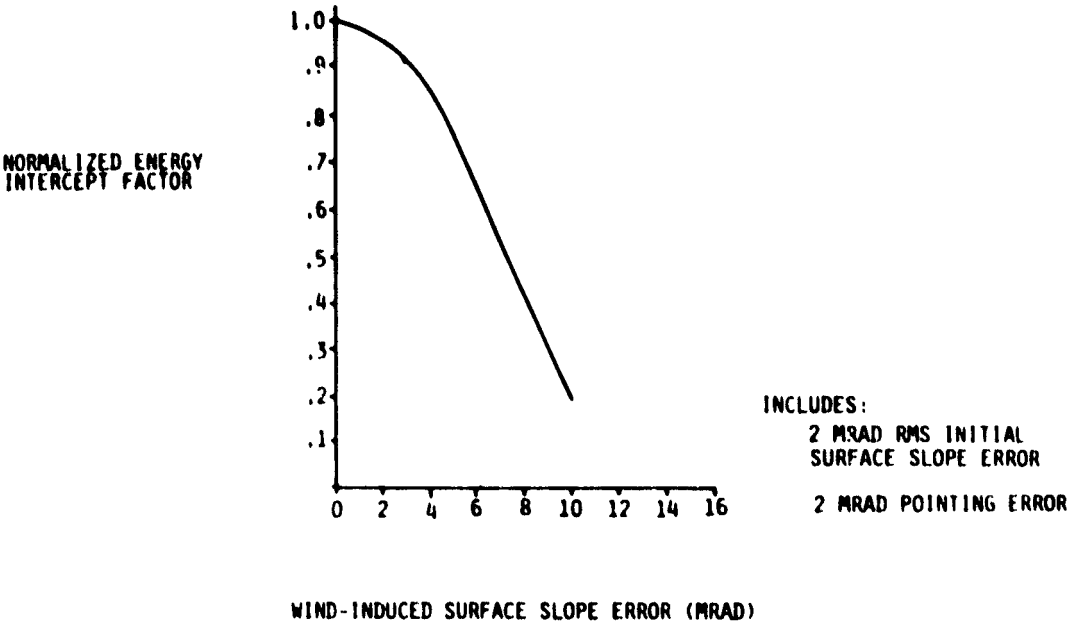

Figure 3.1-9 Concentrator Intercept Factor Related to Wind

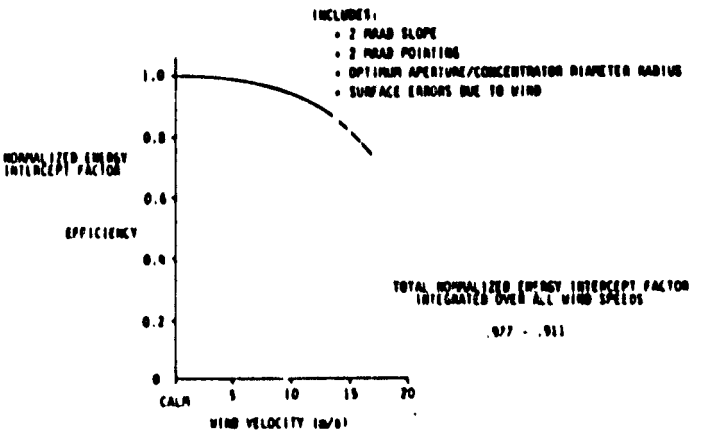

Figure 3.1-10 Concentrator Performance vs. Wind Speed

Table 3.1-9 Wind Loads Used on Panel Sizing

CONDITION	MAXIMUM OPERATIONAL WIND 13.9 m/s	ULTIMATE WIND 41.7 m/s
CONCENTRATOR ORIENTATION	HEAD-ON	YAW
PRESSURE COEFFICIENT (C_p)	1.0	2.1
UNIFORM DESIGN PRESSURE	107.3 g/m^2 (2.20 lb/ft^2 psf)	1706 g/m^2 (37.3 lb/ft^2 psf)

Table 3.1-10 Concept Screening Model Features

FEATURE	CONCEPT	
	STIFFENED SKIN	SANDWICH
SKIN CONFIGURATION STIFFENER CONFIGURATION COST CONFIGURATION BENDING STIFFNESS EI	SHEET OR BALANCED LAMINATE MAT-TYPE SKIN INTEGRAL WITH STIFFENERS	SHEET OR BALANCE LAMINATE HONEYCOMB NEGLECT CORE
SURFACE SLOPE ERROR	COMBINE STIFFENER AND SKIN ERRORS	NEGLECT INTRACELL DEFLECTIONS
FAILURE MODES	SKIN YIELDING STIFFENER YIELDING	SKIN YIELDING
DIMENSION VARIABLES	SKIN CLADDING THICKNESS SKIN CORE THICKNESS STIFFENER THICKNESS STIFFENER FLANGE WIDTH STIFFENER HEIGHT STIFFENER SPACING CORE ANGLE INNER AND OUTER GORE RADII	SKIN THICKNESS SKIN CORE THICKNESS CORE DEPTH CORE ANGLE INNER AND OUTER GORE RADII
ANALYSES	MATERIAL WEIGHT MATERIAL COST	MATERIAL WEIGHT MATERIAL COST

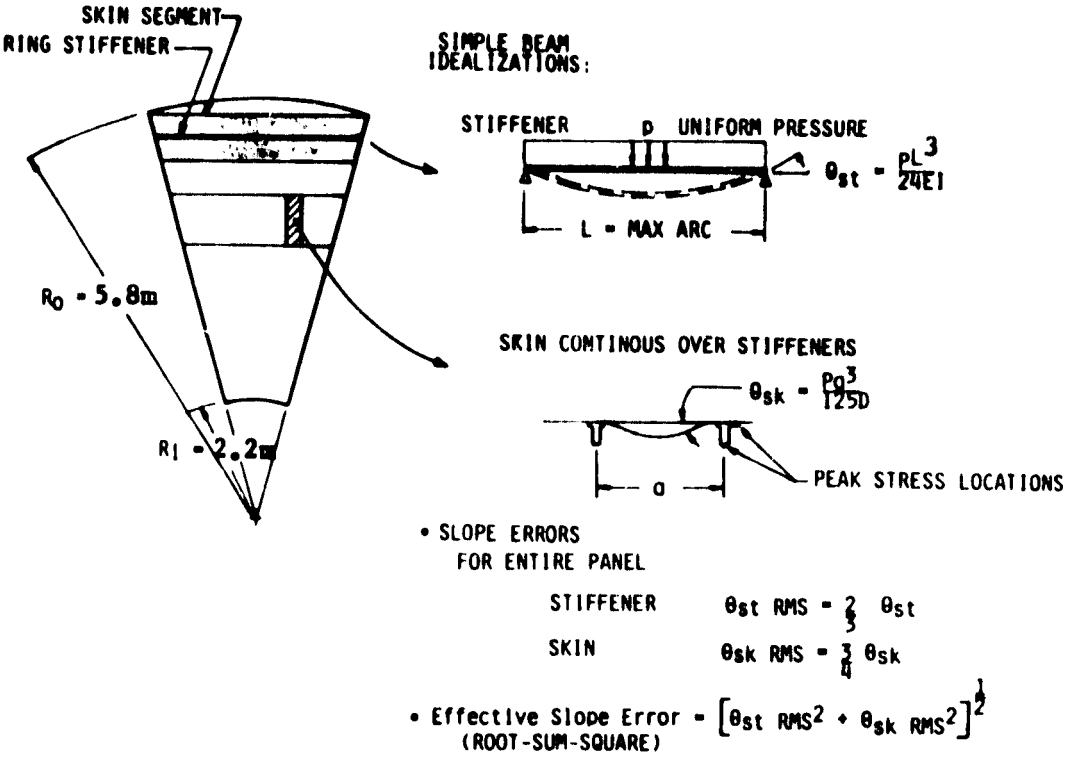

Figure 3.1-11 Computer Model for Panel Concept Screening

Table 3.1-11 Optimization Strategy for Panel Sizing

- SELECT NOMINAL GAGES FOR SHEET MATERIALS BASED ON AVAILABILITY AND HAILSTONE RESISTANCE
  - STEEL SHEET .076cm (.030in.) For Skins and Stiffeners
    .020cm (.008in.) For Laminate Cladding
  - WOOD FIBER HARDBOARD .318cm (.125in.)
  - POLYPROPYLENE .076cm (.030in.)
  - PAPERBOARD .127cm (.050in.)
- SELECT HONEYCOMB CORE
  0.224 kg/m^2 (1.74 lb/ft^3)
- SELECT HAT STIFFENER WIDTH
  2.54cm (1.0in.) For Spacing < 38.1cm (15.0in.)
  5.08cm (2.0in.) For Spacing ≥ 38.1cm (15.0in.)
- SELECT GORE CONFIGURATION
  ANGLE 20°
  OUTER RADIUS 5.84m (19.2 Ft)
  INNER RADIUS 2.18m (7.17 Ft)
- VARY OTHER DIMENSIONS TO FIND LEAST COST
  STIFFENER SPACING AND HEIGHT
  HONEYCOMB CORE THICKNESS

Results from the panel sizing study are shown in Figures 3.1-12 through 3.1-14, and Table 3.1-12. In all cases, stiffener depth or sandwich core thickness is optimized for minimum panel material cost. Also, all cases are governed by deflection limits at the operational wind condition. Initially, a trade study comparing costs of the two types of construction at varying gore angles indicated stiffened skin construction is consistently lower in cost than sandwich construction. Detailed parameter optimizations were then conducted at a representative fixed gore angle of 20°.

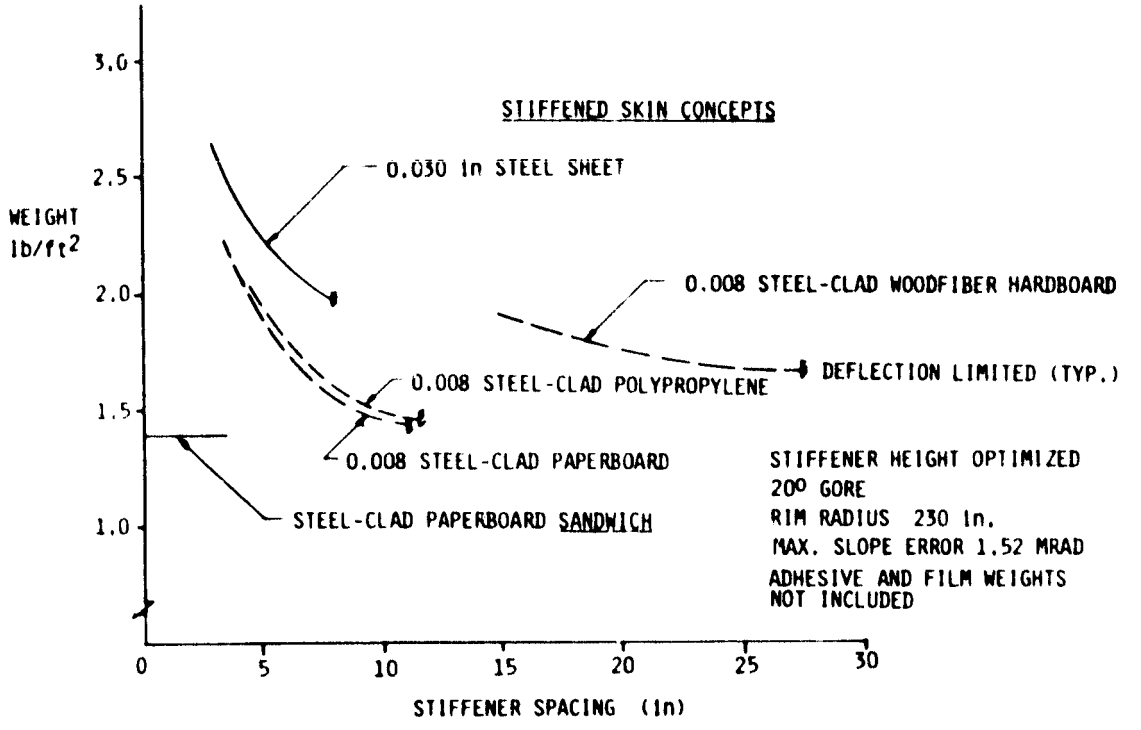

Figure 3.1-12 Panel Structural Material Weight Comparisons

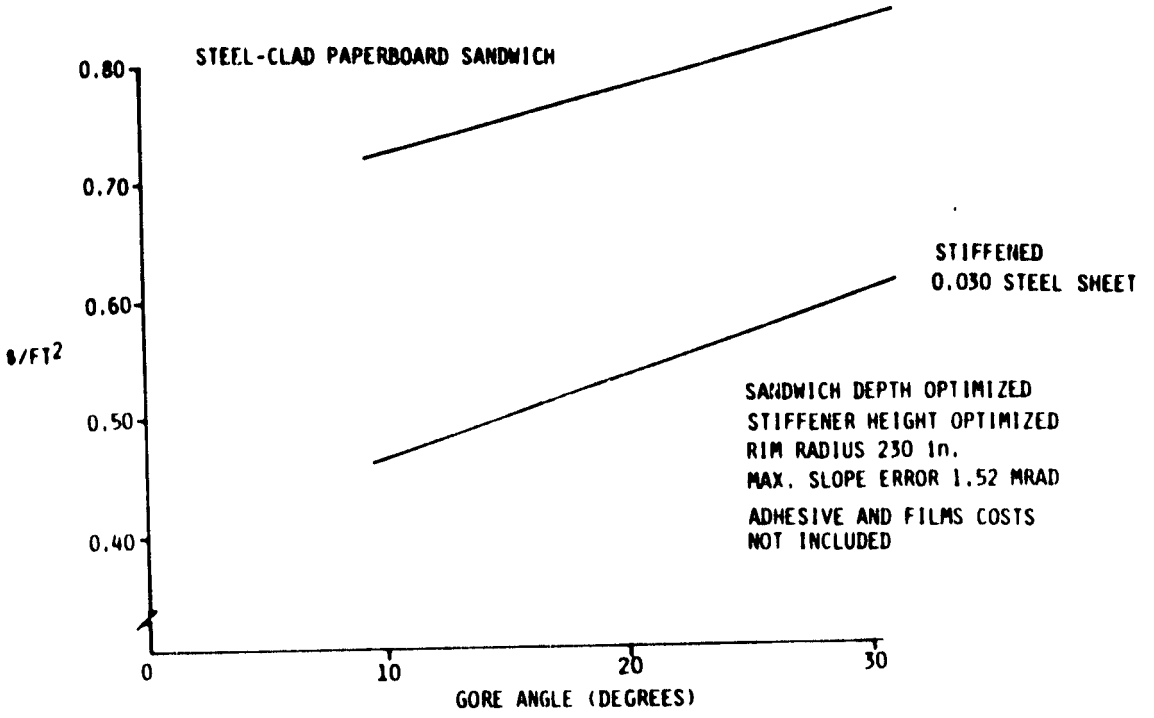

Figure 3.1-13 Panel Structural Material Cost vs. Gore Angle

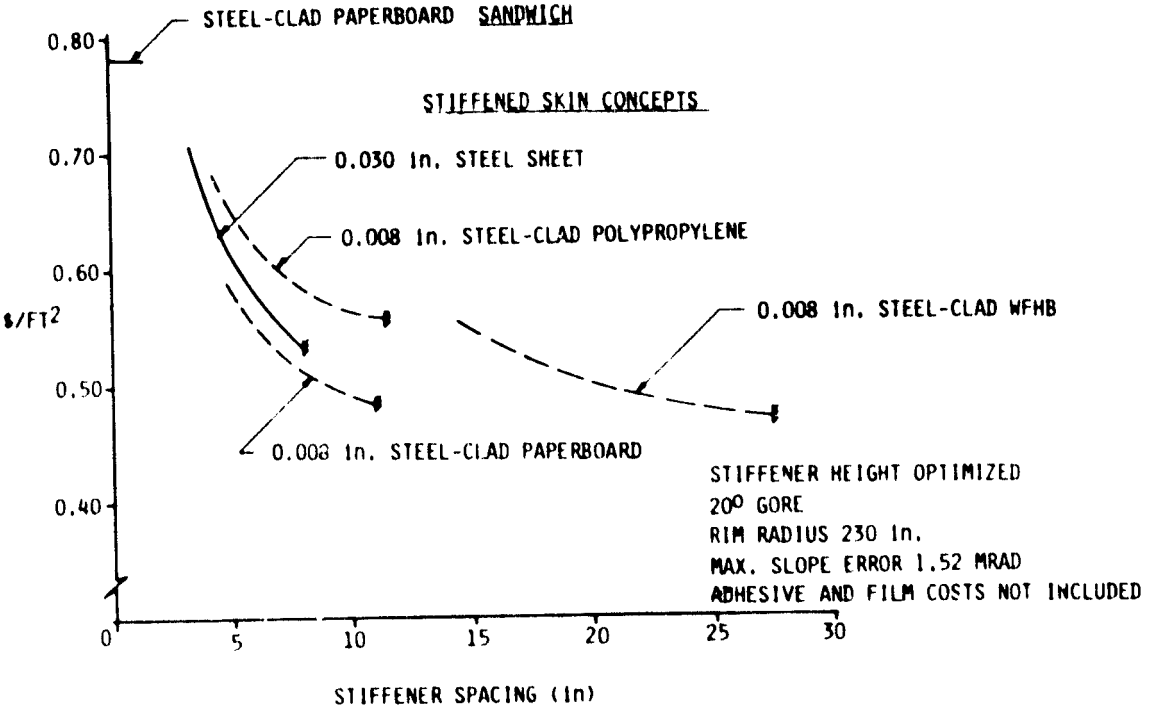

Figure 3.1-14 Panel Structural Material Cost Comparisons

Table 3.1-12 Material Costs

	STIFFENED STEEL SKIN $/M^2	STIFFENED STEEL CLAD PLASTIC CORE LAMINATE $/M^2	STIFFENED STEEL CLAD WFHB CORE LAMINATE $/M^2	ALUMINUM CLAD PAPER HONEYCOMB SANDWICH $/M^2	STEEL CLAD PAPER HONEYCOMB SANDWICH $/M^2
STRUCTURAL MATERIALS	5.70	6.03	5.06	8.37	8.30
STRUCTURAL LAMINATION ADHESIVE	NONE	SELF-BONDING	0.80	0.80	0.80
STRUCTURAL STIFFENER ADHESIVES	0.15	0.15	0.12	NONE	NONE
REFLECTIVE FILM	5.38	5.38	5.38	5.38	5.38
HOLD DOWN ADHESIVES	0.50	0.50	0.50	0.50	0.50
TOTALS	11.73	12.06	11.86	15.05	14.98

Total panel material costs were then compiled by adding adhesive and reflective material costs to the structural material costs from the computer model. When total material costs are compared, the stiffened skin concepts are preferred over sandwich concepts. This is primarily due to the sandwich concept being penalized by minimum material thickness constraints. All three competing stiffened skin concepts are close in terms of cost, the final selection is dependent on life cycle costs, manufacturing complexity and technical risk, which are evaluated in the following discussion.

Illustrations of the 5 study finalists appear in Figures 3.1-15 and 3.1-16.

Life Cycle Cost Factors

Life cycle costs for the panel candidates were computed based on certain simplifying assumptions: 1) design concepts influence energy costs primarily by capital costs, which are dominated by raw material prices; 2) all concepts have similar installation costs, film replacement and/or refurbishment requirements and film reflectivity. Further details assumed appear in Table 3.1-13. It is assumed that most of the selling price of the panels would be attributable to material costs as is typical of similar mass-produced consumer products. A panel capital cost of 1.2 times panel material cost was selected. Also, all panel concepts are judged to have similar film reflectivity (performance) and replacement requirements (ten year interval assumed, actual weatherability needs further investigation). The annual maintenance cost based on replacing YS-91 film at ten year intervals and cleaning at six month intervals is estimated to be seven percent of capital cost. These assumptions result in the panel life cycle costs being directly proportional to the panel material costs. Using the analysis method presented in JPL document 5040-29, The Cost of Energy from Utility-Owned Solar Electric Systems, life cycle costs were computed for each panel candidate which are presented later in Table 3.1-16.

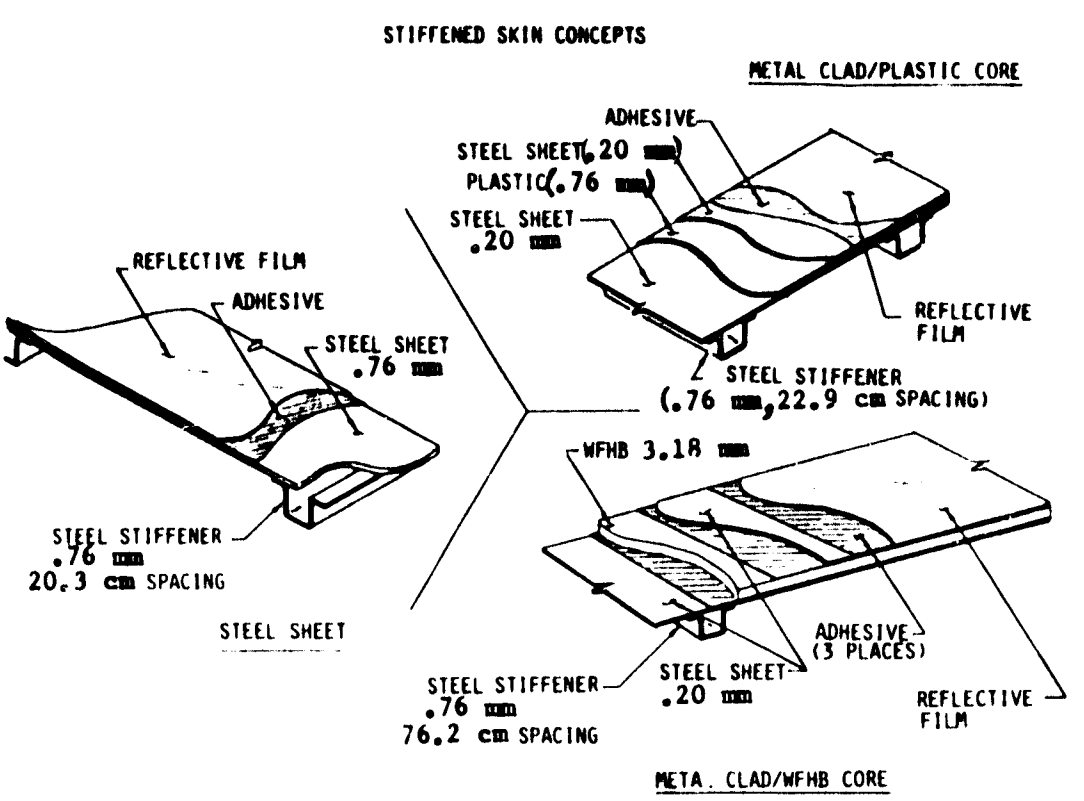

Figure 3.1-15 Structural Sizing

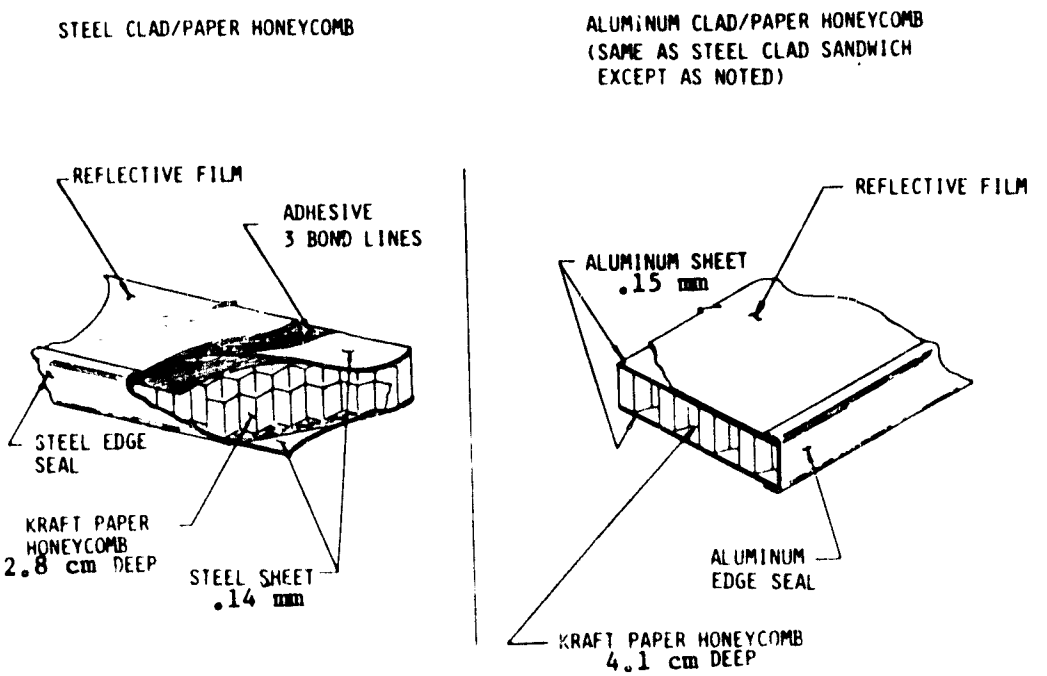

Figure 3.1-16 Structural Sizing

Table 3.1-13 Energy Cost Analysis Assumptions

CAPITAL COSTS = 1.2 (PANEL MATERIAL COSTS)	
1980 DOLLARS	
30 YEAR LIFETIME	
YEAR OF COMMERCIAL OPERATION	1985
YEAR OF CAPITAL INVESTMENT	1984
GENERAL ESCALATION RATE	8%
DISCOUNT RATE	20%
INCOME TAX RATE	50%
NONINCOME TAX FRACTION	0.0025
INSURANCE FRACTION	0.02
INSOLATION	800 W/m2
EFFICIENCY	80%
ANNUAL HOURS OF OPERATION	3,000 HRS.
ANNUAL MAINTENANCE COST CLEANING + REFURBISHMENTS	7% OF CAPITAL COST

Manufacturing Evaluation

Each panel candidate was evaluated with respect to the number and type of manufacturing operations required. (See Figures 3.1-17 through 3.1-21). This evaluation led to a qualitative ranking of manufacturing complexity which was one of the criteria in the final concept selection process. (See Table 3.1-14). The all-steel stiffened skin concept is least complex because it has the fewest number of parts and manufacturing steps. In addition, the metal components of the stiffened steel sheet concept can be fabricated by state-of-the-art methods by a number of suppliers.

Technical Risk Assessment

An assessment of overall technical risk was made for the panel candidates by rating the candidates in several risk categories. (See Table 3.1-15).

An overall best ranking was given to the stiffened steel sheet concept primarily because: 1) the metal components can be fabricated on conventional stretch forming equipment with good potential for tolerance control, 2) the design details are relatively simple, 3) special sealing of the structural parts will not be required, and 4) the design will have minimal temperature gradients.

- STIFFENED STEEL SKIN CONCEPT

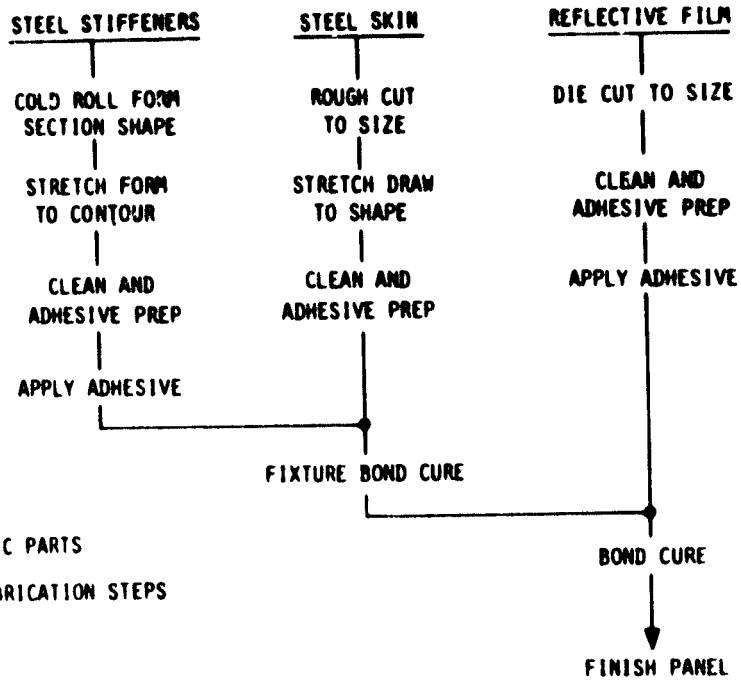

Figure 3.1-17 Manufacturing Requirements

- STIFFENED STEEL CLAD/PLASTIC CORE LAMINATE CONCEPT

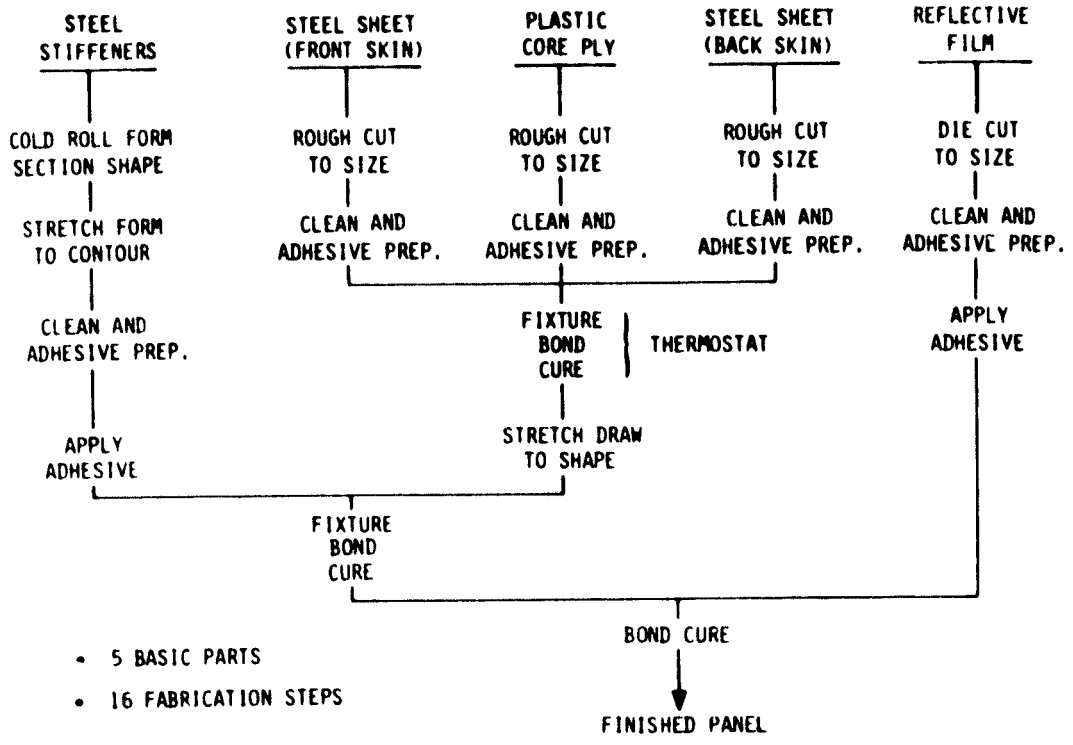

Figure 3.1-18 Manufacturing Requirements

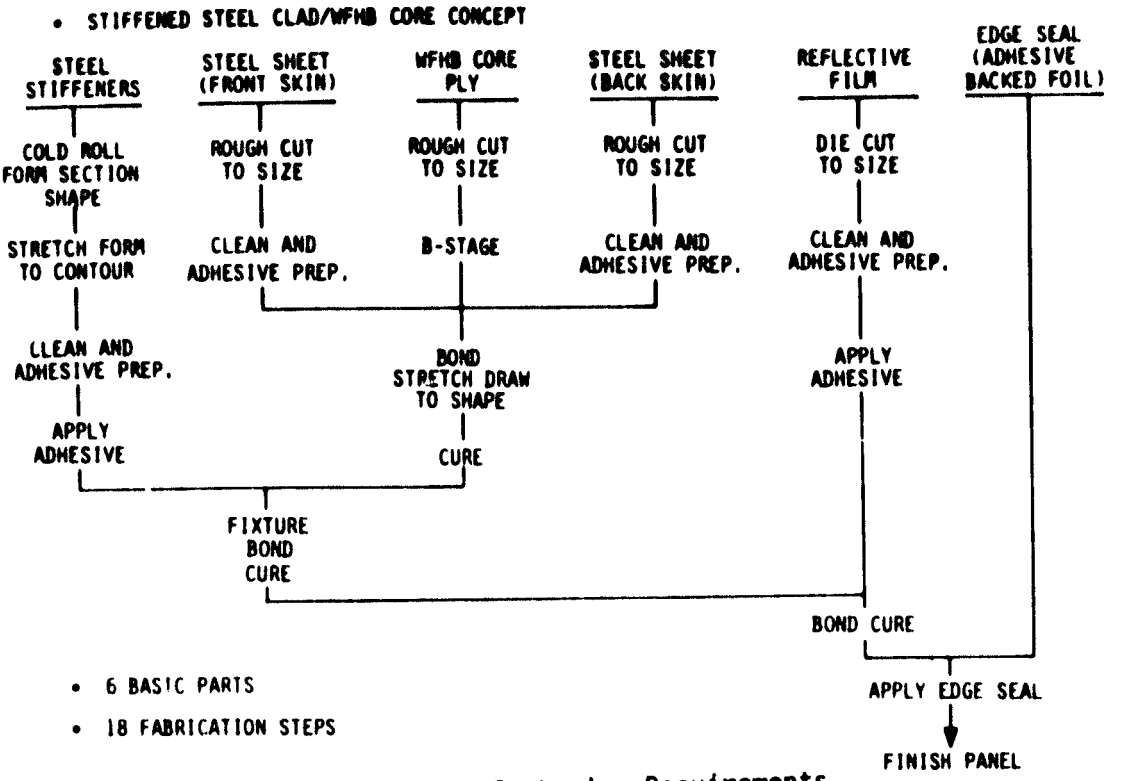

Figure 3.1-19 Manufacturing Requirements

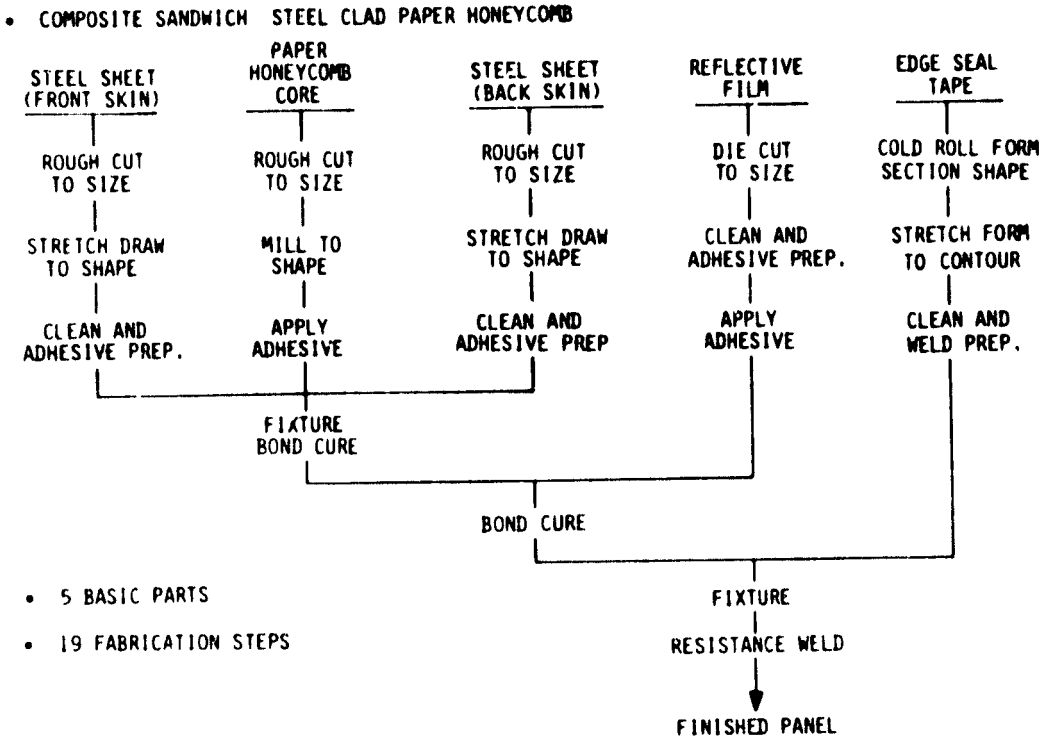

Figure 3.1-20 Manufacturing Requirements

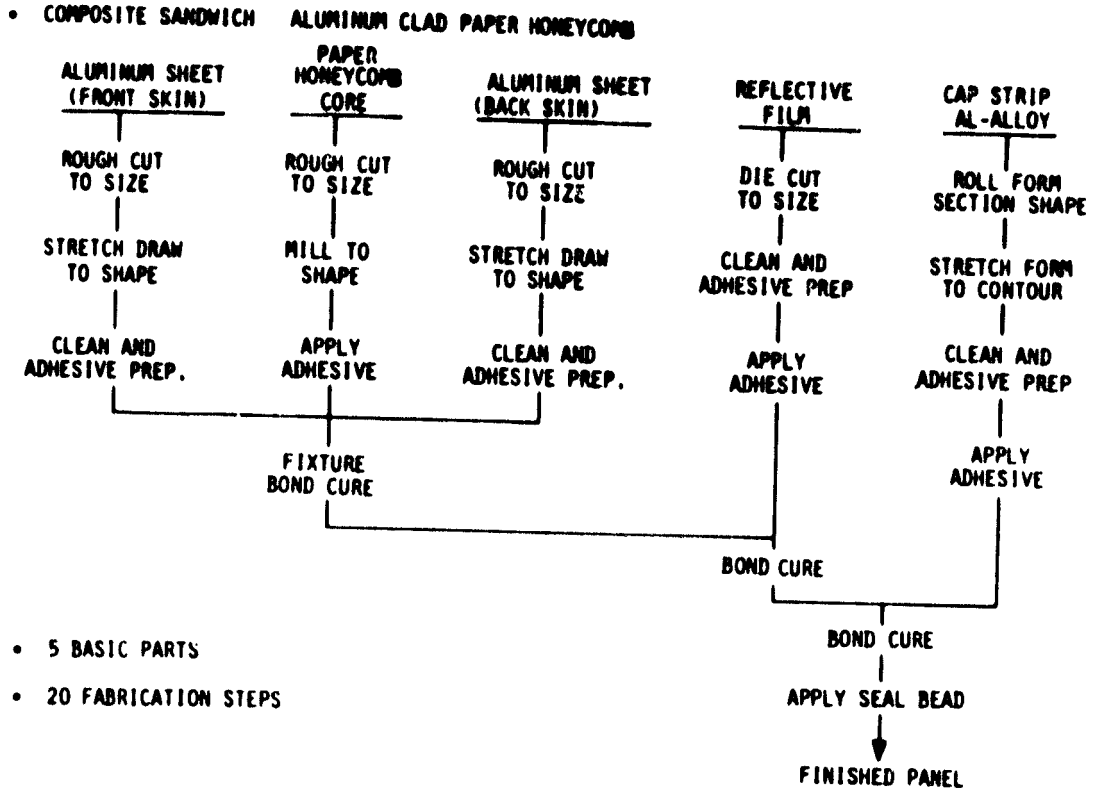

Figure 3.1-21 Manufacturing Requirements

Table 3.1-14 Manufacturing Requirements Summary

CONCEPT	BASIC PARTS	FABRICATION STEPS	MANUFACTURING COMPLEXITY
STIFFENED STEEL SKIN	3	12	LOW
STEEL CLAD/ PLASTIC CORE	5	16	MODERATE
STEEL CLAD/ WFHB CORE	6	18	MODERATE TO HIGH
COMPOSITE SANDWHICH STEEL CLAD/ PAPER HONEYCOMB	5	19	HIGH
COMPOSITE SANDWICH ALUMINUM CLAD/ PAPER HONEYCOMB	5	20	HIGH

Table 3.1-15 Technical Risk Assessments

	SUBSTRATE SURFACE FINISH	FILM TO SUBSTRATE BONDING	SUBSTRATE CONTOUR TOLERANCE CONTROL	SUBSTRATE SEALING AND DELAMINATION	PANEL THERMAL CONSIDERATIONS	INDUSTRY CAPABILITY	RISK RANKING
STIFFENED STEEL SKIN	32 TO 64 RMS AS FORMED	BI-AXIS STRAIN	EXCELLENT	NOT APPLICABLE	MINIMUM ★ ΔT ACROSS PANEL	EXCELLENT	LOW
STIFFENED STEEL CLAD PLASTIC CORE LAMINATE	32 TO 64 RMS AS FORMED		GOOD	NOT LIKELY	MISMATCHED COEF. OF EXP.	BEING DEVELOPED FOR AUTO-MOTIVE MARKET	LOW TO MEDIUM
STIFFENED STEEL CLAD WFHB CORE LAMINATE	32 TO 64 RMS AS FORMED		DIFFICULT	POTENTIAL PROBLEM	MISMATCHED COEF. OF EXP.	LIMITED TO BUILDING PRODUCTS	MEDIUM
ALUMINUM CLAD PAPER HONEYCOMB SANDWICH	POTENTIAL CORE MARK-OFF		DIFFICULT	INHERENT PROBLEM	INTERNAL PRESSURE BUILD-UP	LIMITED TO SPECIALIZED PRODUCTS	HIGH
STEEL CLAD PAPER HONEYCOMB SANDWICH	32 TO 64 RMS AS FORMED	BI-AXIS STRAIN	DIFFICULT	INHERENT PROBLEM	INTERNAL PRESSURE BUILD-UP	LIMITED TO SPECIALIZED PRODUCTS	HIGH

★ **Good Thermal Match to Supporting Structure**

Concept Selection

In summary, the panel concept evaluation resulted in selection of the stiffened steel sheet as the preferred concept for development. This selection is based on a composite rating of the evaluations discussed previously and summarized in Table 3.1-16 --manufacturing complexity + technical risk + busbar energy cost.

Weight is shown in the table, although not an evaluation criterion. The selected concept has the highest weight. This is consistent with recent findings that laminated steel products can save weight in automotive applications and many examples of light weight sandwich structure. However, higher weight is not necessarily detrimental since a larger portion of the stiffened steel sheet material will effectively stiffen the panel support trusses as part of a composite.

Table 3.1-16 Concept Evaluation and Ranking

Concept	Weight LB/M^2	Material cost $\$/M^2$	Manufacturing complexity	+ Technical risk	+ BBEC $mils/kW_{th}\text{-}h$	= Ranking
Stiffened steel skin	21.3	11.73	Low	Low	3.7	1 (Selected)
Stiffened steel clad plastic core laminate	15.6	12.06	Moderate	Moderate	3.9	2
Stiffened steel clad WFHB core laminate	17.7	11.86	Moderate to high	Moderate	3.8	3
Aluminum clad/ paper honeycomb sandwich	11.8	15.05	High	High	4.8	5
Steel clad/paper honeycomb sandwich	14.9	14.98	High	High	4.8	4

3.1.3 Selected Panel Concept Details

Design information related to the selected stiffened steel skin concept is presented in Tables 3.1-17 and 3.1-18 and Figures 3.1-22 and 3.1-23. This concept represented the basis for the conceptual design activities of Task 2.

A number of critical issues related to the selected thin film panel concept remained to be addressed in the next task. These were: 1) specular reflectance versus film application method; 2) steel sheet forming tolerance which influences film adhesive thickness and panel slope errors, 3) high speed film bonding; 4) corrosion protection; 5) film replacement procedure, 6) minimum gage needed for hailstone resistance; and 7) assessment of developments in overcoated reflective films.

3.2 Coupon Development

3.2.1 General

This work established the basic design techniques, the feasibility and fabrication methods for the reflective film on steel sheet substrate concept.

Table 3.1-17 Selected Concept

- STIFFENED STEEL SHEET
  - LOWEST DEVELOPMENT RISK
  - NO ENVIRONMENT SEALING REQUIRED
  - FEW PARTS
  - SIMPLE INTERFACE WITH SUPPORT STRUCTURE
  - MODERATE WEIGHT
  - USES EXISTING MATERIALS AND FABRICATION TECHNOLOGY
  - EXCELLENT PROSPECTS FOR REASONABLE LIMITED PRODUCTION COST
  - LOW MASS PRODUCTION COST

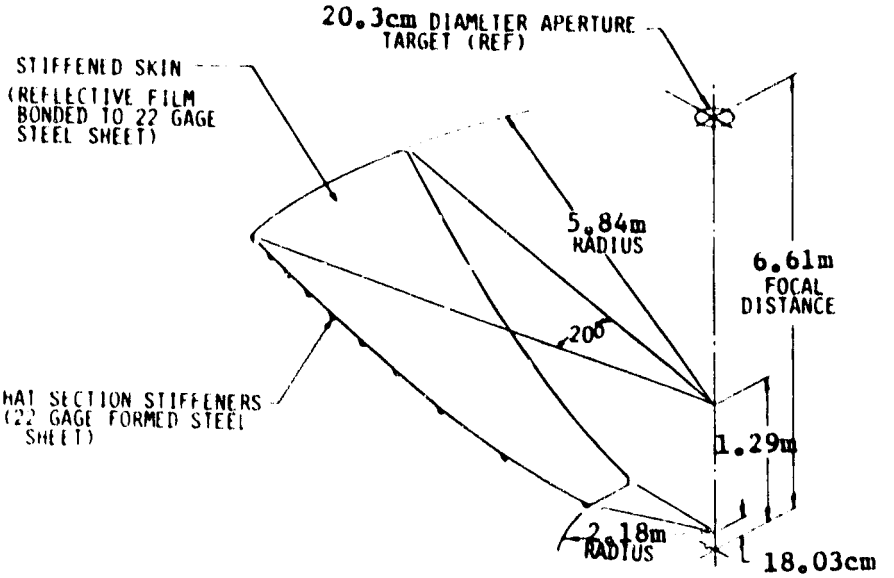

- PANEL AREA: 5.4M^2 (8369 In^2)
- PANEL WEIGHT: 51.8Kg (114 lb)

Figure 3.1-22 Selected Concept Configuration

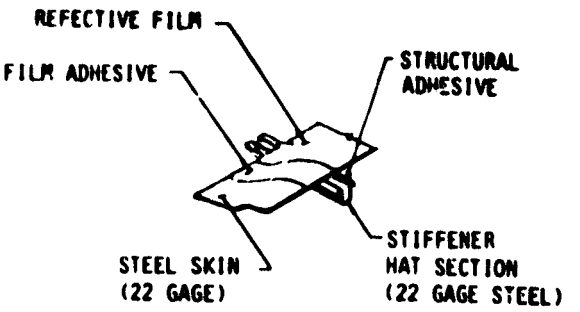

• PANEL COMPONENTS

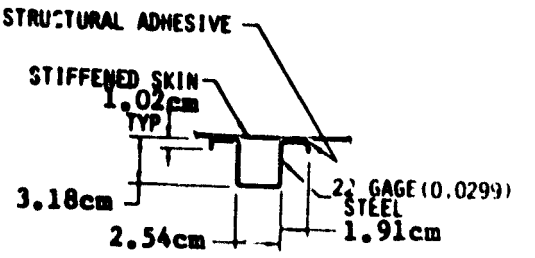

• DETAIL HAT SECTION STIFFENER

• MATERIAL/USAGE

COMPONENT	MATERIAL	QTY./PANEL
REFLECTIVE FILM	ALUMINIZED 4 MIL POLYESTER FILM WITH ACRYLIC OVERCOAT	5.4m^2 (8369 in^2)
STEEL SKIN	STEEL SHEET, LOW CARBON 22 GAGE, COLD ROLLED	29.3Kg (72.8 lbs)
STIFFENER HAT SECTION	FORMED STEEL SHEET, LOW CARRON 22 GAGE, COLD ROLLED	22.5 Kg (41.2 lbs)
STRUCTURAL ADHESIVE	REACTIVE ACRYLIC	.6Kg (1.5 lbs)
FILM ADHESIVE	T.B.D	---

Figure 3.1-23 Selected Concept Details

Table 3.1-18 Selected Concept Features

SKIN BENDING STIFFNESS	1070 $\frac{cm^4}{m}$ (65.3 $\frac{in^4}{in}$)
HAT STIFFENER AREA	.871cm^2 (.1351n^2)
HAT STIFFENER MOMENT OF INERTIA	1.37cm^4 (.033in^4)
COMBINED SKIN STIFFENER MOMENT OF INERTIA	8.07cm^4 (1.94in^4)
STIFFENER SPAN USED IN ANALYSIS	2.04m (80.3in) (At Rim)
STIFFENER SPACING	2.03cm (8.0in) (Minimum)
PEAK SIMPLE SPAN BENDING MOMENT	189Nm (1671 in-lb)
MAXIMUM STIFFENER STRESS	1.76MPa (25,5/8 lb/in^2)
MAXIMUM SKIN STRESS	38.6MPa (5603 lb/in^2)
PEAK STIFFENER SHEAR LOAD	417N (93.7 lb)
MAX. SKIN STIFFENER BONDING SHEAR FLOW	7.59 $\frac{N}{m}$ (67.2 lb/in)

The selected materials and processes resulted in reflective surfaces exhibiting 85% spectral reflectance and a 1 specular reflectance of 1.6 mrad, corresponding to a 0.8 mrad slope error. The .76 mm thick substrate survived hailstone impact without damage. Preliminary temperature/humidity tests indicated a potential problem with 3M's YS91A which has since been resolved.

3.2.2 Background

A series of flat reflective coupons were fabricated and tested. Each coupon represented a changed process or design variable. The initial coupon consisted of aluminized plastic film bonded to bare steel sheet. Its reflective surface exhibited an orange peel texture, i.e., small scale (1/8 inch diameter or less) protrusions or waviness. The final coupon in the series used a higher grade of steel sheet with a sanded epoxy primed faying surface. This approach significantly reduced the visual evidence of orange peel. However, data from specular reflectance tests indicated no significant difference between the initial coupon and the final coupon.

All coupons were constructed using 22 gage flat steel sheets 21 x 27 cm and 3M's YS91A reflective film. For film component description see Figure 3.2.2-1.

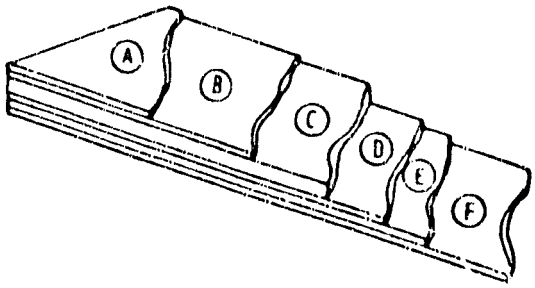

Ⓐ PROTECTIVE OVERCOAT ~ .2 MIL ACRYLIC COPOLYMER, PRECISION ROLL COATED

Ⓑ METALIZED REFLECTIVE SURFACE ~ 800 - 1000 A THICK VAPOR DEPOSITED SPECIAL HIGH PURITY ALUMINUM

Ⓒ CARRIER FILM ~ 2 MIL THICK POLYESTER FILM BI-AXIALLY ORIENTED (TENTED)

Ⓓ ADHESIVE LAYER ~ 1/2 MIL THICK PRESSURE SENSITIVE ACRYLIC, PRECISION ROLL COATED

Ⓔ RELEASE COATING ~ WATER SOLUBLE DETACKIFYING SOLUTION, CURTAIN WALLED

Ⓕ RELEASE LINER ~ 1 MIL THICK POLYESTER FILM BI AXIALLY ORIENTED (TENTED), SALVAGABLE

Figure 3.2.2-1 Reflector Film Description

3.2.3 Selected Materials and Processes

Figure 3.2.3-1 depicts the fabrication sequence and methods which were selected based on tests and evaluations.

No optical performance advantage for the ASTM-A620 steel substrate was indicated by the test data. Therefore, the initial selection of ASTM-A366 was retained, based on its lower cost and availability.

The use of the epoxy primer is required to prevent oxidation of the substrate faying surface. This oxidation begins once the mill oil is removed from the steel sheet in preparation for bonding. Therefore, the primer was applied immediately after cleaning.

The method of film application which 3M refers to as "wet application" was selected based on its simplicity. The film is easily positioned and no air is trapped. Dry film application was tried; the elimination of air bubbles was difficult and exact positioning of film before contract with the substrate was required.

Table 3.2.3-1 lists the coupon configurations examined and evaluated.

3.2.4 Coupon Testing

Optical and physical tests were conducted on several coupons to determine the effects of process and material variables. The test results facilitated selection of the final processes and materials for follow-on development hardware.

3.2.4.1 Spectral Reflectance Test

Purpose:

Determine spectral reflectance characteristics of surface

Test Method:

Spectrophotometer intensity measurement of reflected beam compared to air reference beam

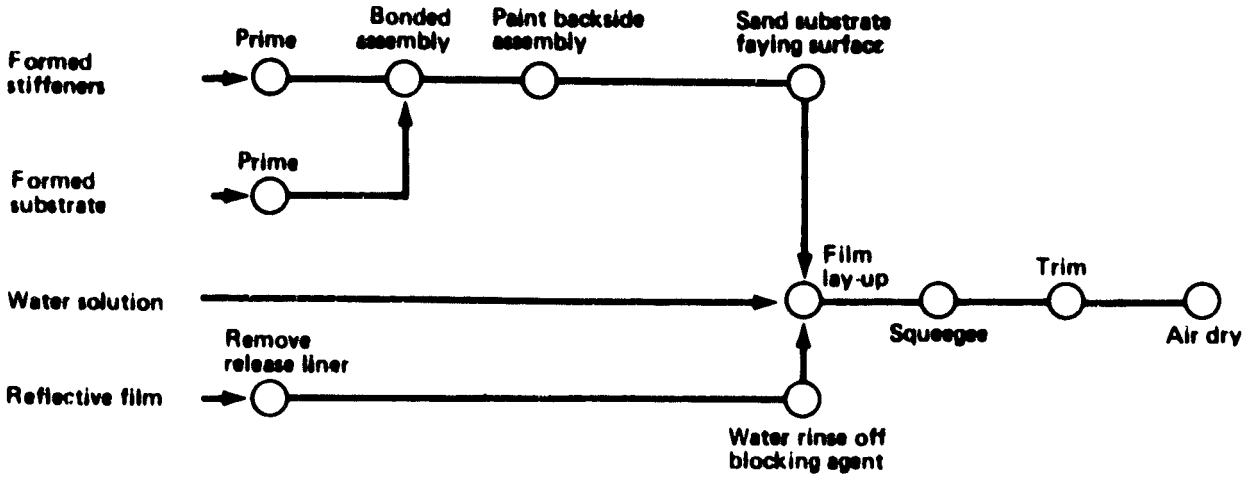

Figure 3.2.3-1 Selected Assembly Sequence

Table 3.2.3-1 COUPON CONFIGURATIONS EXAMINED

(All Coupons Used YS91A Reflective Film)

ASTM 366 Steel	Bare Bare-Dichromate* ① Bare-Sanded-Dichromate ② Epoxy Primed ③ Epoxy Primed-Painted ③ Epoxy Primed-Sanded Galvanized Galvanized-Epoxy Primed ③	Water/Detergent* Water/Detergent/ Dichromate Water Only Dry	Squeegee* Press Vacuum Bag
ASTM 620	Bare-Dichromate Epoxy-Sanded** ① Epoxy-Painted	Water/Detergent**	Squeegee**

* Baseline concept coupon

** selected design coupon

① Tested for spectral and specular reflectance and reflector figure

② Tested for specular and reflector figure

③ Tested for specular reflectance

Test Article(s):

Flat coupons

Test Data:

Percent reflected energy vs. wavelength (see Figure 3.2.4-2 for typical data sheet)

Test Parameters:

Discrete measurement over - 341 nm wavelength to 1923 nm, 29 mrad aperture

3.2.4.2 Specular Reflectance Test

Purpose:

Determine specularity error, beam divergence caused by high spatial frequency variations in reflective surface elements

Test Method:

Fourier image intensity distribution evaluation (see Figure 3.2.4-3)

Test Article(s):

Flat reflector panel coupons

Test Data:

Specularity plot, power normalized to 29 mrad full aperture (see Figure 3.2.4-4 for typical data sheet)

Test Parameters:

568 nm light source, 0.3 cm (1/8 inch) beam

Test performed by Battelle Northwest Laboratories

3.2.4.3 Reflector Figure Test

Purpose:

Determine reflective surface slope errors caused by physical deformations on the surface

Figure 3.2.4-2 Spectral Reflectance Test Data

Thermophysics Lab. Sample: 2 Date 1-5-81
Beckman DK-2A Spectrophotometer.
Air mass 2. (Reference handbook of Geophysics 1960)
For. SOLAR REFLECTANCE - 83.3 corrected = 85.00

λ	100%	Sample	Correct	λ	100%	Sample	Correct	λ	100%	Sample	Correct
341		59.8	65.1	685		73.6	80.9	1253		86.7	86.9
399		68.8	73.7	700		73.7	81.0	1301		86.9	86.0.
424		73.3	78.5	716		73.7	80.7	1437		87.0	87.8
462		74.4	79.7	729		73.7	80.2	1590		87.0	88.0
457		74.8	80.0	745		73.8	80.2	1640		86.4	87.8
471		75.0	80.2	763		74.0	80.4	1923		83.3	84.2
484		75.4	80.6	780		74.6	80.9				
496		76.0	81.3	797		75.4	81.7				
508		76.4	81.6	815		76.3	82.7				
521		76.6	81.7	833		76.8	83.2				
533		77.2	82.1	851		78.0	84.2				
546		77.2	82.1	870		79.2	85.3				
558		77.4	82.3	896		81.1	87.2				
571		77.5	82.4	932		82.2	88.2				
583		77.6	82.5	968		83.2	89.1				
596		77.5	82.4	991		84.3	89.2				
609		77.1	82.3	1015		85.0	89.7				
621		77.0	82.4	1060		85.2	91.5				
634		77.0	82.5	1067		85.4	87.0				
647		76.7	82.2	1114		85.7	87.3				
659		76.6	82.2	1171		86.2	89.1				
672		73.5	80.5	1213		86.9	89.1				

WBS # .
Correction -
+85.815
-84.116

Total - 4167.039
Average - 83.341
= 84.966

ORIGINAL PAGE IS
OF POOR QUALITY

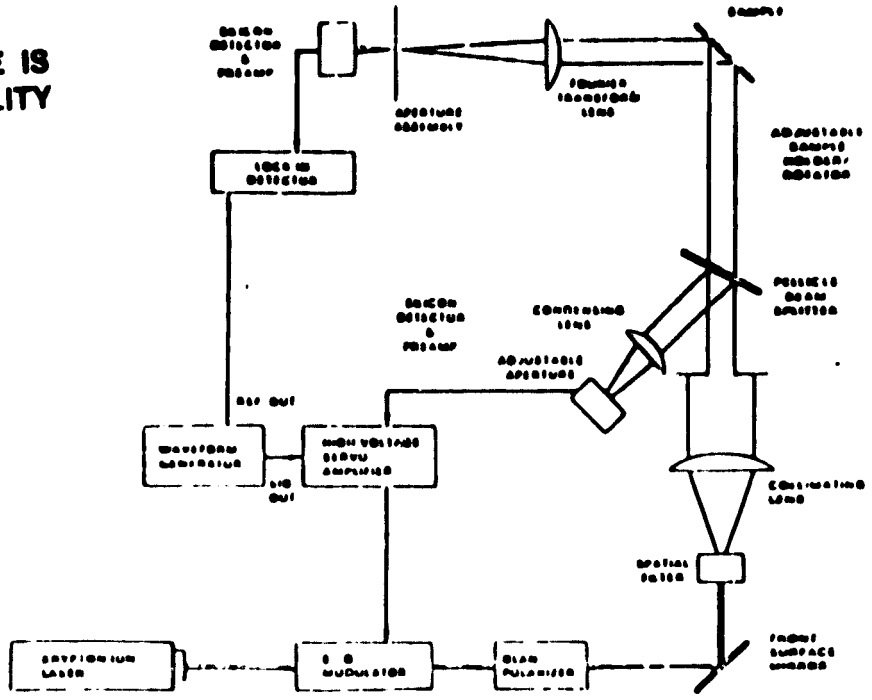

Figure 3.2.4-3 Optical Configuration for Specularity Measurement

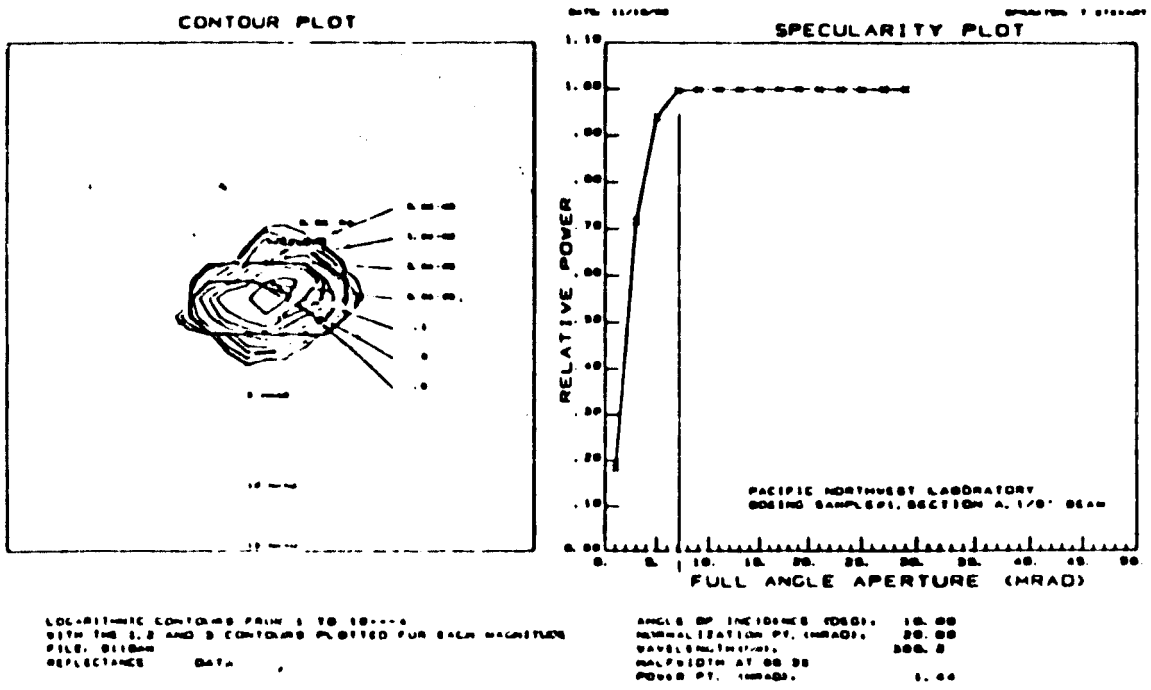

Figure 3.2.4-4 Specularity Test Results

Test Method:

Laser ray trace

Basic Test Principle:

Deviation of reflected beam angle from mean angle, with gross panel curvature removed

Test Article(s):

Flat reflector panel coupons

Test Data:

Deviation of surface normal vs. linear length position (see Figure 3.2.4-5 for typical data)

Test Parameters:

HeNe laser, 1 mm beam diameter, 0.25 mm travel resolution

Test performed by Battelle Northwest Laboratories

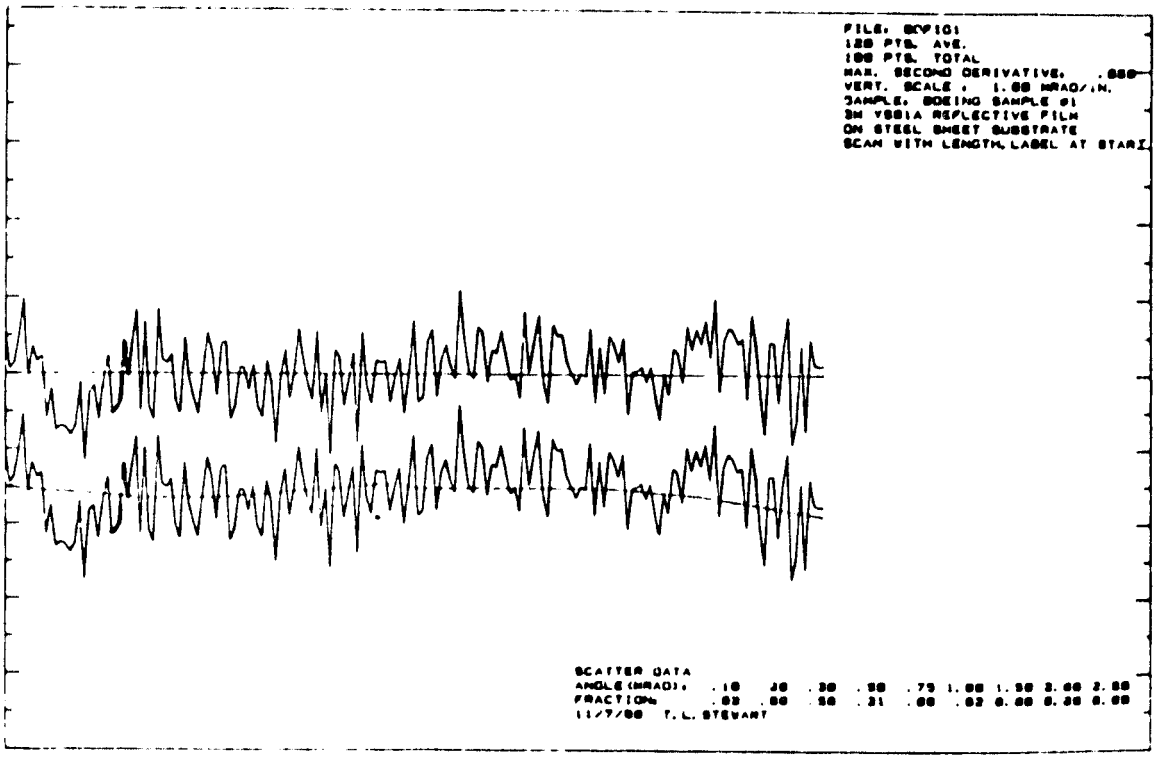

Figure 3.2.4-5 Reflector Figure Test Results

3.2.4.4 Substrate Surface Roughness Test

Purpose:

Determine substrate finish requirement based on optical testing of finished coupons

Test Method:

Mechanical measurement of height deviation vs. length using a stylus recorder

Test Article(s):

Finished substrates for flat coupons and development panels

Test Data:

RMS micro inch value (see Figure 3.2.4-6 for typical data plot)

Test Parameters:

Measurements to be made per ASME B461.1 standard

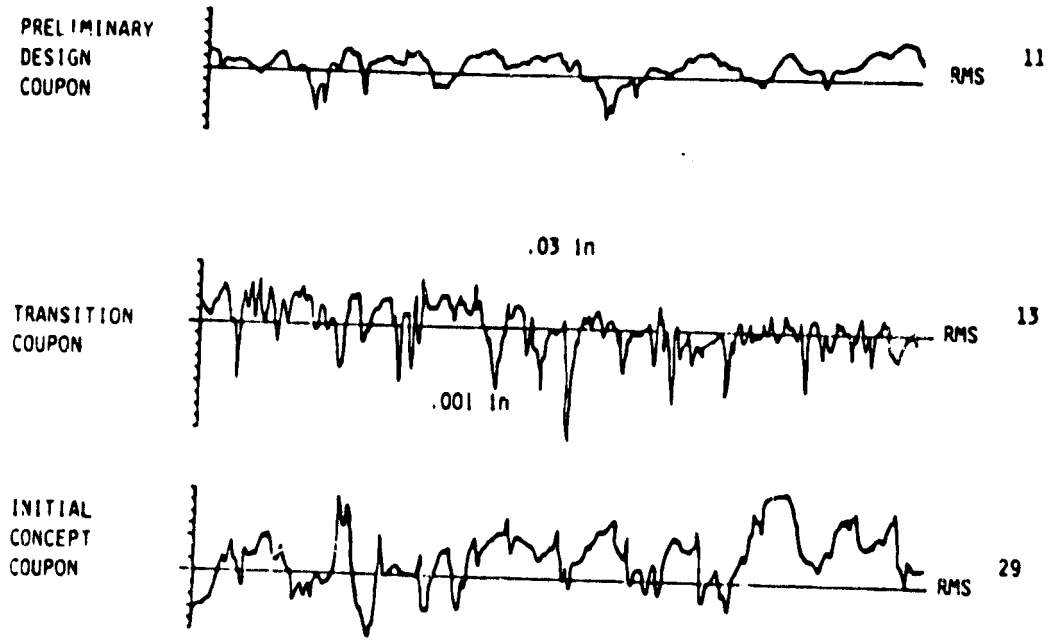

Figure 3.2.4-6 Surface Roughness Test Results

3.2.4.5 Hailstone Impact Test

Purpose:

Determine damage resistance of panel to hailstone impact. Test results will be used for design specification verification.

Test Method:

Simulated hailstone impact using pneumatic fired ice balls (see Figure 3.2.4-7).

Test Article(s):

Flat reflector panel coupons.

Test Data:

Visual damage assessment.

Test Parameters:

2.54 cm diameter ice ball - hardness 2-3 MOHS, velocity 21±.9 m/sec at 45° and 90° front surface incidence angles.

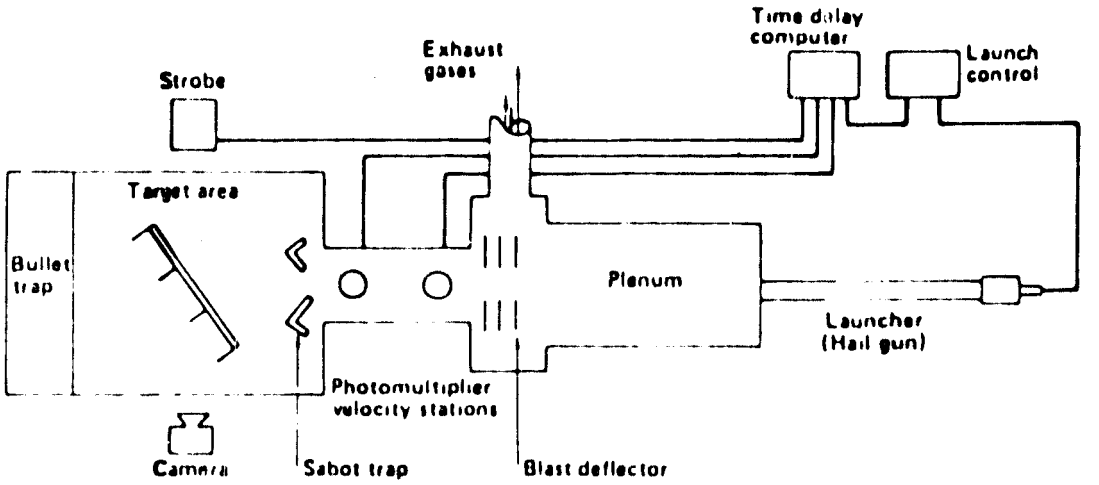

Figure 3.2.4-7 Hailstone Impact Test Range

3.2.4.6 Preliminary Temperature Tests

Purpose:

Determine temperature effects on panel elements.

Test Method:

Exposure in temperature controlled chamber.

Test Article(s):

Selected design coupon cut into two section A and B.

Test Data:

Visual assement

Test Parameters:

Vary temperatures in 10°C increments between ±50°C (122°F) to -30°C (-22°F), soak 1 hour at extremes and 10 minutes at steps between. No humidity control required (see Figure 3.2.4-8 for test profile).

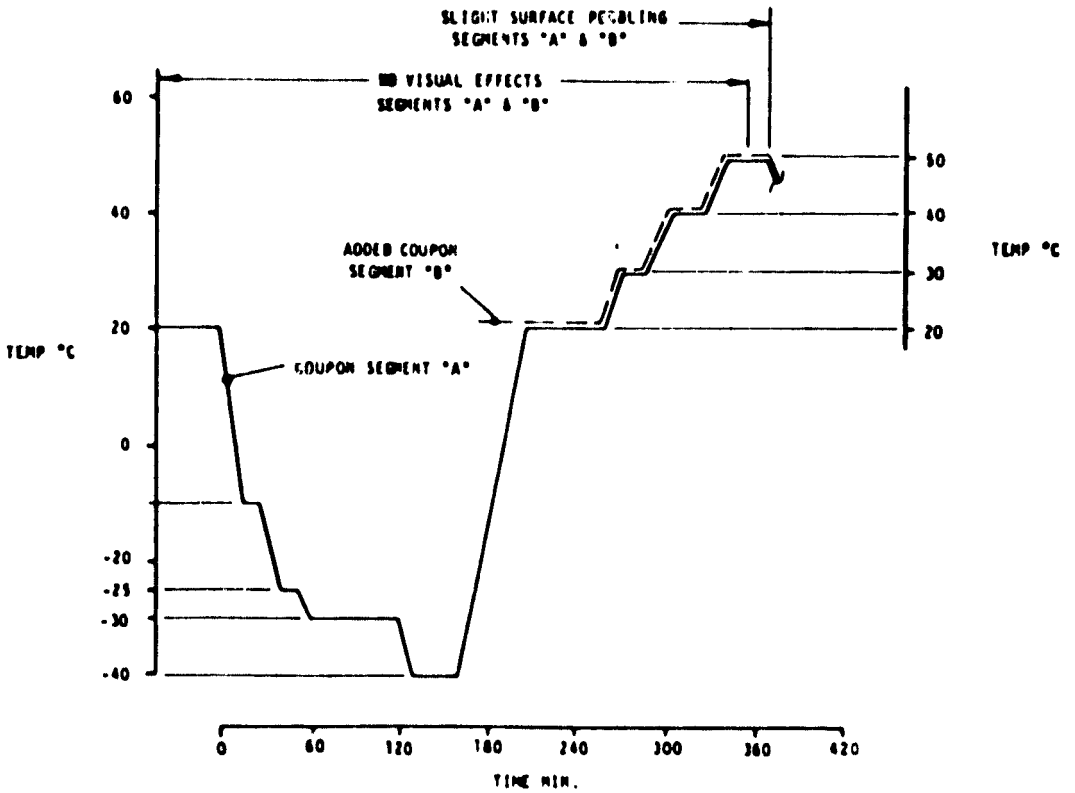

Figure 3.2.4-8 Temperature Cycle Test Profile

3.2.4.7 Coupon Test Results

Results for the tests described in the preceding paragraphs are presented in Table 3.2.4-1.

Optical test data (spectral reflectance specularity and reflector figure) were used in the initial film selection, coupon screening and in the concentrator optical performance analyses (presented in Section 4.3).

Substrate surface roughness data needed to aid in the selection of substrate preparation shows the improvement of surface quality achieved during the development program. The initial concept involved the use of bare steel and the selected design uses sanded epoxy primer. It should be noted that while the surface roughness was reduced (visually and by measurement) no significant optical improvement was observed. The epoxy primer is required, however, for corrosion protection of the substrate.

Simulated hail testing indicated that the substrate thickness (.76 mm) was adequate. No reflective film damage was observed.

Preliminary testing at the specifications temperature extremes, -30°C (-22°F) and +50°C (122°F), revealed a problem of film blistering at +50°C. The problem was reported to the 3M company. 3M investigated samples in their laboratory and identified the problem as a failure at the interface between the polyester film and the adhesive. Water captured during the film application process migrated through the adhesive, expanded upon heat addition and formed the blisters. 3M recognized the problem and its solution from experience with other films and made a small process change to the YS-91A. Samples tested at BEC and 3M subsequent to the process change have not exhibited the blistering problem.

Table 3.2.4-1 Coupon Tests/Results

TEST	PURPOSE	RESULTS	
		INITIAL CONCEPT	Selected DESIGN
Spectral Reflectance (Air Mass 2, 29 mrad)	Coupon Screening Optical Performance Analysis	84%	85%
Specular Reflectance (1σ Half Angle Aperture), mrad		1.4 - 1.8	1.5
Reflector Figure (1σ Area Slope Error), mrad		.3 - .5	.3 - .4
Substrate Surface Roughness (RMS - micro-inches)	Substrate Design Drawings Specification	29 ✓	11 ✓
Hailstone Impact (1 Inch Diameter at 70 Ft/Sec)	Verify Substrate Thickness	0.03 Inch Marginal	
	Determine Film Damage	No Film Damage	
	Design Specification Compliance	Requires Assessment	
Temperature Extremes Soak at -30°C, +50°C	Determine Temperature Effects	Surface Pebbling at +50°C	

4.0 CONCENTRATOR CONCEPTUAL DESIGN

4.1 Concentrator Design

4.1.1 General

The Point Focus Thin Film Concentrator Conceptual Design is shown in Figure 4.1.1-1. It is a 12 meter diameter, 80 kW, 1500°F concentrator with a 20 cm diameter receiver aperture, and a focal length to diameter ratio of 0.6.

The primary features of the concentrator are:

a. Azimuth elevation drive system gimballed at the concentrator center of gravity.

b. Inverted stow with receiver boom mechanically locked to base of pedestal.

c. Zero blocking reflector design and receiver support structure boom.

d. Prestressed cast concrete pedestal/foundation.

e. Low weight concentrator 60 lbs/m^2 estimated, pedestal/foundation not included.

The reflector panels are bolted to the circumferential rings shown in Figure 4.1.1-2. Alignment of the individual panels is accomplished using this bolted connection. Radial trusses support the circumferential rings.

Figure 4.1.1-3 shows orientation of the parabolic gore section reflector panels. There are 15 inner panels and 30 outer panels.

4.1.2 Reflector Panel Design

The reflector panels are 3 meter long parabolic gores with 7.2 meter focal lengths. The panels are comprised of radial rib stiffened s l substrates with bonded on aluminized plastic film. They have a spectral reflectance of 85% and a 1σ specularity of 1.5 mrad (slope error 0.75 mrad). The panels are

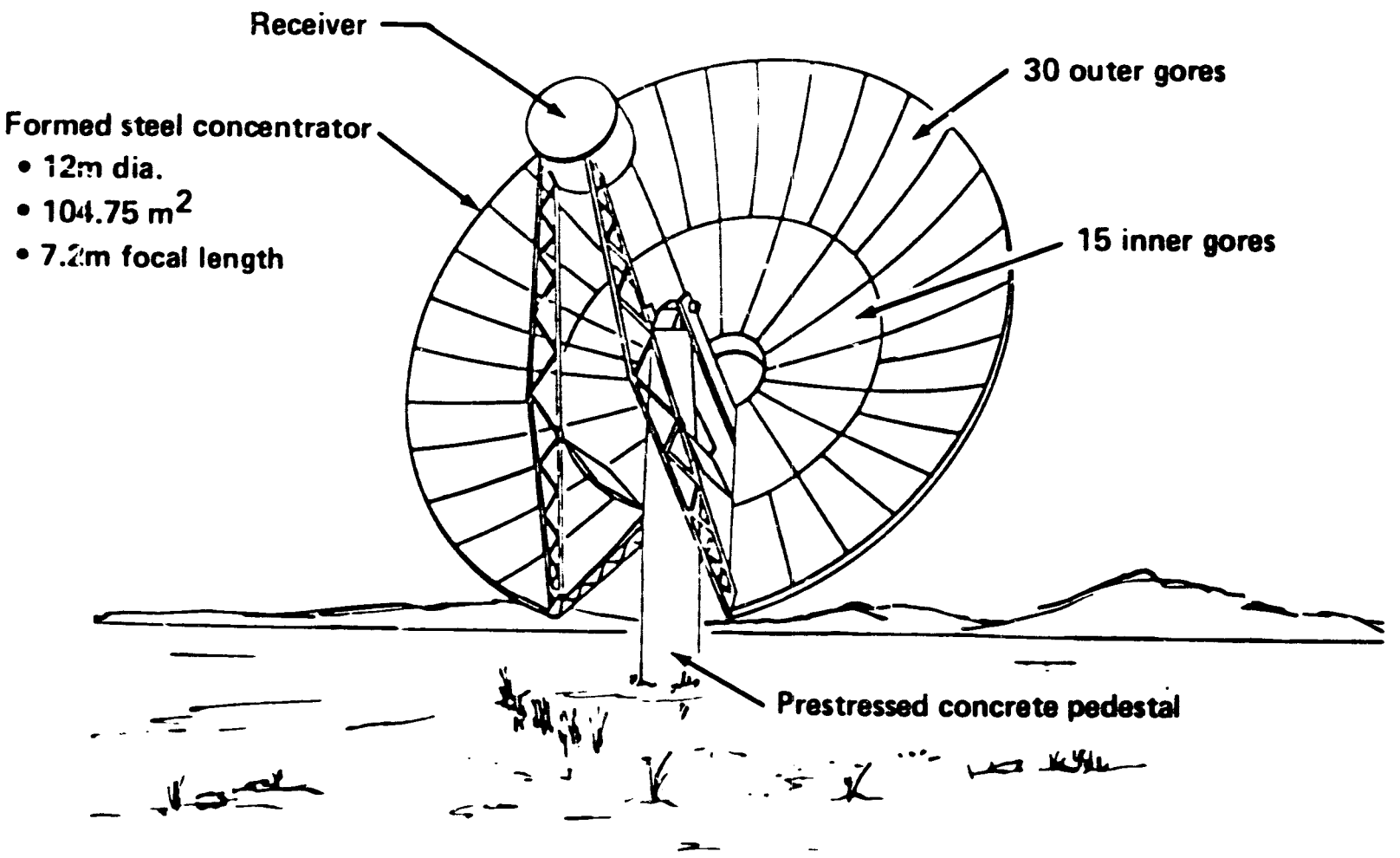

Figure 4.1.1-1 Thin Film Concentrator Conceptual Design

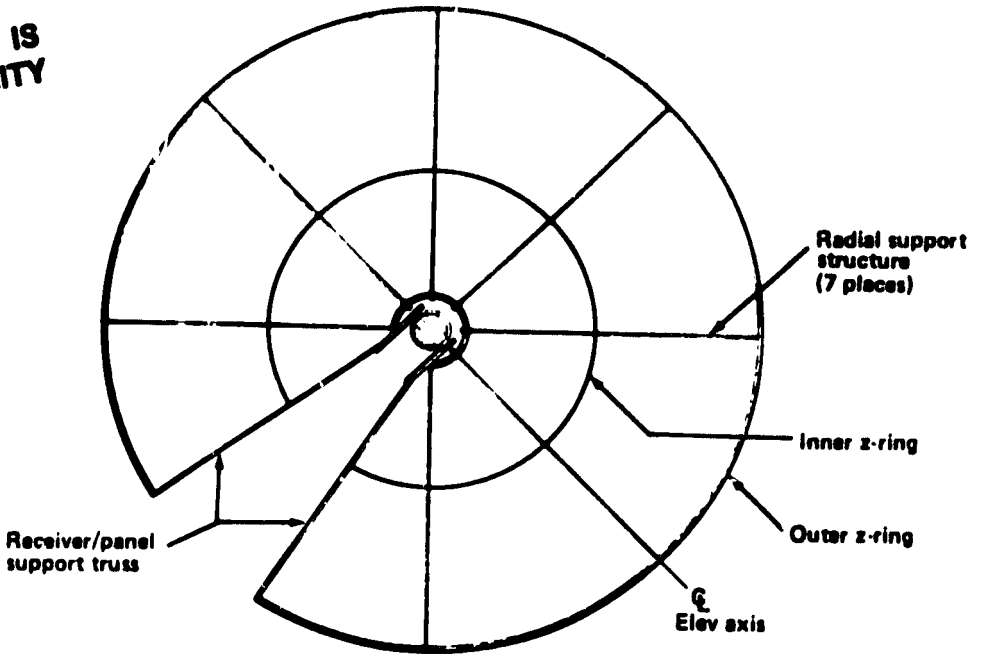

Figure 4.1.1-2: Support Structure

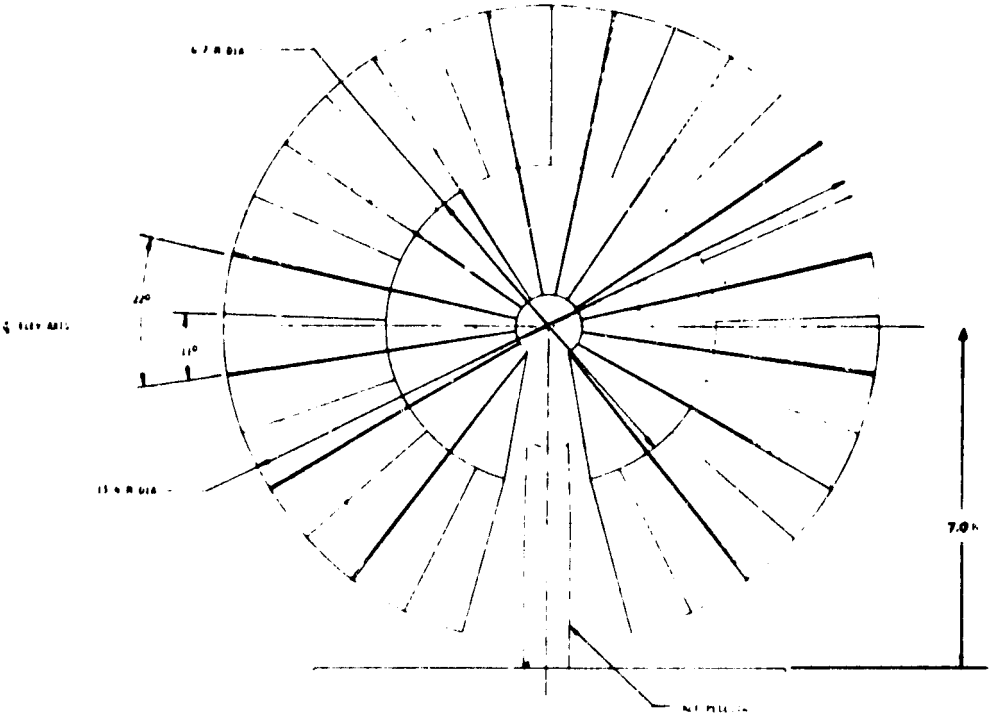

Figure 4.1.1-3: Reflector Panel Layout

designed to achieve a fabricated contour error of 2.0 mrad or less over 90% of their area. The wind load deflection of the panel is 0.6 mrad RMS at 14 m/s.

The major components of the panels are shown in Figure 4.1.2-1. A 22 gage low carbon steel sheet per ASTM A-336 is stretch formed into a parabolic contour, and an aluminized plastic film (3M's YS91A) is bonded to it. Five 22 gage steel (A-366) hat section stiffeners are bonded to the steel sheet with acrylic adhesive. The stiffeners are equally spaced and oriented in the radial direction. Four steel hat section spreaders provide panel torsional rigidity.

A two part zinc rich epoxy primer is applied to all the steel surfaces for corrosion protection. The reflective film is bonded to the primed surface of the steel stubstrate. All other steel surfaces are finish coated with a white, two-part polyurethane paint.

The steel components primed and painted as specified are designed to last 30 years in the southwest United States. Preliminary experiments with coupons indicate the reflective film is easily removed and replaced.

Table 4.1.2-1 lists the panel materials and material costs. The steel costs are based on direct purchase from the steel mill. The break point where direct purchase becomes possible occurs at 18,200 kg (40,000 pounds) which is equal to 2,500 m^2 of reflectors or twenty-two 12 m diameter concentrators.

4.1.3 Reflector Panel Fabrication

The manufacturing methods described in this section utilize present technology and existing facilities.

The steel sheet substrate is stretch formed. The advantages of stretch forming this part versus conventional press forming methods are:

1. About 70% less force is needed than for conventional methods;
2. Spring back is greatly reduced and is easily controlled by over forming,
3. Minimum residual stresses remain in the part after forming;
4. Because the entire part is stretched, uniform deformation occurs,
5. Accuracy of the formed parts is highly repeatable because of items 2, 3, and 4 listed above;

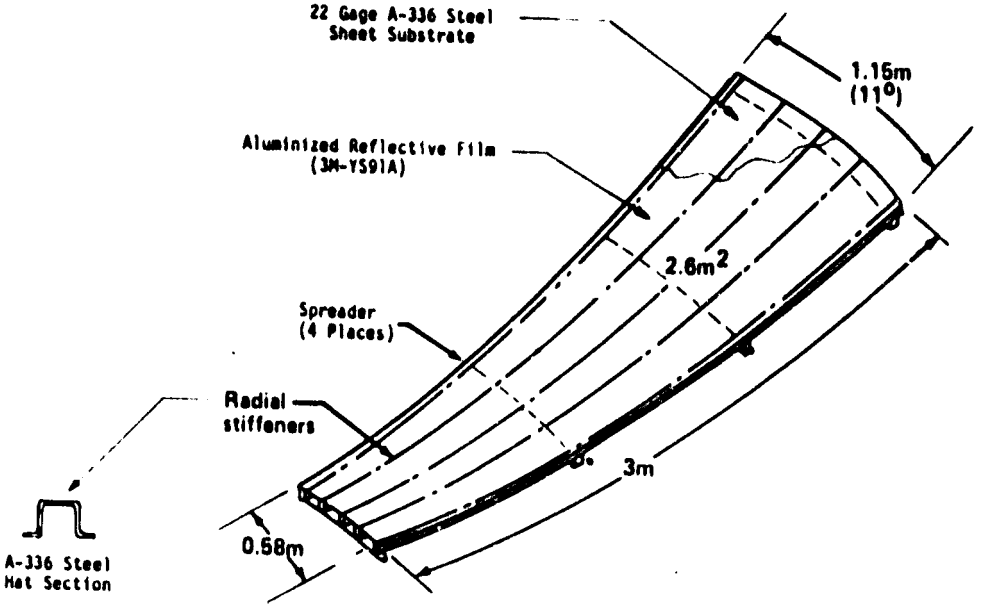

Figure 4.1.2-1 Reflector Panel Components

Table 4.1.2-1 Reflector Panel Material Usage and Costs

Material	LB/M²	$/Unit	$/M²
Reflective Film	1.9	0.60/ft²	6.80
Steel Sheet Substrate	14.2	0.27/lbs	3.80
Steel Hat Section Stiffeners	11.5	0.25/lbs	2.80
Acrylic Adhesive	0.1	8.0/lbs	0.80
Epoxy Primer	-	0.06/ft²	0.70
Polyurethane Paint	-	0.06/ft²	0.70
TOTALS	28.0		$16

6. Long die life results because there is no scuffing between the work piece and the die and relative movement is small.

Setup time required for stretch forming the part is a disadvantage when short runs are considered. However, for high production rates, the blank can be automatically loaded and unloaded. This automation step makes stretch forming competitive with other press forming methods.

The contour accuracy of the finished part depends directly on the contour of the forming die. Therefore, a comprehensive die design/development phase is required. The profile accuracy of the finish will be 0.25 mm (0.001 in) RMS. This will assure finished panels with 2 mrad or less slope errors.

The steel hat section stiffeners and spreaders are fabricated by first contour roll forming low carbon coil stock into the desired hat section shape. These hat sections are then parabolically contoured by stretch forming.

For small production lots, the formed steel parts will be spray primered after forming. For high production, the coil stock would be coil coated at the mill.

The primered stiffeners and spreaders are then positioned on the stiffener subassembly die (Figure 4.1.3-1) and fastened together by resistance spot welding the flanges of the spreaders to the hat section stiffeners. The combination of jigging and sequential spot welding provides a rigid stiffener subassembly without distorting the substrate mating flanges of the stiffeners.

The formed steel substrate is vacuum chucked down on an accurately contoured master tool (Figure 4.1.3-2). This smooths out any long period surface deformations. The stiffener subassembly is then bonded to the chucked substrate using a rapid cure structural acrylic adhesive. The rigidity of the stiffener subassembly maintains the assembled contour of the substrate after removal from the master tool.

The stiffener side of the steel panel assembly is then finish coated with a white 2-part polyurethane paint.

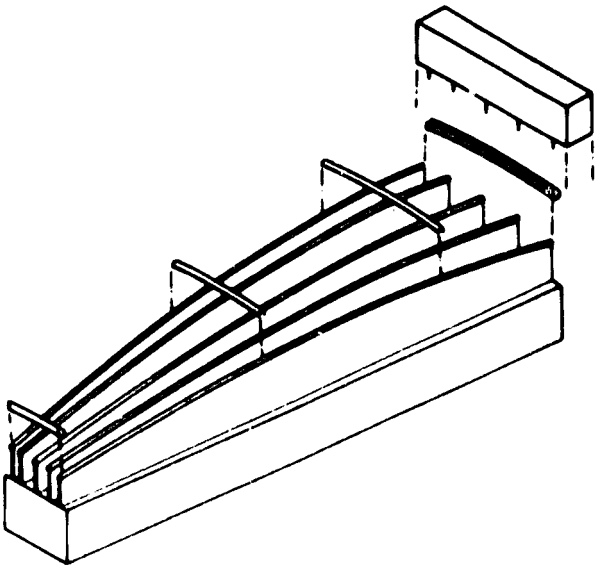

Figure 4.1.3-1: Stiffener Subassembly On Die

- Chucked Substrate Replicates Die Contour
- Stiffener Subassembly (Zero Stress State) Bonded to Substrate

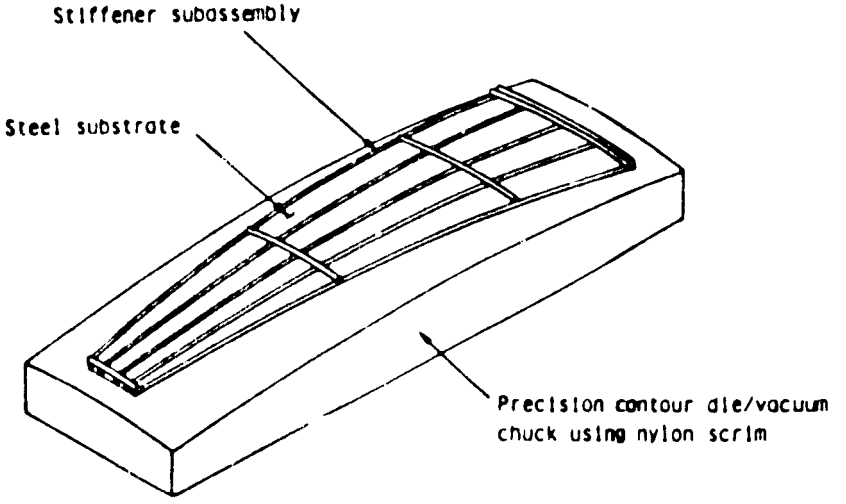

- Rigidity of Stiffener Subassembly Maintains Panel Substrate Contour After Die Release

Figure 4.1.3-2 Reflector Panel Assembly Master Tool

The desired degree of automation for applying the reflective plastic film is affected by production quantities. For prototype concentrator quantities, the film will be applied by hand using the wet application method described in Section 5.3. Some tooling will be designed to facilitate handling the film. This tooling could be refined and expanded on until production quantities warrant installation of an adhesive roll coater machine at the panel assembly facility. This would allow full automation of a dry film application process.

4.2 Structural Analyses

4.2.1 Model Configuration

Two panel configurations were chosen to be studied consisting of radial and circumferential stiffeners (Figure 4.2-1). These two configurations were modeled in sufficient detail (see Figure 4.2-2) to calculate slopes and deflections (deflection analysis) and stresses (strength analysis) for various external loading conditions utilizing the NASTRAN computer program. The external loading conditions applied to the NASTRAN finite element model were wind, gravity, thermal, snow, ice, and seismic (see Table 4.2.1). The wind condition chosen for the panel analysis was a head-on wind that produces a constant wind pressure on the panel. This wind condition is the most severe for a panel but is not necessarily the most severe for a total concentrator. The thermal analysis was based on a temperature difference between the skin and stiffener structure of the panel.

Trade Studies

The slope error of the panels compared to the design slope is critical on point focus concentrators since it directly affects the efficiency of the concentrator. The slope error must be minimized and cannot exceed 1.52 milliradians RMS from the effects of environmental loads. A trade study was performed to evaluate the radial and circumferential stiffener configurations with respect to the slope variations of the two configurations. In order to directly compare the results, the edge condition for both configurations were identical and was chosen to be fixed on the perimeter of the panels. Table 4.2-2 presents the results of this trade study for a

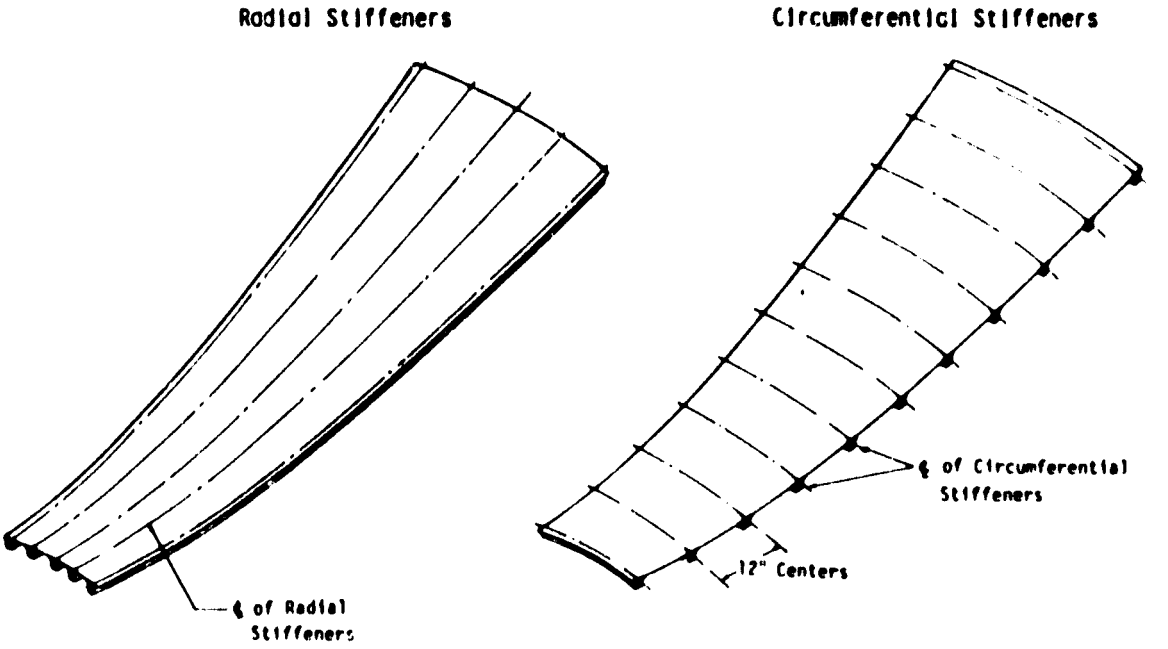

Figure 4.2-1 Model Configurations

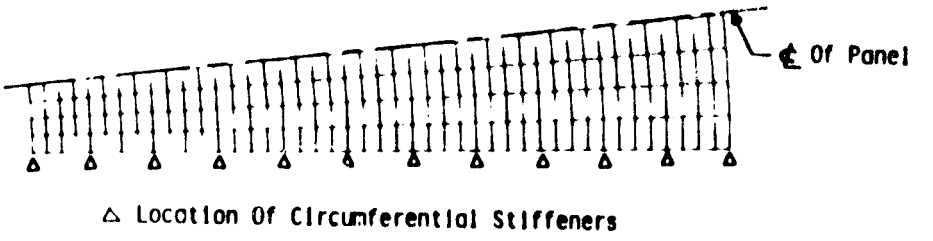

Radial Stiffener Model

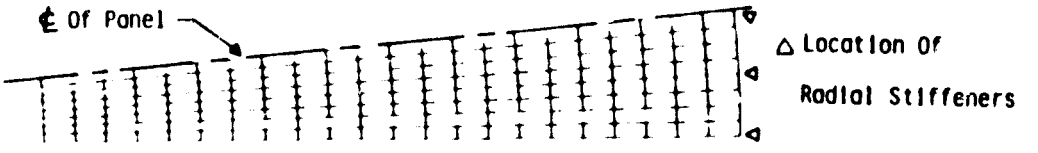

Figure 4.2-2 Finite Element Models

Table 4.2-1 - External Loading Condition

	Deflection	Strength
Wind (uniform pressure load) Cp = 1.4	14 m/s (31 mph) p=165Pa (.0239 psi)	42 m/s (93 mph) p=1482 Pa (.215psi)
Snow		50 cm (19.7 in) p=614 Pa (.089 psi)
Ice		1.0 cm (.3937 in) p=89.6 Pa (.013 psi)
Seismic		$\pm$ .25 g's
Thermal	ΔT between skin and stiffeners	ΔT between skin and stiffeners
Gravity	1 g	1 g

Table 4.2-2 - Stiffener Trade Study (fixed edges)

	RMS Slope Error - Radians	
	Gravity	Wind (14 m/s)
Circumferential	$.353 \times 10^{-3}$	1.067×10^{-3}
Radial	$.205 \times 10^{-3}$	$.63 \times 10^{-3}$

gravity and wind external loading condition. The results show that a radial stiffened panel is superior to the circumferential stiffened panel in minimizing the slope error. However, both the radially and the circumferential stiffener slope errors are below the maximum allowed error.

From the trade study of the stiffener configuration, the radial stiffener configuration was chosen as the candidate configuration for further trade studies. A trade study was conducted to evaluate the support configuration in minimizing slope errors and determination of its strength capabilities. Several support conditions were evaluated consisting of (1) fixed edges, (2) fixed inner and outer circumferential edges, and (3) fixed inner edge and outer support at 0.6 m inward from the outer circumferential edge. Table 4.2-3 shows the slope error results and Table 4.2.4 shows the maximum stresses to be expected in the panel. The minimum RMS slope on the panel was for fixed edge boundary conditions except for the thermal loading condition. The largest RMS slope was for the third support condition.

Although this latter boundary condition yields the largest slope error, it may be the most economical for a total concentrator since the support structure should be lighter than when the outer support is on the concentrator perimeter. The maximum stress in the panel is well below the allowable tensile stress for steel and compressive stresses are within buckling allowables. Consequently, the panel stiffness, rather than strength, is critical.

In conclusion, the structural analysis determined that the rms slope error for a panel with circumferential stiffeners was larger than for a panel with radial stiffeners assuming the same boundary constraints and external loading conditions. The resulting stresses for either panel-stiffener combinations were well below design allowables indicating that the structure is designed by stiffness requirements. The boundary constraints (support configurations) has some effect on the rms slope errors. However, assuming an allowable rms error of 1.52 mrad, there is flexibility on the location and type of support configurations.

Table 4.2-3 - Support Configuration Trades

o Radial Stiffeners

	RMS Slope Error - Radians		
	Gravity	Temperature	Wind (31 mph)
Fixed Edges	$.205 \times 10^{-3}$	$.546 \times 10^{-3}$/ °F	$.630 \times 10^{-3}$
Fixed Inner and Outer Circumferential Edges	$.235 \times 10^{-3}$		$.924 \times 10^{-3}$
Fixed Inner and 0.6m from Outer Circumferential Edge	$.289 \times 10^{-3}$	$.297 \times 10^{-3}$/ °F	1.027×10^{-3}

Table 4.2-4 - Maximum Panel Stresses

o Maximum Stress Due to Wind at 42 m/s

	Stress Mpa (psi)		Stiffener and Support Configuration
	Gravity	Wind	
Panel Skin	1.96 (284)	3.26 (473) 7.15 (-1037)	Radial stiffener supported at inner circumferential edge and at 0.6m. in from outer circumferential edge.
Stiffener	3.45 (501)	50.6 (7337)	

Allowable (steel) = 155 MPa (22500 psi)

4.3 Optical Performance Analysis

4.3.1 Analysis Method

Performance, as measured by net energy into the receiver aperture of the candidate substrates, was analyzed with the aid of a discrete ray tracing computer model (SPLOID). The model treats the various geometrical, optical, and system parameters that are important to performance. The analytical method incorporated in the model is an extension of previous BEC modeling of parabolic mirrors (LOID code). Recent updates to the code allow it to consider image shape, surface specularity profiles, and laser ray trace (angular deflection) profiles, in addition to surface and pointing errors.

Prior to implementing the performance code, the combined effect of the sun's image, surface specularity profile, and laser ray trace deflection (orange peel) profile is determined. The following paragraphs describe the analytic process involved.

Consider an x,y coordinate system in the plane perpendicular to the optical axis of the reflected central unperturbed beam originating from the solar disk. Assume a circular isotropic intensity distribution over the solar disk which is given in the x,y plane by:

$$I(x,y) = i(\sqrt{x^2 + y^2})$$

$I(x,y)$ has its highest value at $(0,0)$ and falls concentrically off to zero as $\sqrt{x^2 + y^2}$ becomes large.

Taking an unperturbed beam from the sun, let its position be (x,y) in the x,y plane. Now consider this location being perturbed by a vector (u,v) which is assumed to have a circular isotropic density in the x,y plane given by:

$$g(u,v) = \rho(\sqrt{u^2 + v^2})$$

This density combines the perturbation effects of surface specularity and reflectivity irregularities. The location of th perturbed beam will then be:

$$(s,t) = (x + u, y + v)$$

The intensity at (s,t) is then given by:

$$j(s,t) = \iint g(s-x,\ t-y)\ I(x,y)\ dxdy$$

The perturbation (u,v) is itself the sum of two perturbation vectors:

$$(u,v) = (u_1,\ v_1) + (u_2,\ v_2)$$

$(u_1,\ v_1)$ has density $g_1(u_1,\ v_1) = \rho_1(\sqrt{u_1^2 + v_1^2})$ which portrays the deflection due to mirror surface specularity.

$(u_2,\ v_2)$ has density $g_2(u_2,\ v_2) = \rho_2(\sqrt{u_2^2 + v_2^2})$ which portrays the deflection due to mirror reflectivity irregularities (laser ray trace data - angular deflection).

Then, $g(u,v) = \iint g_1(u-u_2,\ v-v_2)g_2\ (u_2,\ v_2)\ du_2dv_2$

Converting to cylindrical coordinates to take advantage of symmetry, the overall intensity profile becomes a four fold integral which is modeled using a Riemann sum approximation. The intensity distribution can then be input to the performance prediction code. Figure 4.3-1 summarizes the steps of the image analysis.

The performance model is based on a discrete idealization of the reflector. A grid is projected onto the parabolic reflector dividing it into equal area elements. The unit normals for each element are rotated according to surface slope and tracking errors. A cone of light is simulated by rays clustered around the unit normal. The energy represented by each ray is dictated by the reflected image analysis. The cone of light is then projected onto the focal plane (see Figure 4.3-2). Intercept factors and net useful thermal energy are then calculated for various aperture diameters.

- Combine Effects Of:
  - material specularity
  - surface reflectivity
  - solar intensity profile
- Differentiate and Convolute
  - material specularity
  - surface reflectivity

  to Determine the Combined Energy as a Function Cone Angle
- Convolute the Combined Energy Density Function with the Solar Intensity Profile to Find the Reflected Light Intensity Profile
- Approximate Convolutions with Riemann Sums

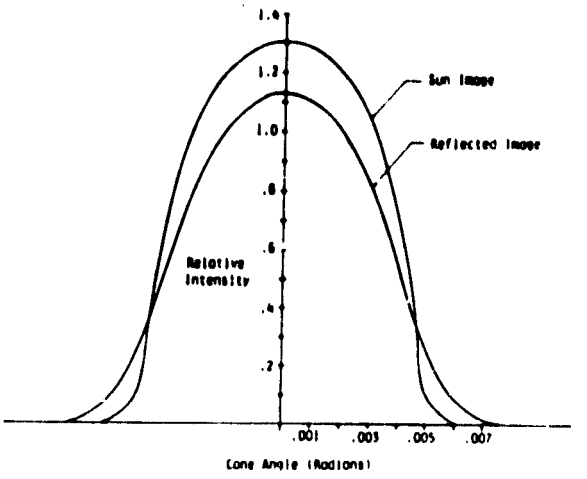

Figure 4.3-1 Reflected Image Analysis

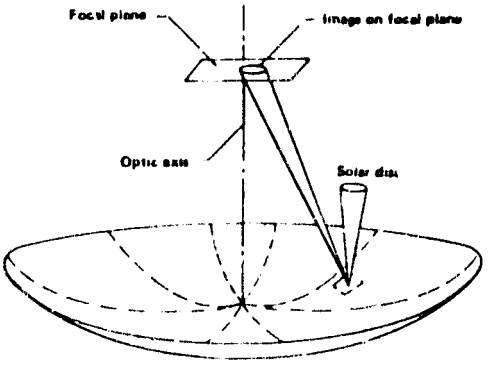

- Energy distribution of reflected light from table look-up of reflected image analysis data
- Model reflected light by cone of rays originating from section of concentrator
- Surface normal of cone of light is perturbed for surface and pointing errors
- Results
  - Intercept factor
  - net useful thermal energy

Figure 4.3-2 Concentrator Performance Analysis

4.3.2 Analysis Results

Computer simulations were run for the concentrator using the selected reflector panel design. Experimentally determined values for reflector surface specularity and reflectivity were used, as well as dimensional data, as input to the computer program. The simulations provided intercept factor curves and curves of net energy to the aperture as a function of aperture size for different surface errors and pointing errors.

Figures 4.3-3 through 4.3-8 are plots of analyses for a 12 meter diameter concentrator with 1000 W/m^2 insolation. Inputs to the analyses included sun shape, hemispherical reflectance and specularity experimentally determined in coupon tests, "orange peel", zero pointing error and 3 receiver temperatures; 815°C, 590°C and 370°C. The net energy curves include reradiation losses from the receiver at the specified receiver temperature and aperture size. Three or more curves are provided on each plot to show the effects of surface error on performance.

The curves for the 815°C case (Brayton cycle) suggest that a surface error of 2 mrad or less will be required to capture the desired 80 kW of thermal energy. As the surface errors increase, the net energy rapidly drops off. This sensitivity to surface error is seen to decrease with the lower receiver temperatures (Figures 4.3-6 and 4.3-8), indicating that greater surface errors could be tolerated on lower temperature systems. For example, at 815°C (in Figure 4.3-4), a peak energy of about 82 kW would be achieved with a 2 milliradian surface error, while at 370°C (Figure 4.3-7), 82 kW would be achieved with about 7 mrad surface error. Therefore, in meeting the low surface error requirements of the high temperature receiver, a concentrator design is created that exceeds the requirements of lower temperature systems.

Figure 4.3-4 shows that surface errors of 1 mrad or lower would add a few percent to the energy collected, provided the aperture diameter is reduced from .25 m (the optimum for 2 mrad surface error) to 0.175 m. However, the effects of pointing error and structural deflections also should be considered. At a 2 mrad pointing error (Figure 4.3-9), the 2 mrad surface

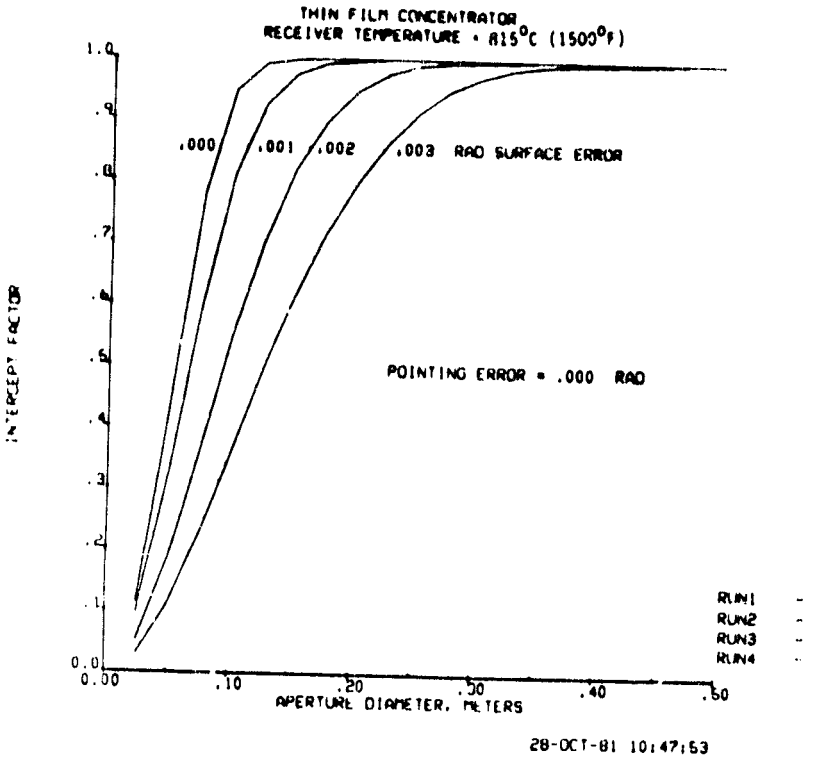

Figure 4.3-3 Intercept Factor Curve 815°C (1500°F)

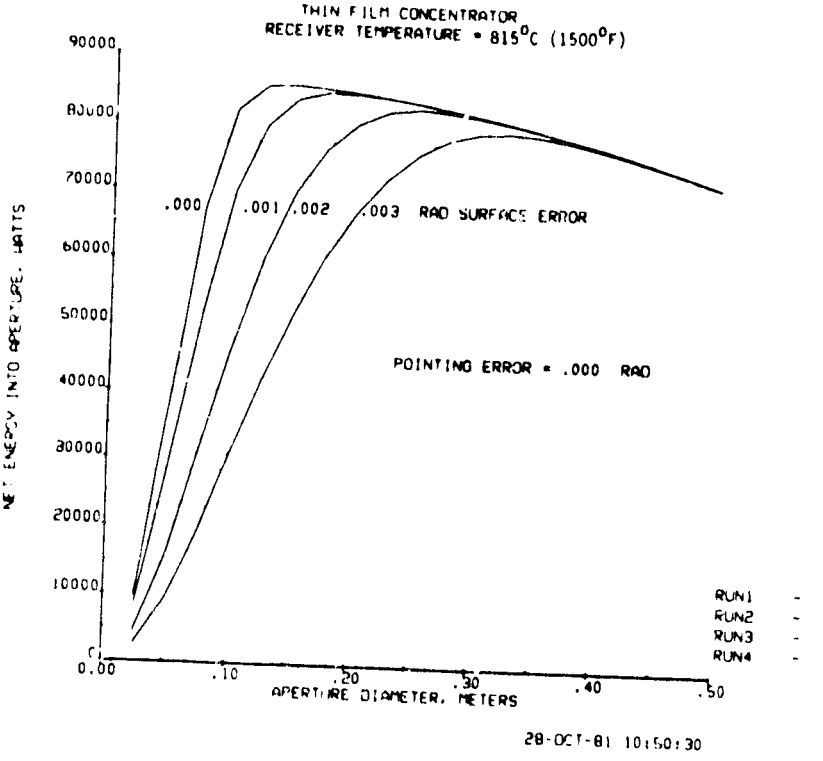

Figure 4.3-4 Net Energy Curve 815°C (1500°F)

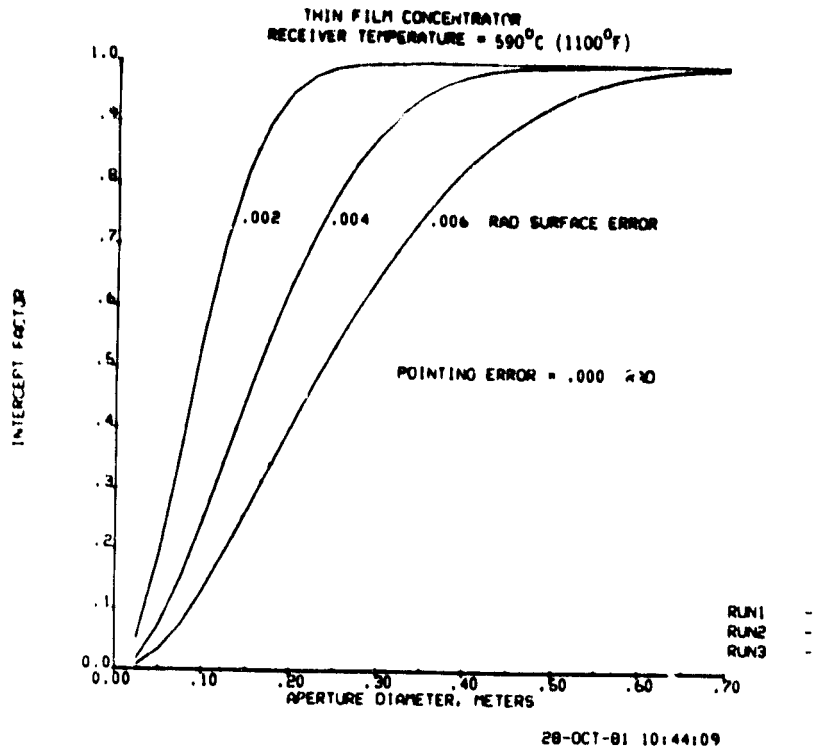

Figure 4.3-5 Intercept Factor Curve 590°C (1100°F)

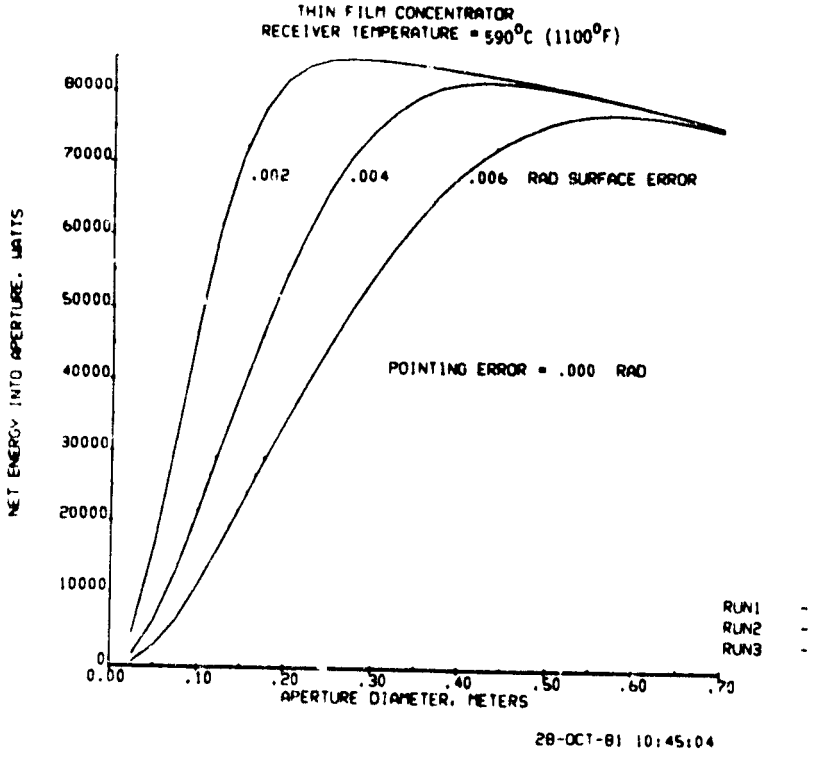

Figure 4.3-6 Net Energy Curve 590°C (1100°F)

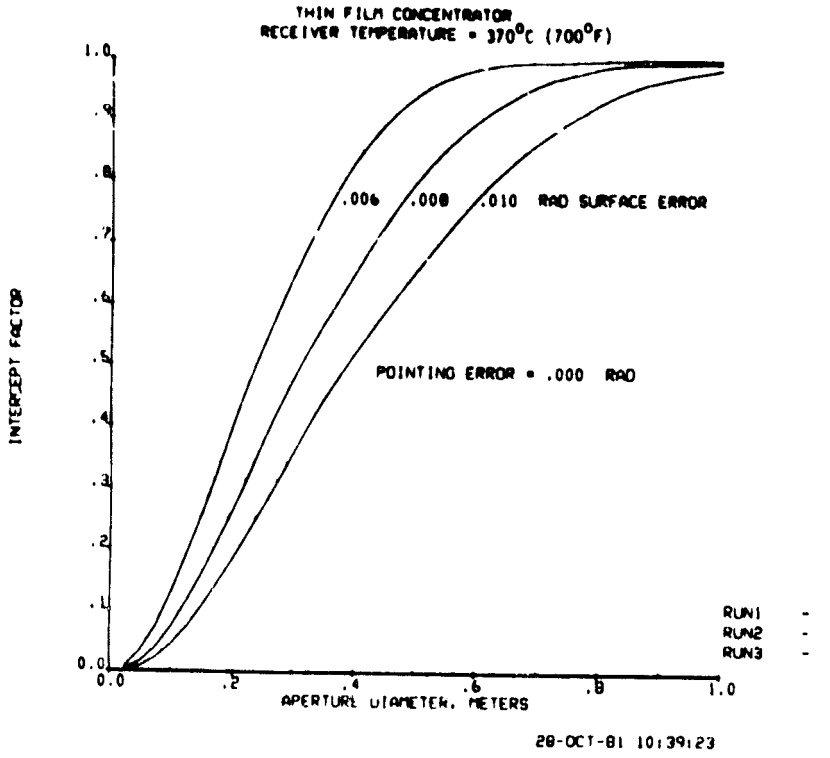

Figure 4.3-7 Intercept Factor Curve 370°C (700°F)

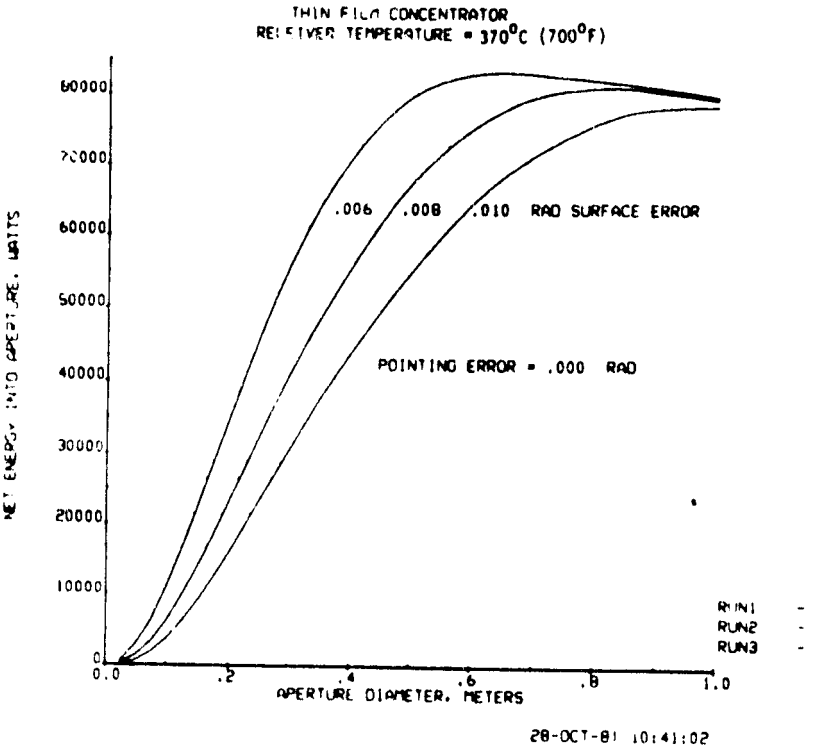

Figure 4.3-8 Net Energy Curve 370°C (700°F)

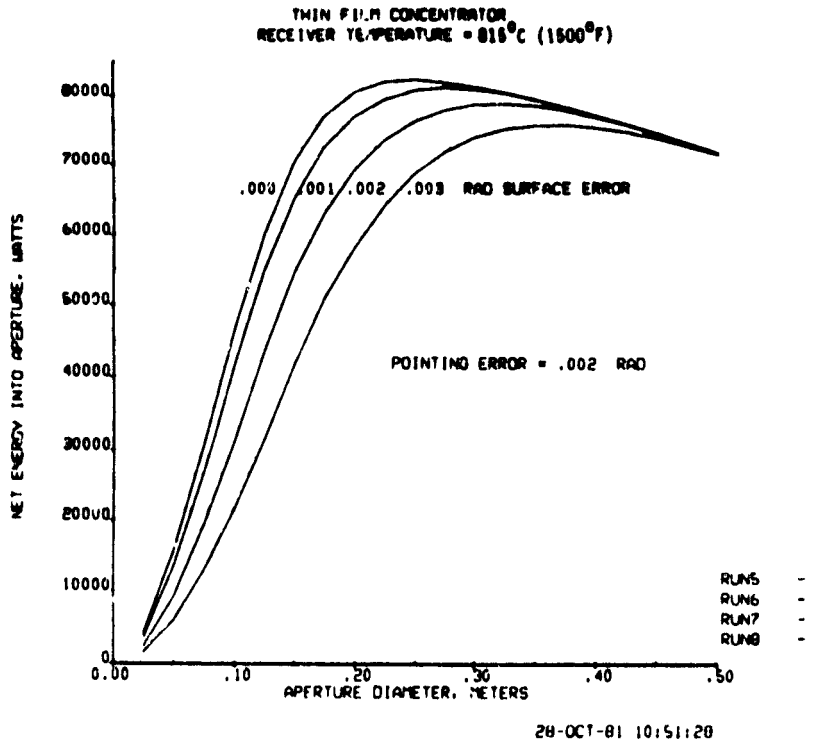

Figure 4.3-9 Net Energy Curve 815°C (1500°F)

error/.25 m aperture drops to 76 kW, but the 1 mrad surface error/.175 m aperture drops even more to 73 kW. Selecting the larger aperture not only permits more surface error but is also less sensitive to other errors. Referring to the bottom figures in Table 4.2-3, it is apparent that some allowance should be given to gravity and temperature deflections. If .5 mrad of the 1.52 mrad budgeted for environmental effects is assigned to these effects, which would be present much of the time, then the manufactured panel error budget should be reduced to 1.5 mrad to achieve a 2 mrad total. Variable deflections due to wind loads will further degrade performance. For the average wind speed in Figure 3.1-7 (about 3 m/s) the equivalent panel surface error will be negligible. At higher wind speeds the concentrator truss deflection will have a significant effect on optical performance. This effect is not shown but it can be concluded that losses would be lower at larger aperture sizes.

Based on these factors it is concluded that (1) achieving panel optical performance suitable for a Brayton cycle would also meet the needs for lower temperature applications, (2) a budget of 1.5 mrad RMS surface error or less for panel manufacturing tolerances is acceptable, and (3) the aperture diameter should be at least .25 m to reduce sensitivity to other errors.

5.0 TEST PANEL DEVELOPMENT

5.1 General

This work concerned the design and fabrication of two panels and the testing of these panels. Test results show that reflectorized plastic film on sheet steel substrates is a feasible design for low cost reflectors. These reflectors are suitable for 816°C (1500°F) concentrator designs. The accumulative RMS optical errors associated with the reflective surface geometry of the test panels were 1.7 mrad for one and 2.2 mrad for the other. There were no fabrication problems or additional technology requirements identified. A tolerancing rationale and inspection method was developed for future metal parts. The finished test panels are shown in Figure 5.1-1.

5.2 Test Panel Design

The test panel design represents a section of a full size parabolic gore reflector. It uses the same stiffener configuration, and its spherical radius of curvature closely matches the parabolic curvature midway on the full size panel. The design is depicted in Figure 5.2-1.

The overall dimensions of the test panel, 60 x 70cm and its 6.45m focal length match those dimensions of the JPL, glass/foamglas test bed concentrator panels. This was done to facilitate testing by JPL.

The test panel design uses the materials and processes selected at the conclusion of the coupon development work described in Section 3.0. The test panel stiffener design and spacing was established based on stress analysis for the full size parabolic gore reflector.

Conventional dimensioning and tolerancing were applied to the detail parts and assembly. A $\pm$.38 mm (0.015 in) profile tolerance was placed on the contoured steel sheet surface.

5.3 Test Panel Fabrication

The test panels were fabricated using the techniques and processes selected at the conclusion of the coupon development work. No special attention or

ORIGINAL PAGE
BLACK AND WHITE PHOTOGRAPH

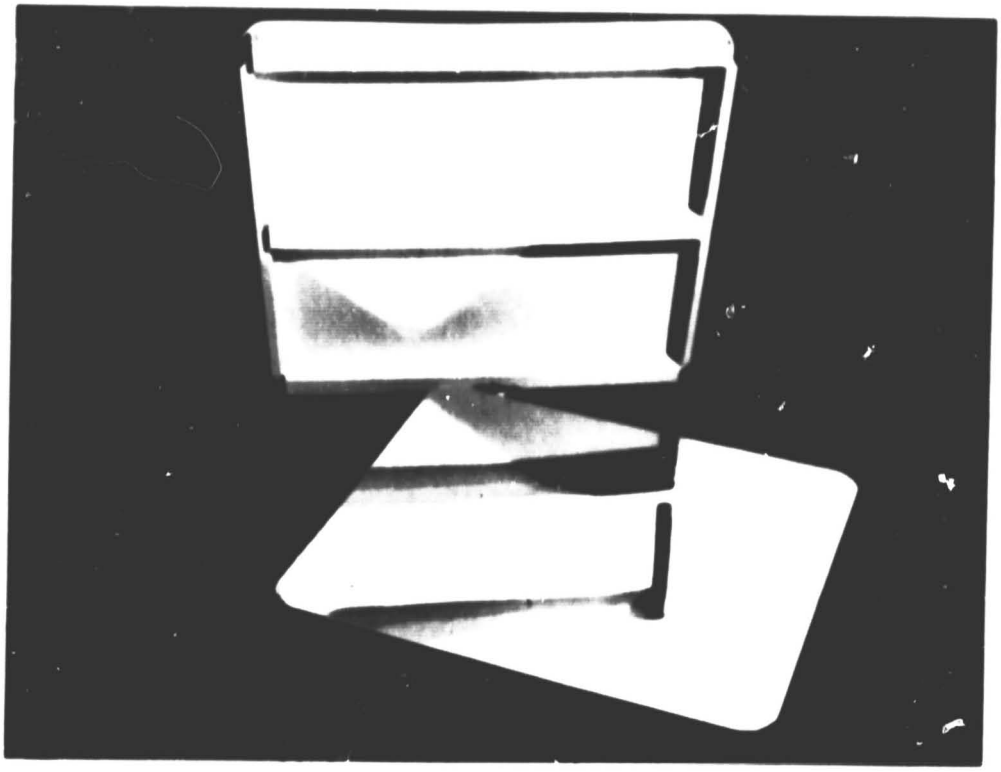

Figure 5.1-1 Test Panels SN-7 and SN-10

- Basic Components
  - Reflective film
  - Steel sheet 22 gage, ASTM-A620
  - Hat section stiffeners
  - Tube end stiffeners
  - Structural adhesive
- Reflective Area
  - 0.4 M^2 (4.3 ft^2)
- Assembly Weight
  - 11.0 lbs calc.

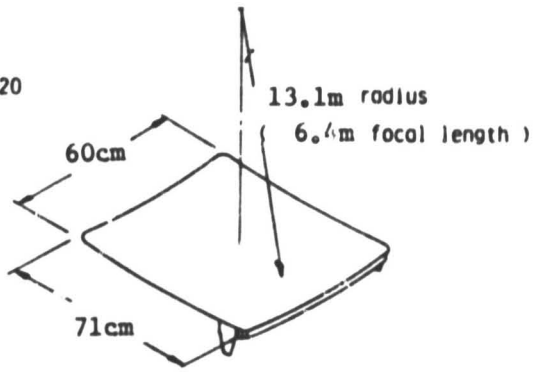

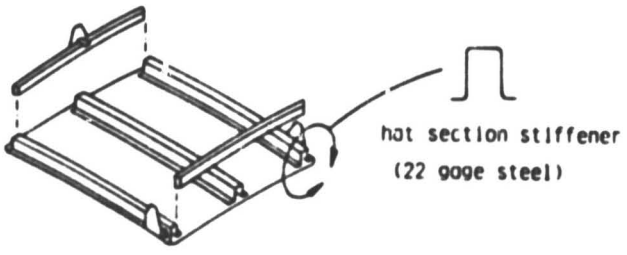

Figure 5.2-1 Test Panel

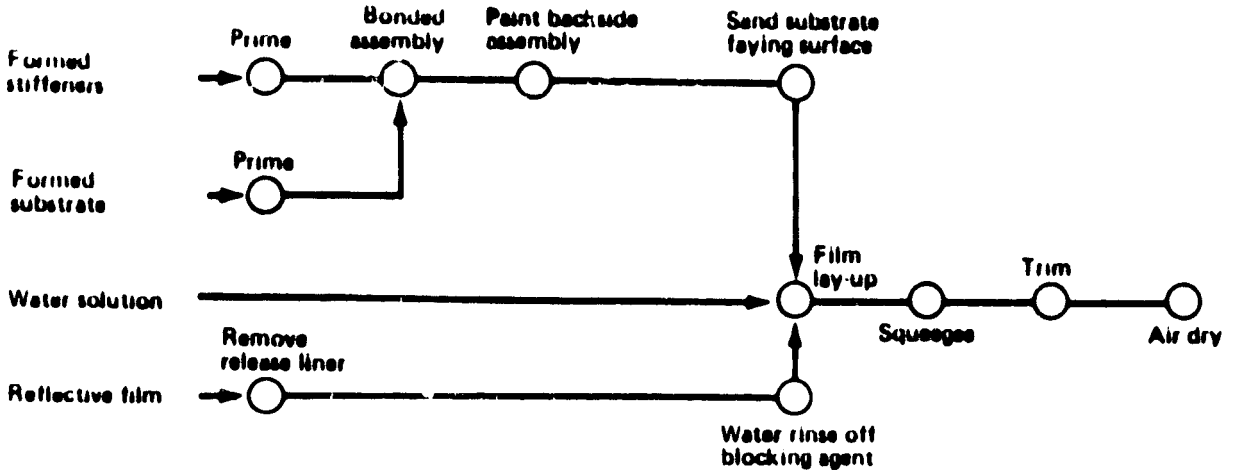

Figure 5.3-1. Development Panel Assembly *Steps*

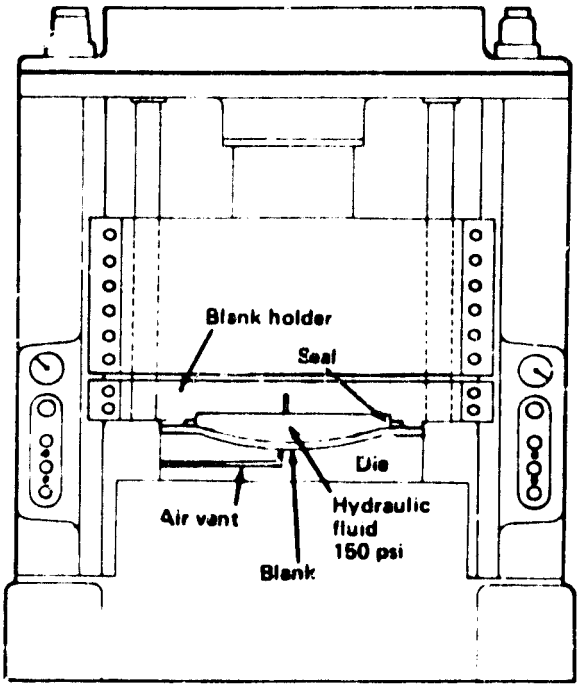

Figure 5.[illegible].2-1 Hydraulic Bulge Forming

methods were required to bond the film to the compound curvature of the substrate. The fabrication sequence is shown in Figure 5.3-1.

5.3.1 Steel Sheet Substrate

1 meter square blanks were sheared from sheet stock and hydraulic bulge formed using a die with a 5.5m spherical radius of curvature, see Figure 5.3.2-1. An abrasive cutting wheel was used to cut out the finished formed blank. The radius of curvature in the forming die was changed three times to adjust the radius of curvatures on the formed part. This is the normal procedure required to achieve accurate forming when springback occurs.

The finished blanks were cleaned to a water break free surface using a vapor degreaser and warm water rinse cycle. The parts were then primered with a zinc rich two-part epoxy primer and oven-baked at 150°C (300°F) for one hour.

5.3.2 Steel Hat Section Stiffeners

The stiffener cross section shape was fabricated by brake forming. The radius of curvature was formed by hand using a mechanical press and roller blocks. After forming the stiffeners were cleaned and primered using the same methods described for the steel sheet substrate, Section 5.3.1.

5.3.3 Stiffener Subassembly

The stiffener subassembly was fabricated by positioning the stiffeners and close-out tubes on the master tool. The parts were then drilled and fastened. This method of fabrication resulted in a stress free stiffener subassembly (Figure 5.3.3-1).

5.3.4 Master Tool

A master tool with a 13.1 meter spherical radius of curvature was fabricated from a steel round. This tool was used for checking parts, fabricating the stiffener subassembly and final assembly of the reflector steel components.

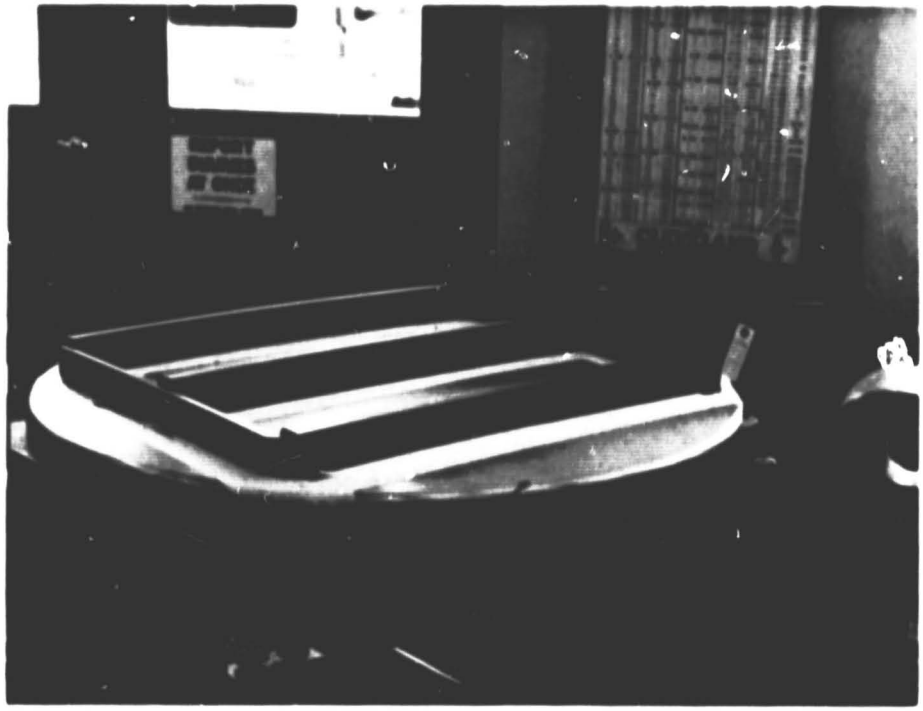

Figure 5.3.3-1 Stiffener Sub-Assembly

5.3.5 Substrate/Stiffener Frame Assembly

Figure 5.3.5-1 shows the steel sheet substrate vacuum chucked to the master tool and the stiffener frame assembly being placed on top. This method of assembly provided precision contour control of the substrate. Figure 5.3.5-2 shows the structural adhesive being applied to the substrate, a gap filling epoxy adhesive was used. The hand formed faying surfaces of the stiffeners were not accurate enough to allow using a thin bond line acrylic adhesive as originally planned. Figure 5.3.3-1 shows the bonded assembly curing on the master tool. No clamps or weights were used to hold the stiffener frame, so that no residual stresses would be induced in the frame. After the 24 hour cure the bonded assembly was painted with a white 2-part polyurethane paint on its frame side. The primered reflective film faying surface of the substrate was lightly sanded using 400 grid wet/dry paper.

5.3.6 Reflective Film Application

3M's wet film application method was used. Figure 5.3-1 lists the process steps. Figures 5.3.6-1, -2, -3, -4, -5, and -6 are photographs of the film application process steps.

Figure 5.3.5-1 Substrate Sheet Vacuum-Chucked to Master Tool

Figure 5.3.5-2 Adhesive Application

Figure 5.3.6-1 Removal of Release Liner

Figure 5.3.6-2 Rinse of Blocking Agent

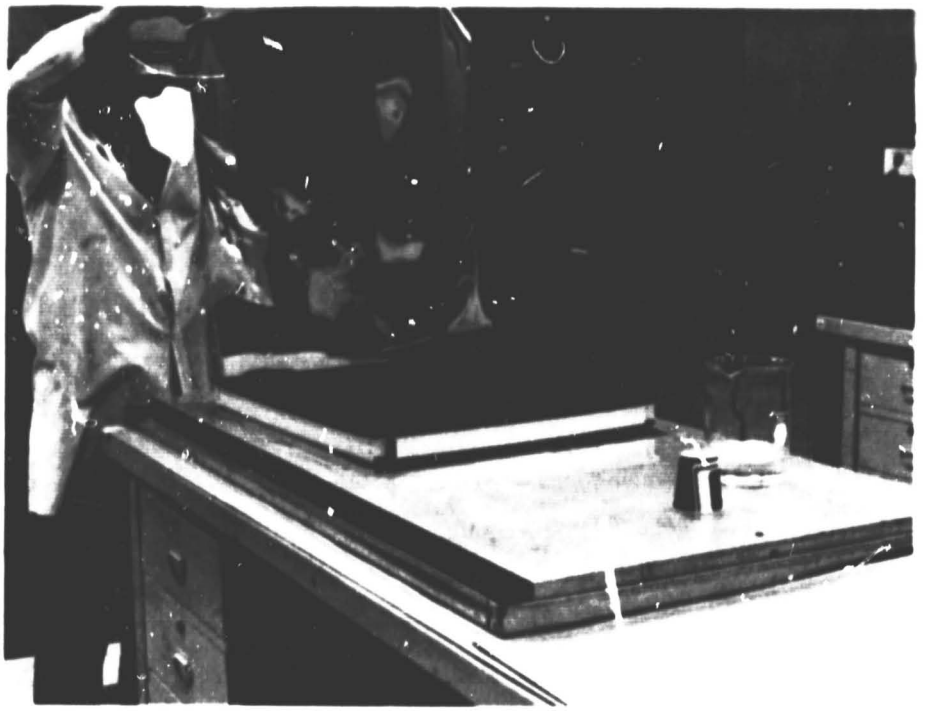

Figure 5.3.6-3 Film Layup

Figure 5.3.6-4 Removal of Water with Squeegee

C-2

5.4 Test Panel Evaluation

This section of the report presents the test and evaluation program that was performed on the two test panels. Test purposes, procedures, and results are presented for optical tests using both point source and sun source approaches. A test was also conducted on one of the test panels to determine the effects of temperature upon the image quality. Data from the two optical tests are compared with analyses and with each other for validation.

5.4.1 Evaluation with Point Source

5.4.1.1 Purpose of Testing

The purpose of this test was to measure the radius of curvature and surface error distribution for each of the test panels.

5.4.1.2 Method

The technique used was similar to the one developed by M. Argoud as described in Reference 5-1. The optical apparatus uses a point source geometry where the source and target lie in the same plane which is located at a distance equal to the radius of curvature from the test panel. Figure 5.4-1 is a schematic of the apparatus used for this work.

A 1.3 cm (0.5 in) diameter carbon arc source was used. The source was located outside the light tight enclosure, which was provided to shield the test panel and target optics from stray light. Light from the source was directed down the length of the enclosure via a folding mirror. The test panel then returned the light to the target plane. The distance between the source centerline and the target centerline at the source/target plane was approximately 61 cm (24 in).

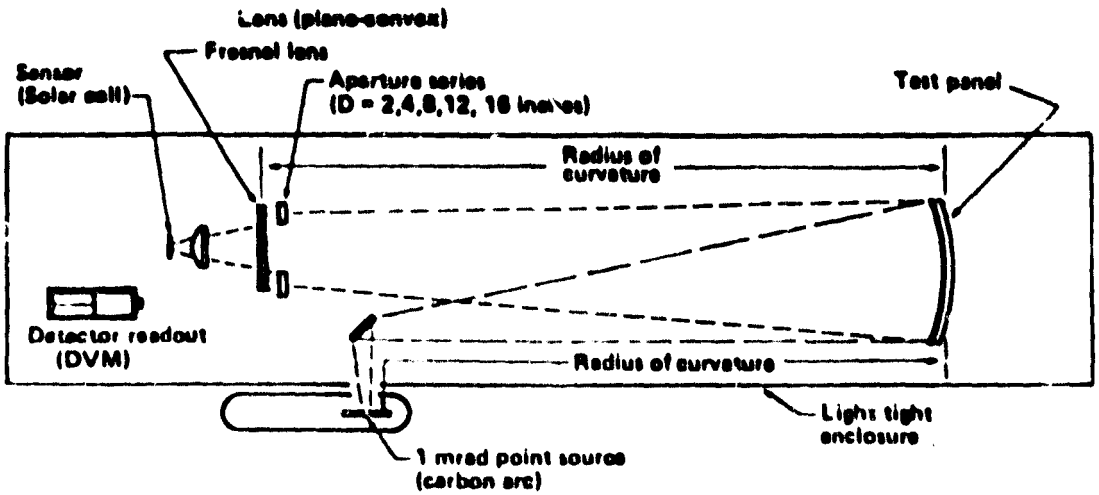

Figure 5.4-1 Point Source Panel Evaluation Apparatus

The target plane consisted of a frame that supported a 46 x 61 cm (18 x 24 in) fresnel lens and a set of removable apertures. The lens used had a focal length of 56 cm (22 in). A second lens (plano-convex) was positioned at the fresnel lens focal point to further reduce the image size to well below the outer dimensions of the photovoltaic detector. Response from the detector, in millivolts, was read out on a digital volt meter. Figures 5.4-2, -3 and -4 are photographs of the point source optical apparatus. Figure 5.4-5 is a plot of the detector output versus light level in a calibration facility, showing the linearity of the instrument.

5.4.1.3 Procedure

Radius of Curvature

The test panel was mounted on a support fixture equipped with wheels. The panel could be moved forward or backward along axis of the enclosure, while keeping its aim point on the target approximately fixed. A clean, white surface was positioned at the target plane. Next, the carbon arc source was illuminated. The test panel was positioned at a distance from the target plane approximately equal to the anticipated radius of curvature. The panel was then slowly moved forward down the tunnel while observing the image shape

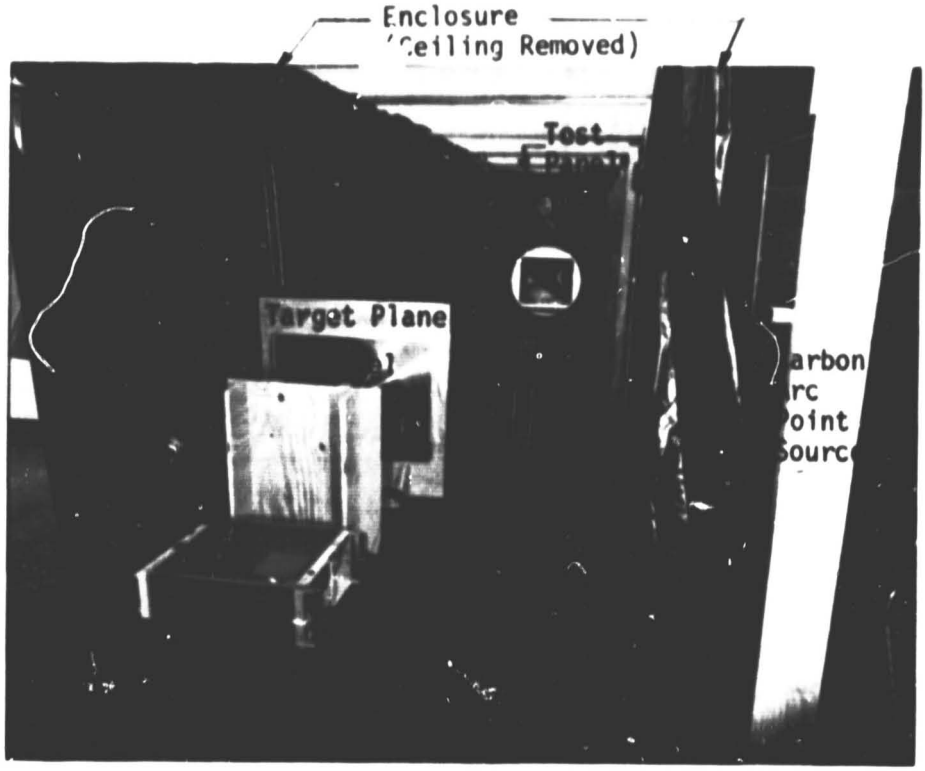

Figure 5.4-2 Point Source Optical Elements

Figure 5.4-3 Target Plane, Lenses and Detector Readout

Figure 5.4-4 Lens and Photovoltaic Sensor

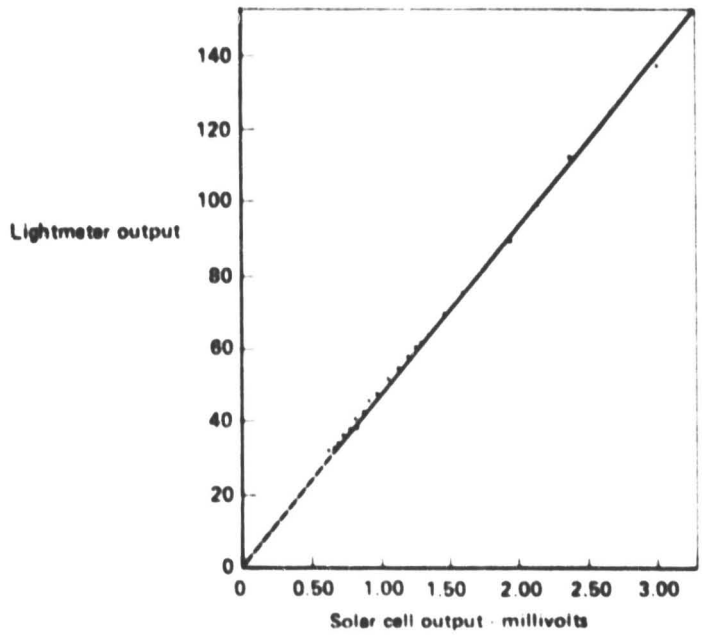

Figure 5.4-5 Solar Cell Linearity Check

on the target surface. Then the panel was moved in reverse, up the tunnel, while observing the image shape. This process was repeated until a position was obtained where the image diameter was observed to be a minimum. A tape measure was used to measure the distance from the panel to the target plane. This distance is the radius of curvature.

Surface Error Distribution

The test panel was positioned at the measured radius of curvature and adjusted so that the reflected image was placed approximately on the centerline of the target plane. The aperture series, consisting of 5 cm (2 in), 10 cm (4 in), 20.5 cm (8 in), 30.5 cm (12 in), and 40.5 cm (16 in) diameter holes cut from the cardboard sheets was installed. These apertures were arranged on hinge lines so that they could be sequentially positioned one after the other over the Fresnel lens. The centers of the aperture were coincident with the center of the Fresnel lens and the centerline of the optical train. The aperture sizes were selected to cover the range of wide open (collects all light) down to about 1 mrad of surface error. Individual apertures allowed only light rays included within the cone angle defined by the aperture to be passed through the lenses. These rays were concentrated on the sensor by the lenses and quantified by the digital voltmeter (DVM). By observing the sensor response for each aperture and normalizing the results to the wide open aperture result, a surface error curve was generated. This curve provided information about what percentage of the total image was contained in each surface error panel. Further data manipulation resulted in intercept factor curves.

5.4.1.4 Test Results

Radius of Curvature

The radii for the test panels were measured to be:

Panel SN7: 13.11 m (516 in)
Panel SN10: 12.80 m (504 in)

The repeatability of the measurements was found to be ± 30.5 cm (12 in), or ± 2.4%.

Surface Error Distribution

The error distributions were determined by taking a number of aperture series data sets for each panel and finding the averages and standard deviation (1σ) error bands. Gradual drifting in the output of the carbon point source would occur resulting in an eventual reduction of the peak output. It was determined that no significant drifting occurred during a single series of readings. Since each series was normalized to maximum output, effects of drift on series-to-series data were eliminated.

Table 5.4-1 summarizes the data taken for panels SN7 and SN10. Twenty-three sets of data were taken for SN7 and 8 sets for SN10. The same data is plotted in Figures 5.4-6 and 5.4-7.

Computer simulation of the test panels was performed. Assuming a 1 mrad point source at infinity and using the specularity from the coupon test, intercept factor vs. aperture angle curves were generated. Curves for 0, 1 and 2 mrad surface error are shown as the solid lines in Figure 5.4-8. Test data for SN7 and SN10 are also shown. Comparison of analysis and test data clearly indicates that the 1σ surface errors for these two panels are between 1 and 2 mrad. To obtain a closer estimate, the intercept factor curves are linearized, assuming the curves can be adequately represented by an error function:

$$\bar{Q} = 1 - e^{-\frac{R^2}{2\sigma_o^2}}$$

where $\bar{Q}$ = intercept factor
R = aperture radius (mrad)
σ_o = standard deviation of the function

As shown in Figure 5.4-8b, the analytical curves conform very well up to intercept factors of .98 or so. The slope of these curves is equal to σ_o^{-2}.

A correlation between σ_o and panel surface error is obtained by plotting the analytical data as shown in Figure 5.4-8c. It is evident that the computer

Table 5.4-1: Point Source Surface Error Test Data

APERTURE DIAMETER CM (INCHES)	SN 7			SN 10		
	APERTURE RADIUS MR	NORMALIZED OUTPUT		APERTURE RADIUS MR	NORMALIZED OUTPUT	
		$\bar{x}$ (AVG)	σ (STD DEV)		$\bar{x}$ (AVG)	σ (STD DEV)
5.08 (2.0)	1.9	0.268	± 0.0044	2.0	0.175	± 0.002
10.20 (4.0)	3.9	0.728	± 0.014	4.0	0.560	± 0.009
20.30 (8.0)	7.8	0.968	± 0.021	7.9	0.958	± 0.015
30.50 (12.0)	11.6	0.984	± 0.017	11.9	0.987	± 0.012
40.60 (16.0)	15.5	1.000	± 0	15.9	1.000	± 0

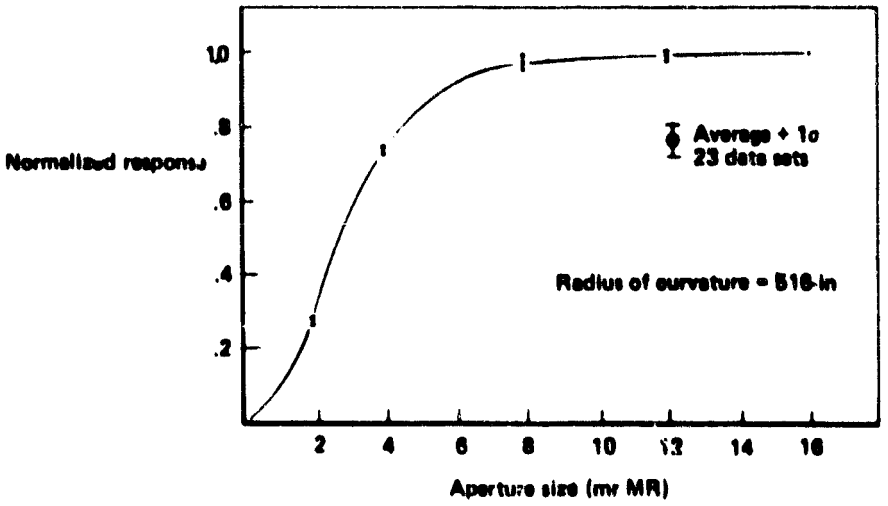

Figure 5.4-6 Mirror No. 7 Point Source Test Data

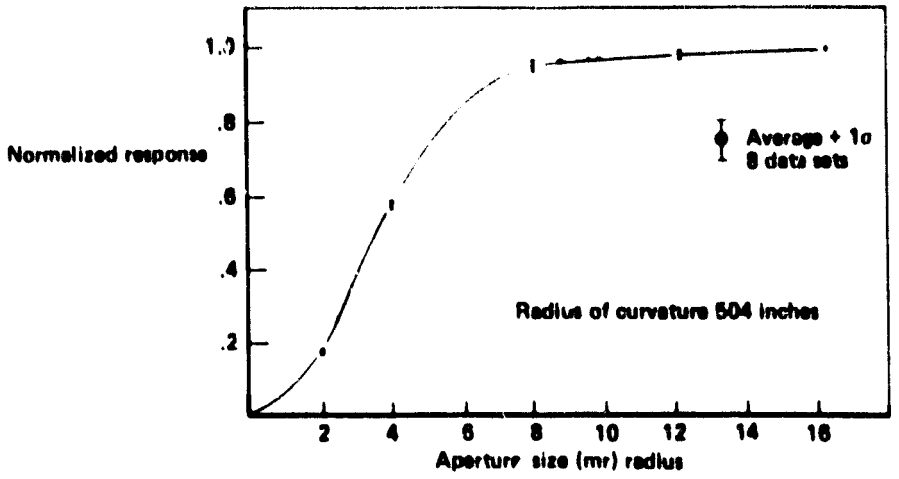

Figure 5.4-7 Mirror No. 10 Point Source Test Data

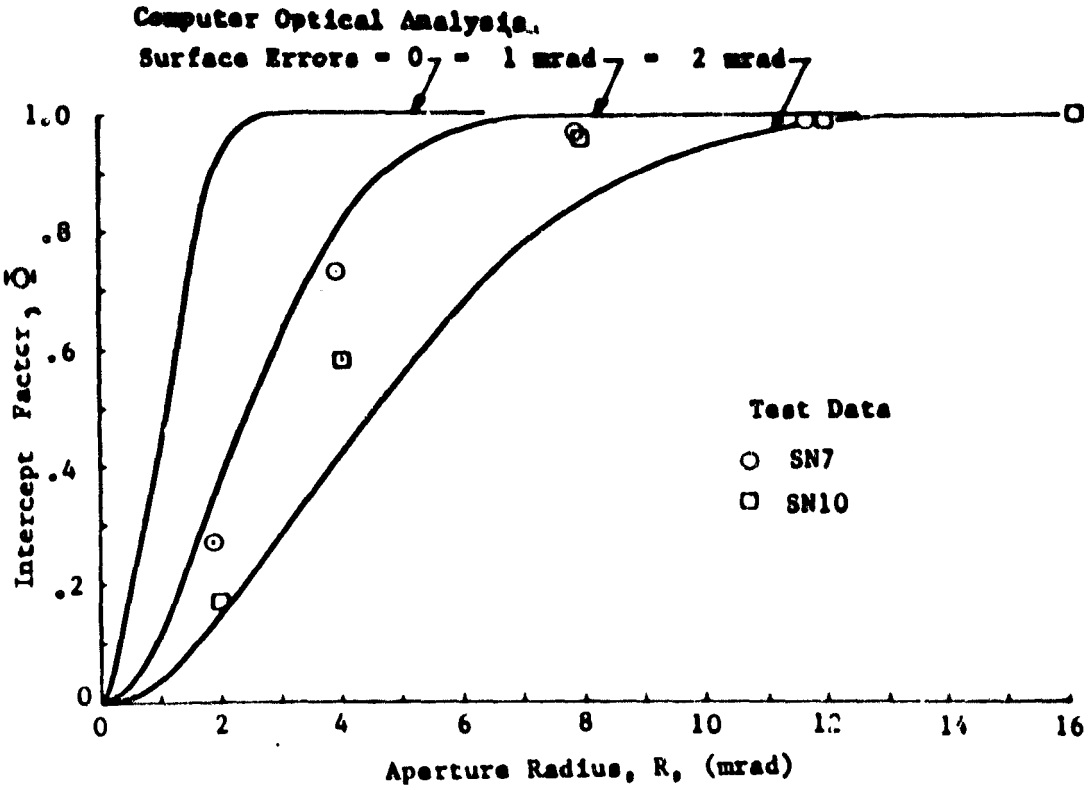

Figure 5.4-8 Test Results - Analysis Comparison

analysis approaches the line where surface error = $1/2\,\sigma_o$ for larger errors. The difference between these lines is the result primarily of the reflective surface specularity effects and secondarily due to the small but finite source image size. Slopes through the test data in Figure 5.4-8b (using a linear regression best fit) are also used to establish values for σ_o. The analytical correlation in Figure 5.4-8c is then used to estimate the panel surface errors corresponding to these test data. Several values are shown based on the number of test data points used to determine σ_o . The dashed lines indicate upper and lower bounds on the data. Because the uncertainty becomes very large in the Figure 5.4-8b curve, when the intercept factor approaches 1.0, the value of the fourth data points (at 12 mrad) is suspect. Basing the best fit "nominal" performance on the first three data points for each panel yields panel 1σ surface errors of 1.4 and 1.5 mrad for panel S/N7 and SN10, respectively.

5.4.2 Evaluation of Temperature Effects on Image Quality (Point Source)

5.4.2.1 Purpose of Testing

The purpose of this testing was to evaluate the sensitivity of the panel performance (image quality) to temperature variations.

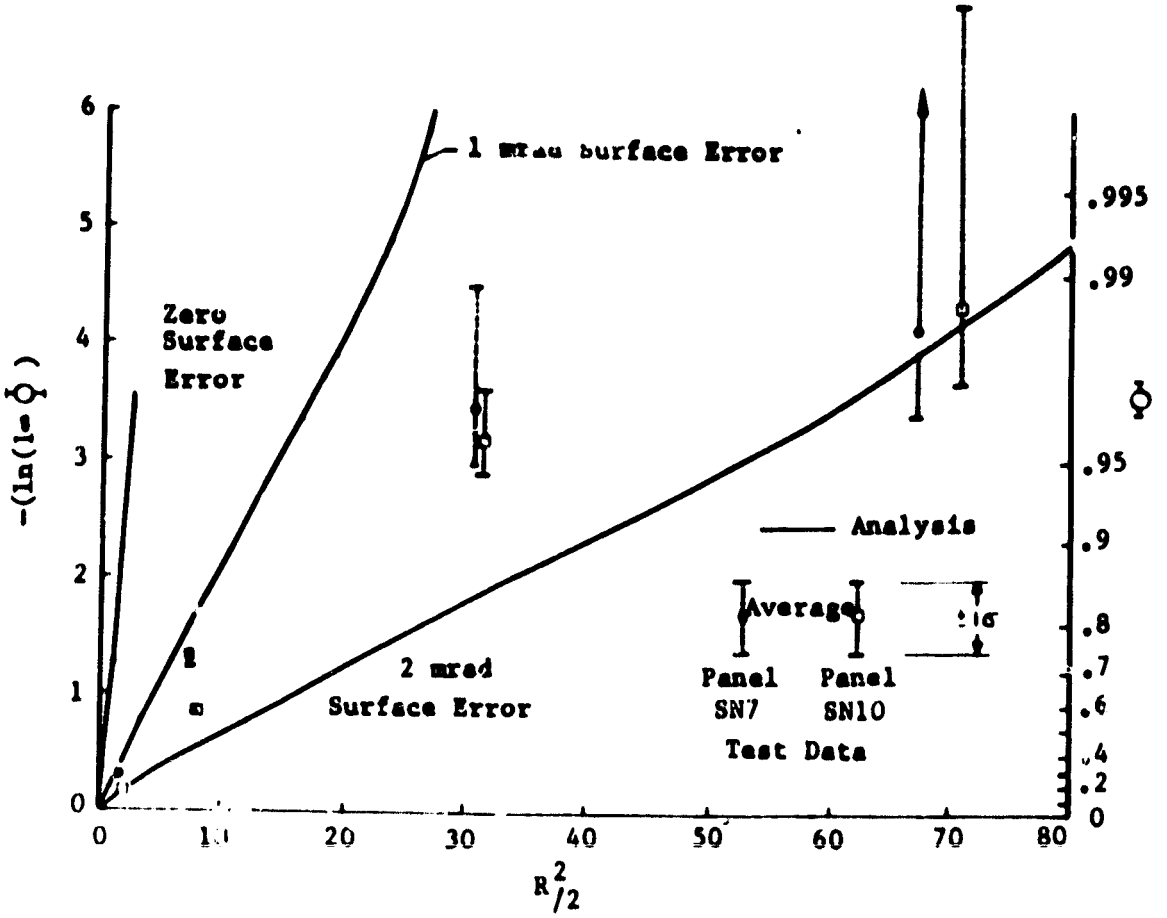

Figure 5.4-8b Test Results - Linearized Plot of Analysis

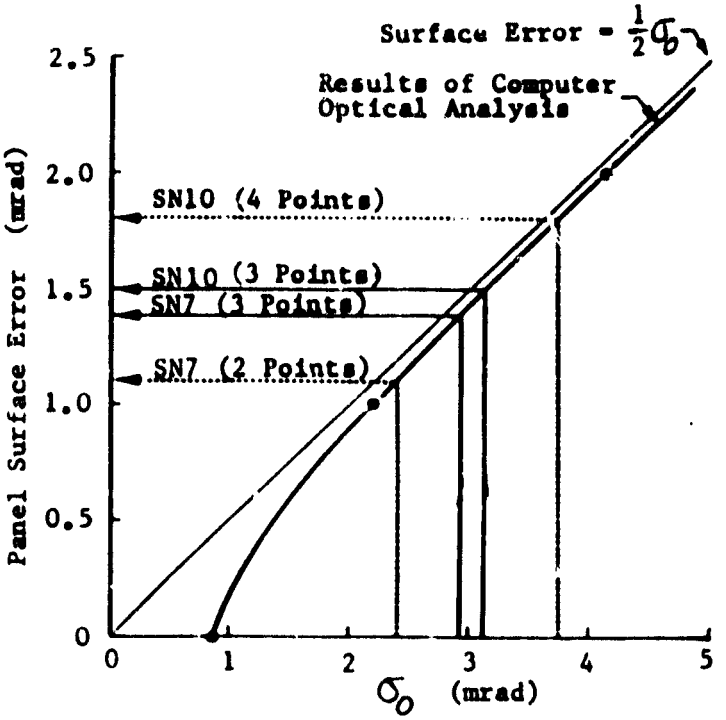

Figure 5.4-8c Panel Surface Error vs. σ_0

5.4.2.2 Method

The apparatus described in Section 5.4.1.2 for point source testing and panel SN7 were used in this test setup. In addition, equipment for heating and cooling of the panel was provided. Cooling was accomplished by enclosing the back side of the panel with a polystyrene foam box and loading the box with dry ice and allowing natural convection air currents to gradually cool the panel to the desired temperature. Heating was accomplished with an array of three 250 watt infrared lamps. A light shield was constructed to block rays from the heat lamps from traveling down the tunnel and entering the test system optics. Two chromel-alumel (Type K) thermocouples were installed on the backside of the panel. One was attached to the steel skin and the other to the structure. Radiation shields were provided on each thermocouple. An ice-bath junction was used and the readout was a Hewlett-Packard dual pen recorder. Figure 5.4-9 shows schematics of the apparatus used.

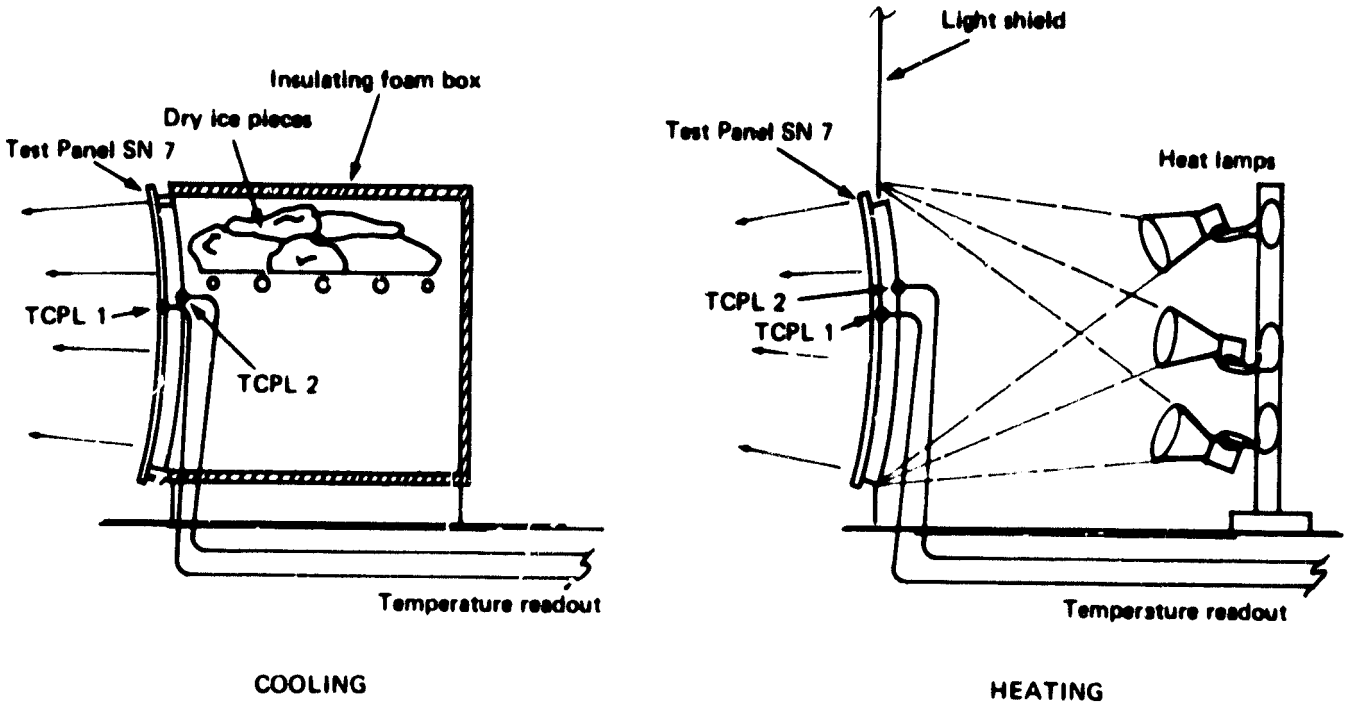

Figure 5.4-9. Temperature Effects Test Apparatus

5.4.2.3 Procedure

Panel SN7 was used for both the temperature tests; therefore, it was positioned at 1311 cm from the target plane.

Low Temperature Heat Test

The optical test apparatus was aligned for testing as in previous tests. The cooling apparatus as shown in Figure 5.4-9 was installed and loaded with dry ice. The onset of condensation on the front surface of the panel was observed at approximately +10°C (50°F), indicating the dew point had been reached. No provisions had been made to prevent or remove condensation, therefore the test was dew-point limited. Thirteen sets of data were taken at an average backskin temperature of +12.2°C (+54°F) and an average structure temperature of +11.7°C (+53°F).

High Temperature Test

The cooling apparatus was removed from the setup. A support stand with 3 clamp-on heat lamps was positioned behind the panel. Each lamp illuminated the entire backside of the panel but at different angles. No gradients were created. The lamp array was moved in relation to the panel until the desired temperatures were achieved. Thirteen sets of data were taken at an average backskin temperature of +41°C (+105°F) and an average structure temperature of +42°C (+107°F).

Ambient Temperature Test

A data series of 11 sets was taken with the panel at ambient temperature. These data were taken for reference purposes.

5.4.2.4 Test Results

Results from the low, ambient and high temperature tests are tabulated in Table 5.4-2. Normalized detector response average values and standard deviations are provided for each aperture size. The average values are also presented graphically on Figure 5.4-10.

The average values with 1σ error bands are seen to overlap at each aperture size. No general trend, such as low temperature data being consistently higher or lower was observed. Within the limits imposed by experimental uncertainty, no temperature effects were observed.

Table 5.4-2: Temperature Effects Test Data SN7

APERTURE		SURFACE ERROR - NORMALIZED OUTPUT					
DIAMETER CM (INCHES)	RADIUS MR	12°C (54°F) ▷		19°C (67°F) ▷		41°C (105°F) ▷	
		$\bar{x}$ (AVG)	σ (STD DEV)	$\bar{x}$ (AVG)	σ (STD DEV)	$\bar{x}$ (AVG)	σ (STD DEV)
5.08 (2.0)	1.9	0.267	± 0.022	0.259	± 0.006	0.228	± 0.009
10.20 (4.0)	3.9	0.687	± 0.037	0.703	± 0.007	0.663	± 0.014
20.30 (8.0)	7.8	0.964	± 0.013	0.968	± 0.009	0.973	± 0.017
30.50 (12.0)	11.6	0.983	± 0.015	0.983	± 0.011	0.994	± 0.007
40.60 (16.0)	15.5	1.000	0	1.000	0	1.000	0

▷ 13 Data Sets

▷ 11 Data Sets

▷ 13 Data Sets

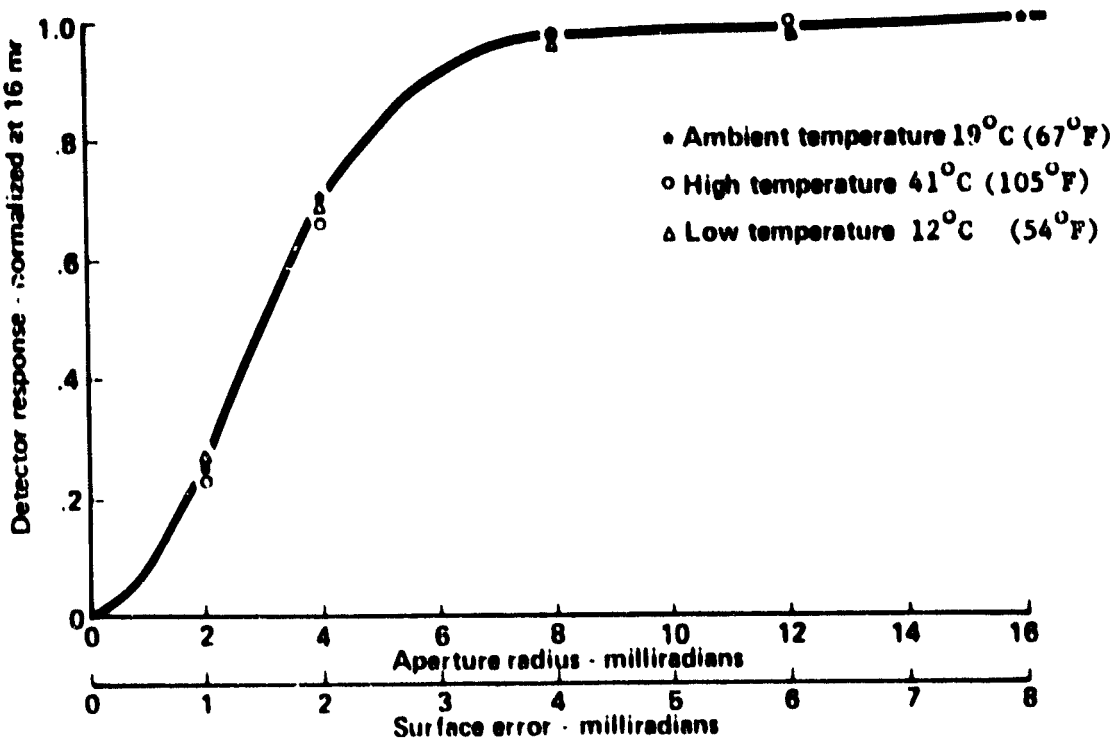

Figure 5.4-10 Temperature Effects Test Mirror No. 7

5.4.3 Evaluation with Sun as Source

5.4.3.1 Purpose of Testing

The purpose of this test was to measure the focal length. the solar image distribution, and to substantiate analytical predictions and point source test results.

5.4.3.2 Method and Apparatus

This test was performed outside on a sunny day using the sun as the light source. A 1.2 m by 2.4 m (4 x 8 ft) target board, with 2.5 cm (1 in) x 2.5 cm grid lines, was supported 3.2 m (12 ft) above ground level on an A-frame on wheels. The target orientation with respect to the test panel and the sun could be adjusted by rolling the entire A-frame to the desired location and/or adjusting the target angle with a hand winch. The orientation was frequently adjusted during testing so as to minimize the angle between the rays coming to the test panel and those reflecting on to the target. A HY-CAL radiometer was flush-mounted in the center of the target board. The radiometer was read out

on a digital voltmeter. Direct insolation was monitored with an Eppley 5° normal incidence pyrheliometer (NIP) or a equatorial mount. The apparatus and setup are shown schematically in Figure 5.4-11 and photographically in Figure 5.4-12.

5.4.3.3 Test Procedure

Focal Length

The test mirror was mounted on the holding fixture and oriented so as to place the image on the target. The target and the mirror were repositioned to place their alignment as near on-axis as possible. The mirror was then moved toward the target and then away from the target until the minimum diameter image was observed. The distance from the center of the mirror to the center of the image on the target (focal length) was measured and recorded for each test mirror.

Solar Image Distribution

The procedure used to obtain a flux distribution for the test mirror was in two parts. The shape of the distribution was determined by moving the image across the radiometer, taking readings at increments of 1 inch. The outside diameter of this image was estimated using photographic transparencies and an optical densitometer.

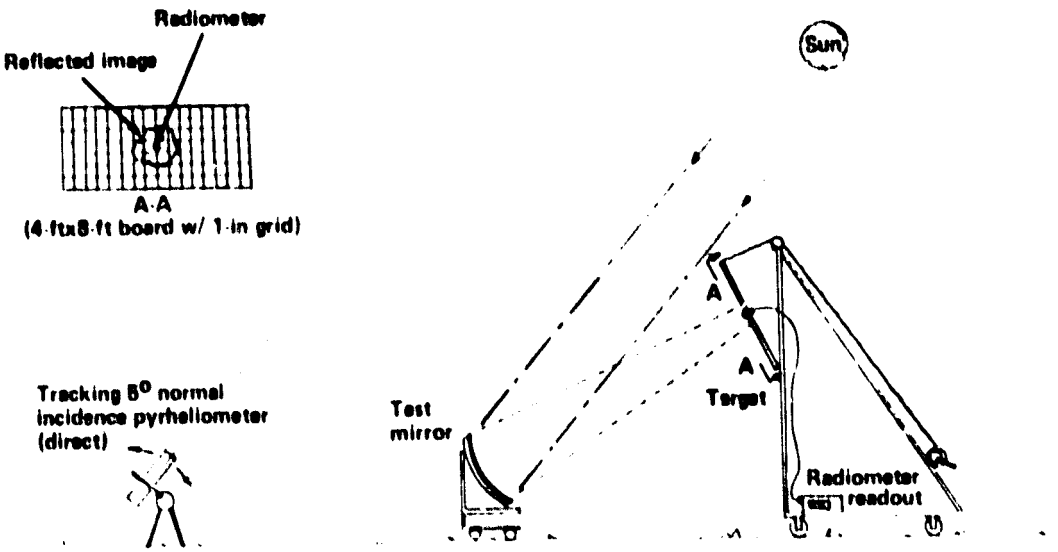

Figure 5.4-11 Sunlight Test Schematic

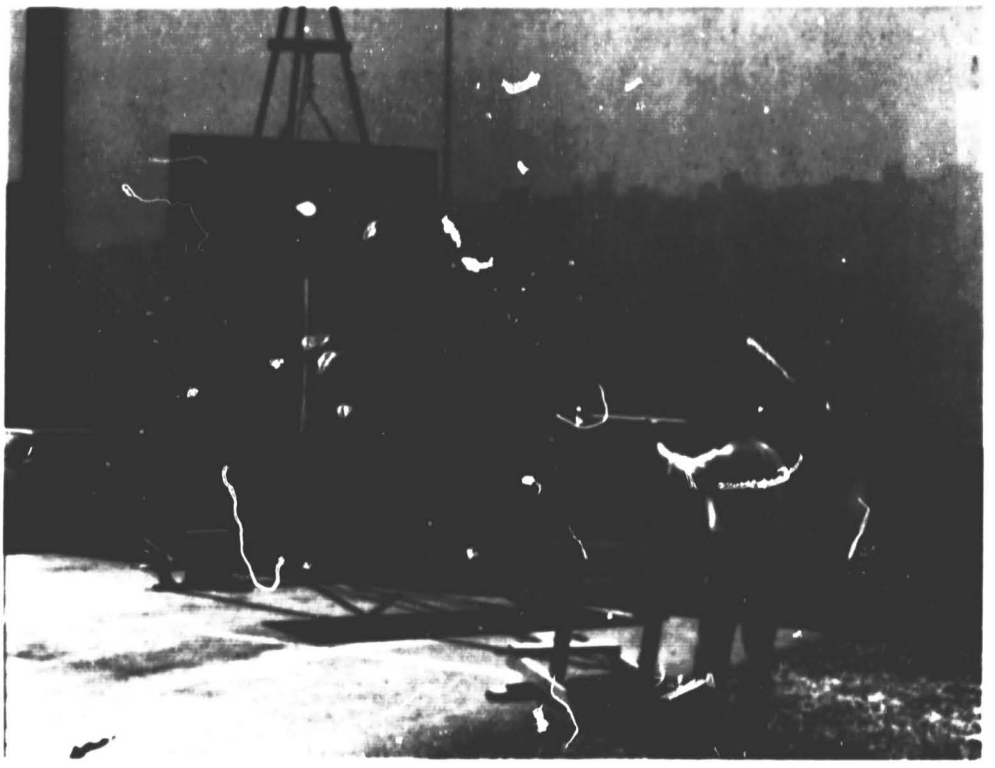

Figure 5.4-12 Sunlight Test Apparatus

The test mirror was manually aimed at the radiometer and moved until the peak output was observed. Next, the mirror was moved in such a manner to stepwise move the image horizontally across the radiometer. Readings were taken every inch across the image, from edge to edge, cutting through the region of peak flux. This procedure was repeated several times for statistical purposes. Figure 5.4-13 shows an image on the radiometer. Direct measurements were taken with the NIP at the same time to provide sun/sky quality and stability information and local intensity. During the time data was acquired, the sky had some transient haze which caused variations in insolation of about $\pm$10%.

Photographs (35 mm) were taken of images at approximately the same time the radiometer scans were made. Several aperture settings and shutter speeds were used to provide a variety of film exposures. The negatives were developed into 8 x 10 inch positive transparencies. These transparencies were scanned in a Macbeth TR524 Densitometer. Since the relationships of film density (opacity) to the exposure is logarithmic, the densitometer scan cannot be used directly as representative of the image distribution. It was used, however, to define the outside diameter of the image. This was defined as the diameter beyond which negligible (<5%) energy remained. Figure 5.4-14 is a typical image photograph with the densitometer scan path shown.

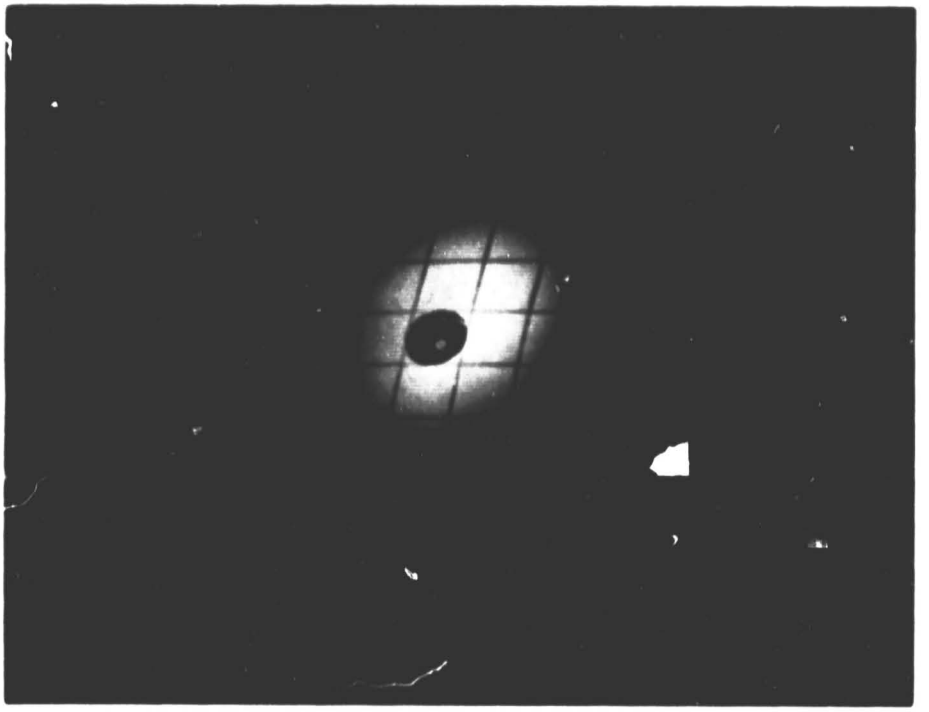

Figure 5.4-13 Reflected Image on Radiometer

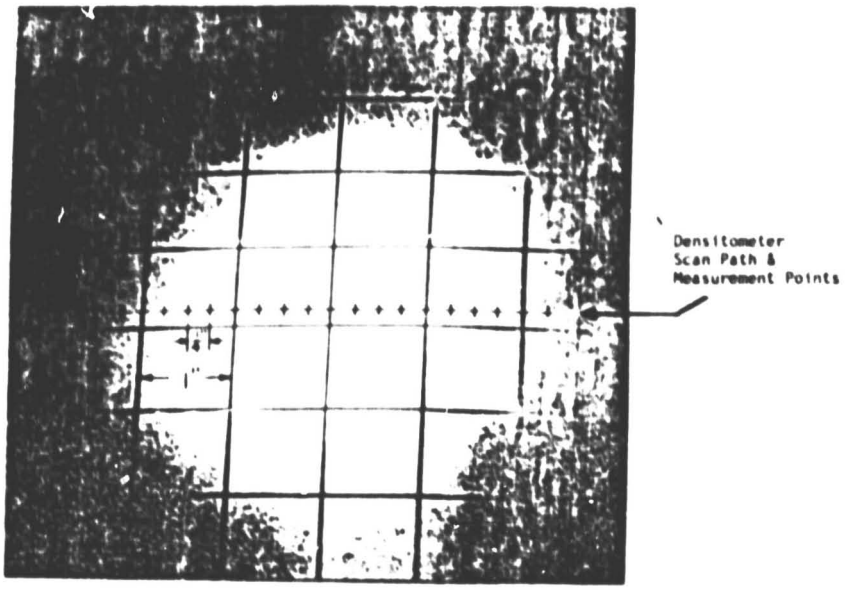

Figure 5.4-14: Reflected Image on Target Board

5.4.3.4 Test Results

Focal Length

The measured focal lengths were:

SN7 F.L. = 6.61 m (518 in)

SN10 F.L. = 6.35 m (490 in)

Solar Image Distribution

Results from the image scans are shown in Figures 5.4-15 and 5.4-16. Detector response vs. horizontal translation (or image diameter) plots are given for each mirror. The curves were made by (1) straight line fitting the fine data points, consisting of average values with 1 σ error brackets in the vertical axis and 1/8 inch error brackets along the horizontal axis; (2) tailing off

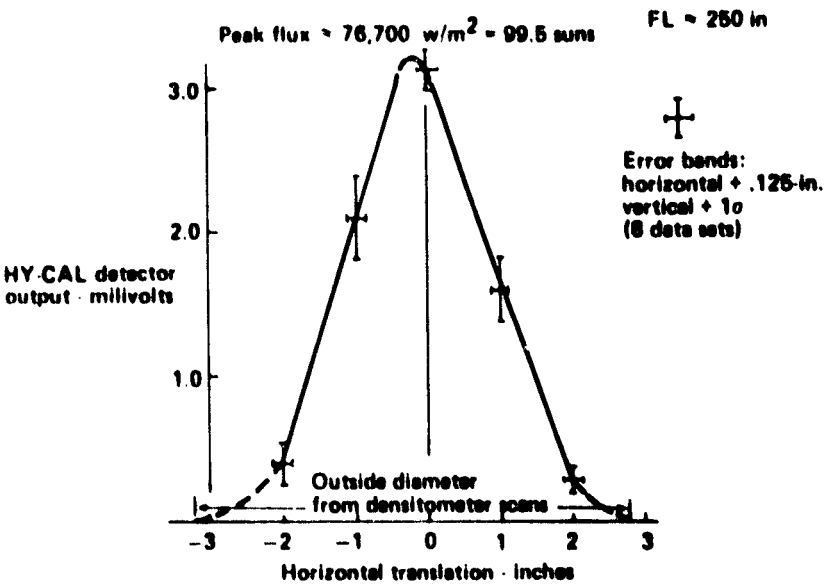

Figure 5.4-15 Mirror 10 Sun Data

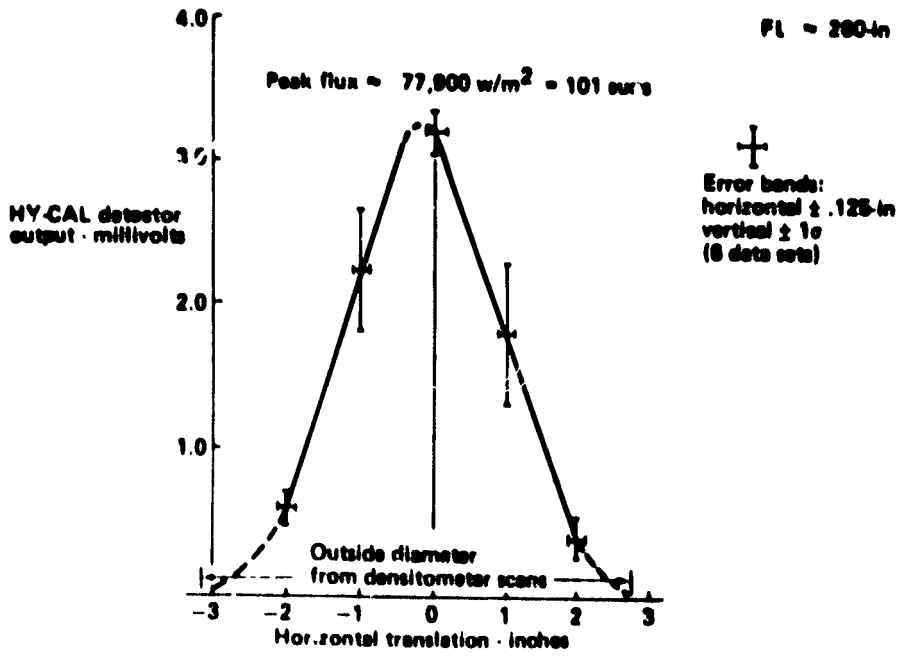

Figure 5.4-16 Mirror 7 Sun Data

the base of the plots to the zero intensity values determined by the densitometer scans. Eight sets of data were taken for SN10 and 6 sets for SN7. Peak fluxes of about 100 suns were estimated for both mirrors.

Calculations were made to predict the flux distribution based upon intercept factor curves produced by point source testing.

The power within an aperture of a given radius is

$$P = P_T IF \qquad \text{where: } P_T = \text{total power}, \quad IF = \text{intercept factor}$$

The intensity is defined as

$$I = \frac{dP}{dA} \qquad dA = \text{differential area} \quad \pi(r+\Delta r)^2 - \pi r^2$$

$$I = P_T \frac{d(IF)}{dA}$$

An equation was developed for the panel SN7 intercept factor curve (1.75 mrad surface error). The equation was differentiated and multiplied by the appropriate total power to obtain a plot of relative flux intensity (I_R) versus aperture radius. Figure 5.4-17 shows this plot. To obtain peak flux the relative flux was multiplied by the test panel area and the reflectance. Values of 103 suns peak and 5-1/2 to 6 inches in diameter are observed. These values compare closely to the experimental values for panel SN7 (Figure 5.4-16).

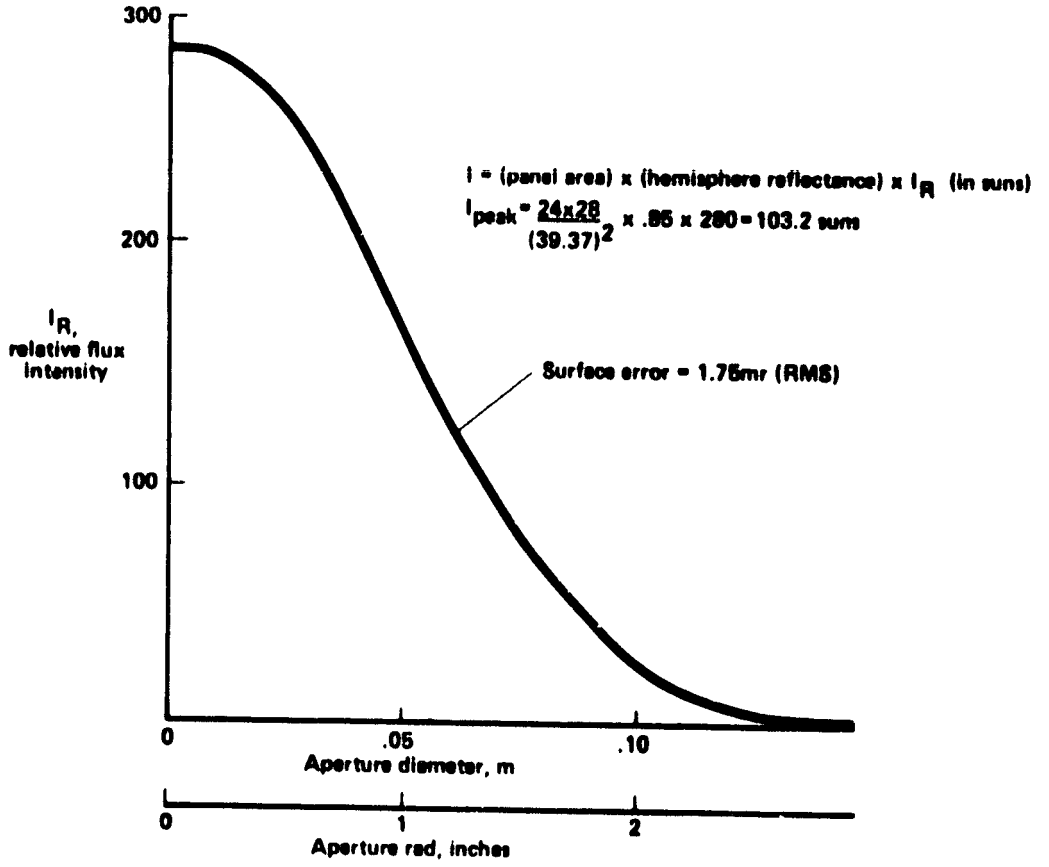

Figure 5.4-17 Calculated Flux Distribution- Sun Source (Mirror 7)

5.4.4 Comparison of Point Source and Sun Source Data

Having evaluated the test panels by two different techniques, it was desired to determine if the two sets of results could be correlated. Figure 5-18 has been prepared to aid in the discussion that follows.

In the light tunnel (point source test) a 1.3 cm (1/2 inch) light source was used as a point source. If the test panel had been perfect, a 1.3 cm (1/2 inch) image would have appeared at the radius of curvature at target plane.

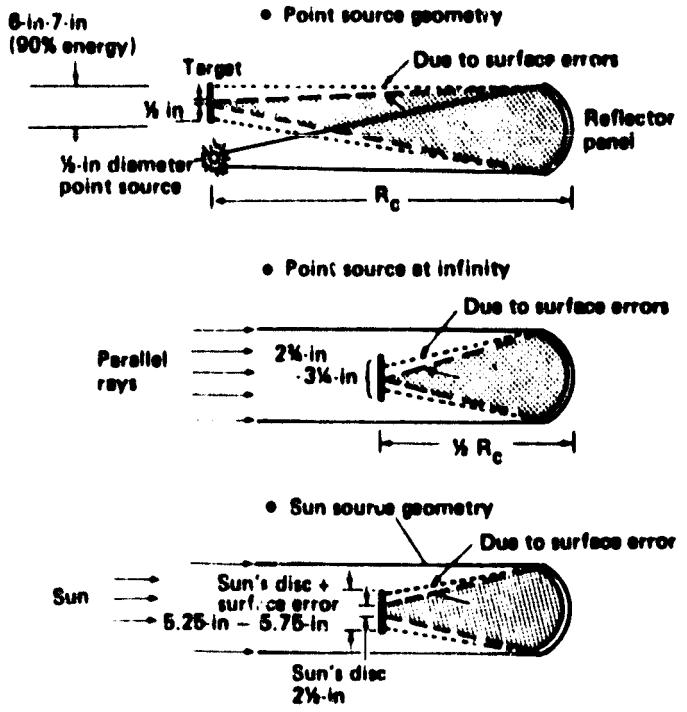

Figure 5.4-18 Point Source/Sun Source Correlation

Due to imperfections, the images of 15 to 18 cm (6 to 7 inches) containing >95% of the energy were observed. If a true point source of negligible diameter had been used, the image diameter then would have been 14 to 16.5 cm (5.5 to 6.5 inches).

Consider next a point source at infinity (the second sketch on Figure 5-18). In this case, the image would be formed at the focal plane because of the parallel incoming rays. Since the focal length is half the radius of curvature, the image size due to surface error would be half that observed at the radius of curvature. The image diameter for the test mirrors would be 7 to 8.3 cm (2.75 to 3.25 inches) for this theoretical geometry.

Finally, consider the real case of the sun source test. The spreading due to the sun's subtense angle result in a image diameter of 6.4 cm (2-1/2 inches) for a perfect mirror with a focal length equal to approximately 6.4 m (252 inches) . This image spreading would be additive to the mirror surface error of 7 to 8.3 cm (2.75 to 3.25 inches) for a total of 13.3 to 14.6 cm (5.25 to 5.75 inches).

Referring back to Figures 5-15 and 5-16, it is seen that the image diameters were determined to be approximately 15 cm (6 inches) from the sun source testing. Therefore, the two test approaches do correlate well (within about 10%) with respect to image diameter.

6.0 Conclusions

This study has met its general objective of developing a rigid panel concept that utilizes a thin film reflector surface for application to a low-cost point-focusing solar concentrator. Through an extensive screening study, a panel concept with low weight, manufacturing complexity technical risk and cost was selected. Figure 6.0-1 and Table 6.0-1 summarize the screening study. A concentrator concept was defined and evaluated which showed panel-concentrator compatibility, defined stiffener orientation and requirements, and provided optical performance goals for the panel. The selected concentrator concept and the resultant panel configuration are shown in Figures 6.0-2 and 6.0-3. The panel concept was validated by characterizing the thin film optical performance, demonstrating substrate/film optical compatibility, showing resistance to hail impact, fabricating test panels and demonstrating acceptable optical performance with the test panels. Figure 6.0-4 contains intercept factor plots predicted analytically and measured in the laboratory. These plots and additional analyses indicated panel surface errors of 1.4 and 1.5 mrad for SN7 and SN10, respectively, suitable for use on solar concentrators, including 816°C (1500°F) applications.

Areas where further investigation is desirable are: 1) weatherability of the film; 2) verification of solution to adhesive problem; and 3) forming tolerance reduction.

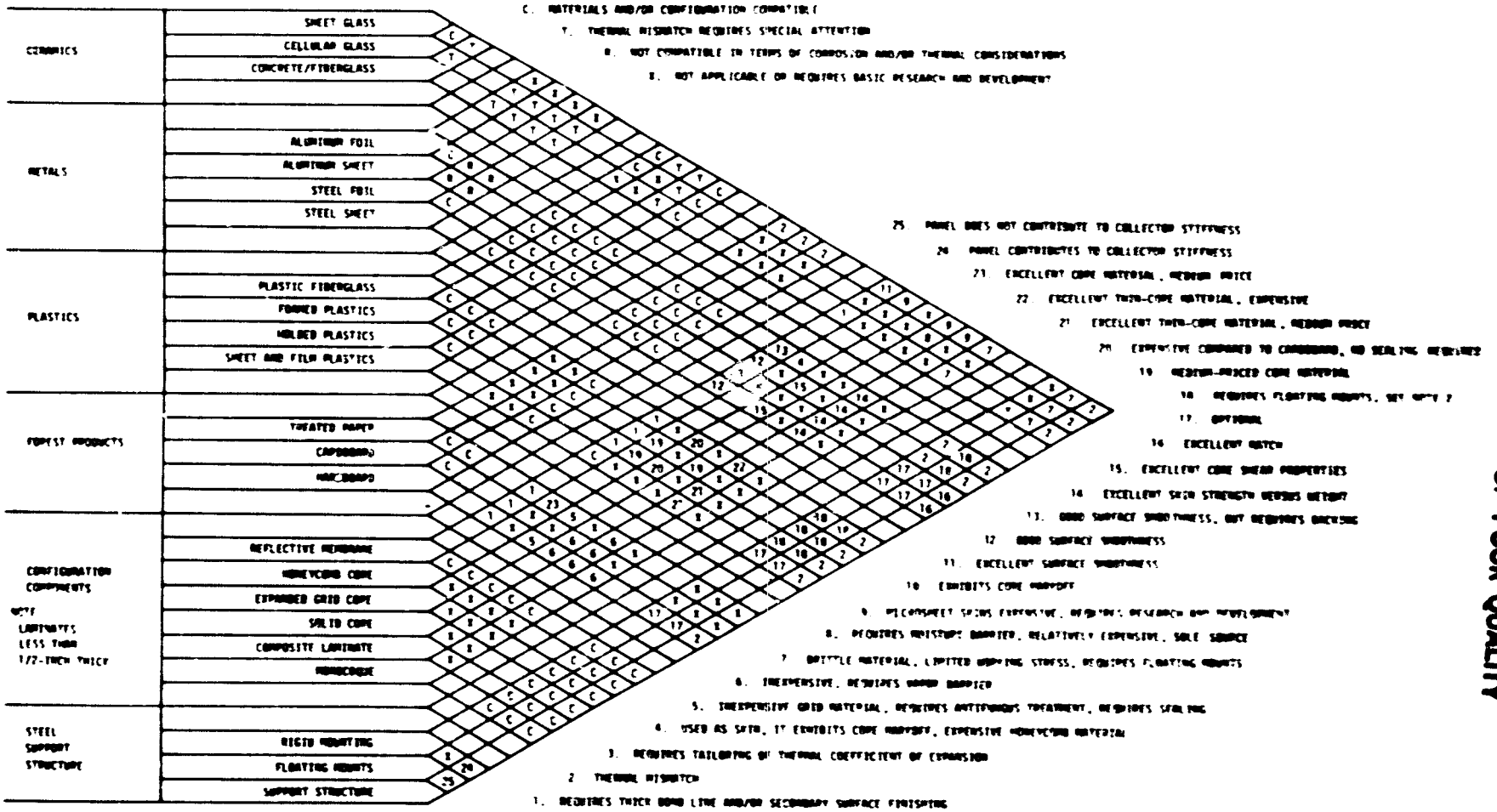

Figure 6.0-1 Potential Material - Configuration Combinations

Table 6.0-1 Concept Evaluation and Ranking

Concept	Weight LB/M^2	Material cost $/M^2	Manufacturing complexity	+ Technical risk	+ BBEC mils/kW_{th}-h	= Ranking
Stiffened steel skin	21.3	11.73	Low	Low	3.7	1 (Selected)
Stiffened steel clad plastic core laminate	15.6	12.06	Moderate	Moderate	3.9	2
Stiffened steel clad WFHB core laminate	17.7	11.86	Moderate to high	Moderate	3.8	3
Aluminum clad/ paper honeycomb sandwich	11.8	15.05	High	High	4.8	5
Steel clad/paper honeycomb sandwich	14.9	14.98	High	High	4.8	4

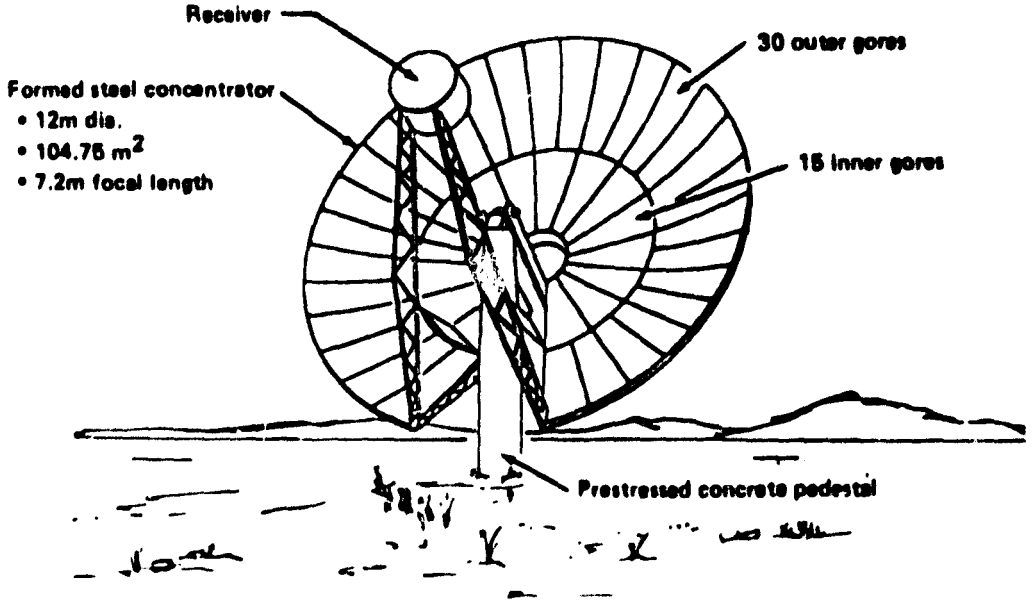

Figure 6.0-2 Thin Film Concentrator Conceptual Design

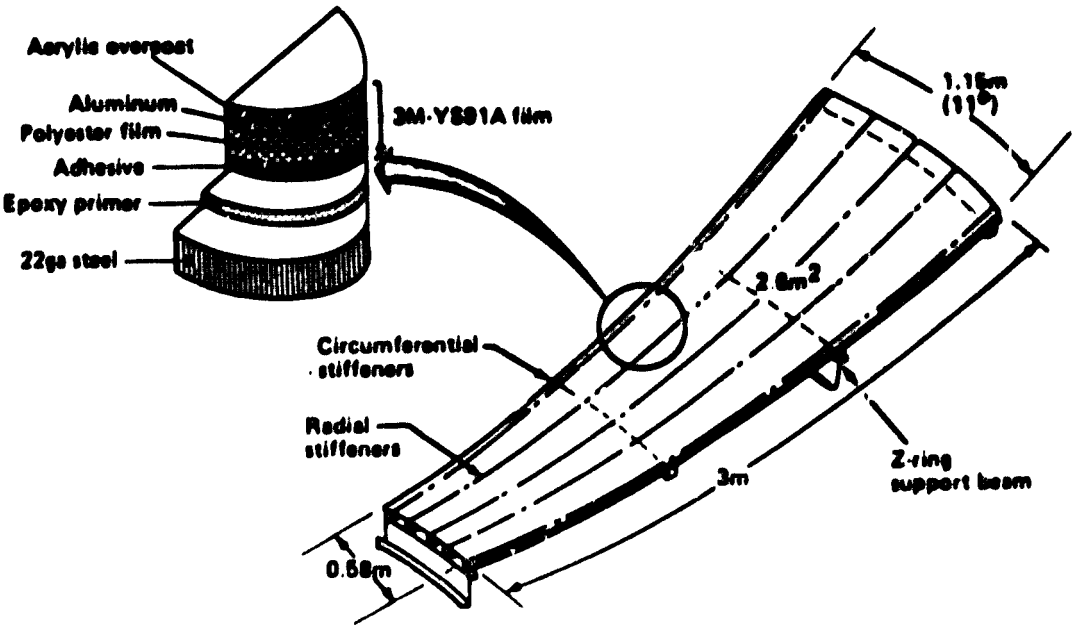

Figure 6.0-3 Outer Reflector Gore Concept

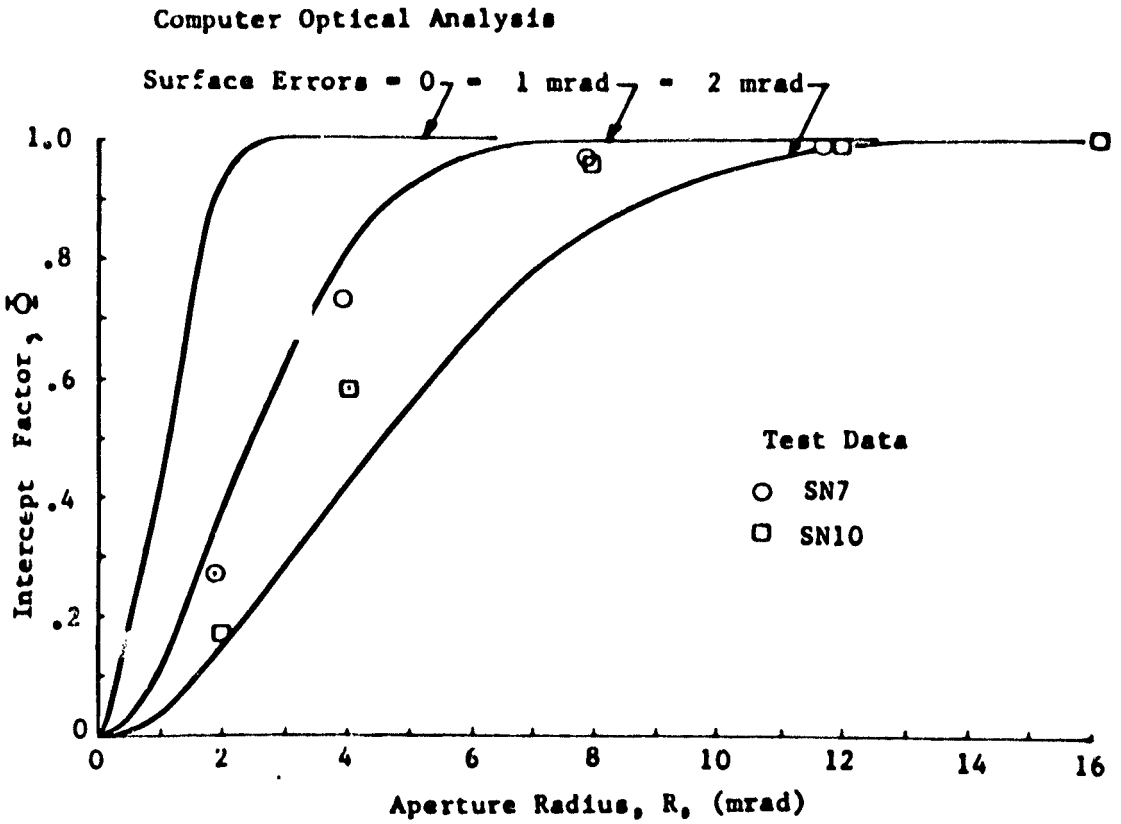

Figure 6.0-4 Test Results - Analysis Comparison

7.0 Recommendations

Recommendations for follow-on phases based upon experience from this study have been prepared and are summarized here (see Figure 7.0-1).

A Phase II is recommended that would address unresolved technical concerns, prepare a preliminary design for a dish concentrator, design, fabrication, and test panels for a 6.7m test bed concentrator and build and demonstrate a 6.7m test bed concentrator. The test bed concentrator would utilize the pedestal/foundation, gimbal actuator, torque tube and support beams from the existing BEC Second Generation Heliostat Design. Figure 7.0-2 shows the interface of the reflector panels and the existing heliostat structure. Phase II would require approximately 16 months (see Figure 7.0-3 for schedule).

A Phase III would follow that would include a detail design for a dish concentrator, production planning, and cost estimation and fabrication and demonstration of a 12m prototype concentrator.

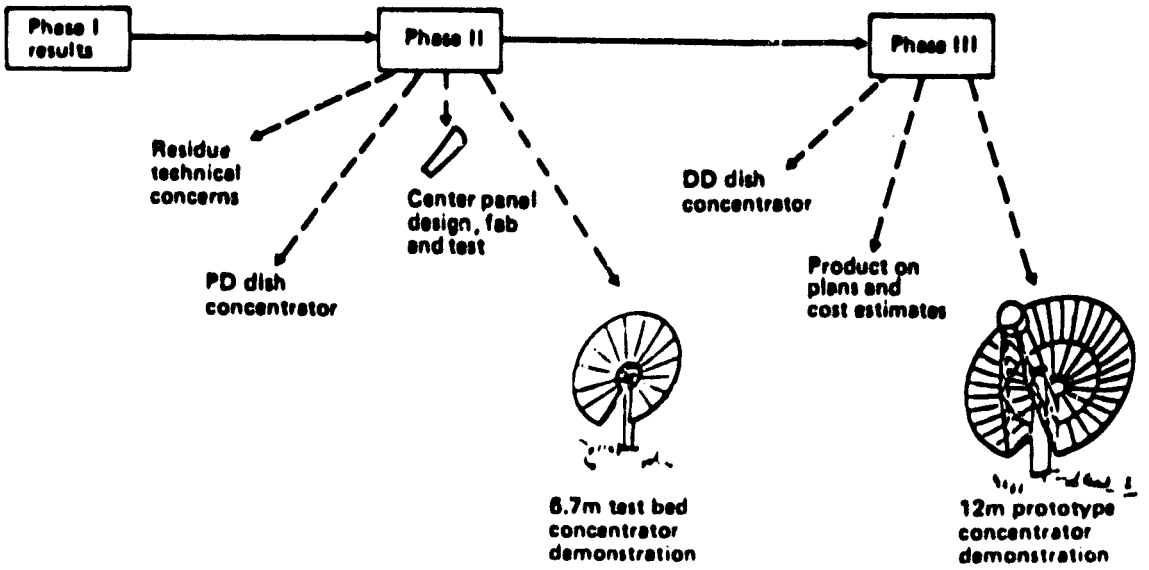

Figure 7.0-1 Program Plan Recommendation

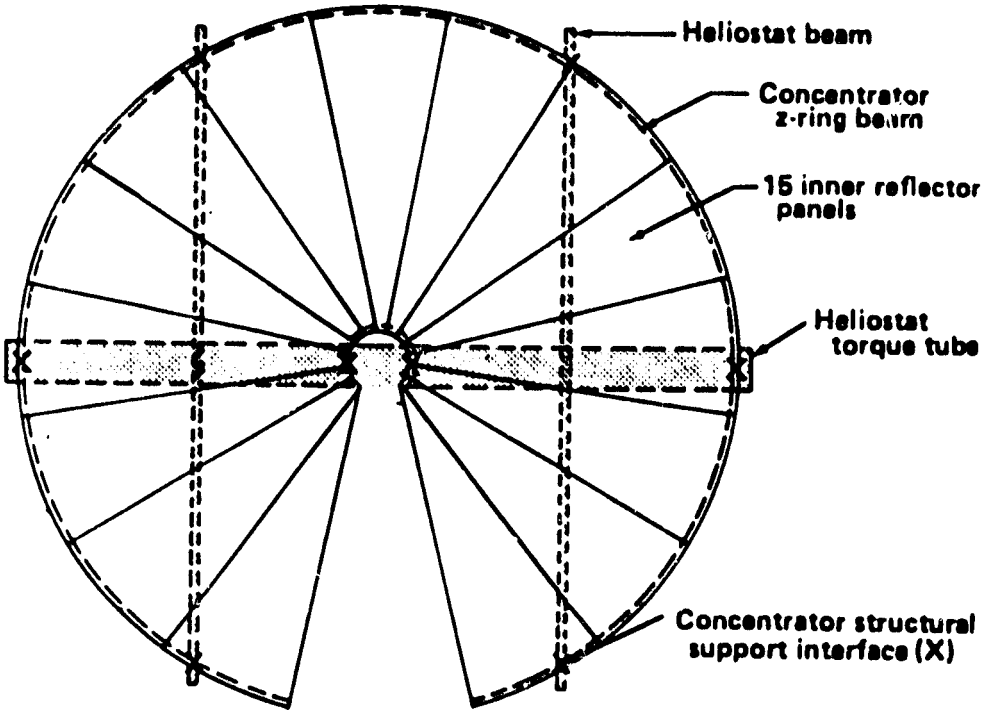

Figure 7.0-2 6.7m Concentrator/Heliostat Interface

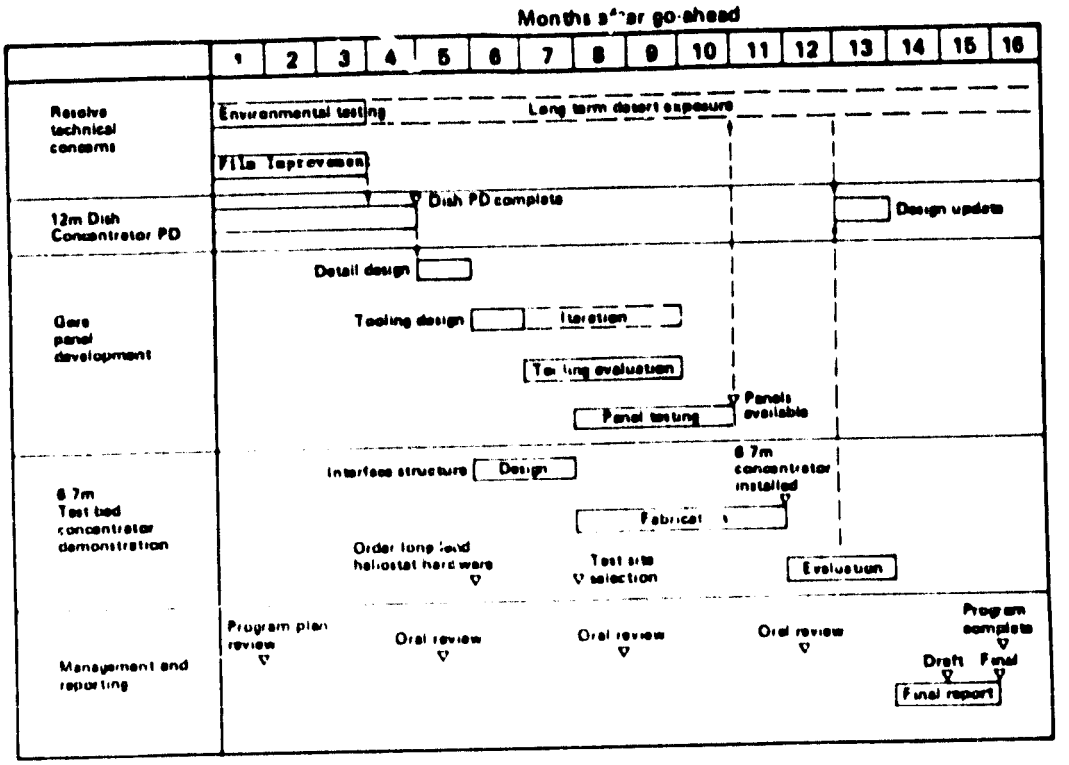

Figure 7.0-3 Phase II Recommended Schedule

8.0 NEW TECHNOLOGY

No reportable items of new technology have been identified by Boeing during the contract of this work.

9.0 REFERENCES

3-1 Donald Zimmerman, "Low Cost Point Focus Solar Concentrator", Phase I Final Report, JPL Contract No. 955209, Boeing Engineering and Construction Company, Seattle, WA, March 1979.

5-1 M. Argoud, "Method and Apparatus for Measuring Surface Errors of Solar Mirror Elements", JPL 2688-2, Jet Propulsion Laboratory, Pasadena, California.